Investigation on Control Strategies for Grid and Off-Grid Connected Inverters in Distributed Generation System

Thesis
Submitted in partial fulfillment of the requirements
for the award of the degree of

Doctor of Philosophy
in
Electrical Engineering

by

Ratna Rahul Tupakula
(Roll No. 714122)

Supervisor
Dr. D.M. Vinod Kumar
Professor

Department of Electrical Engineering
National Institute of Technology Warangal
(An Institute of National Importance)
Warangal – 506 004, Telangana State, India
September – 2019

Approval Sheet

This Thesis entitled **"Investigation on Control Strategies for Grid and Off-Grid Connected Inverters in Distributed Generation System"** by **Mr. Ratna Rahul Tupakula** is approved for the degree of Doctor of Philosophy

Examiners

_____

_____

_____

Supervisor

Dr. D. M. Vinod Kumar
Professor
EED, NIT Warangal

Chairman

Dr. S. Srinivasa Rao
Professor & Head,
EED, NIT Warangal
Date: _____

DEPARTMENT OF ELECTRICAL ENGINEERING
NATIONAL INSTITUTE OF TECHNOLOGY WARANGAL
WARANGAL – 506 004

DEPARTMENT OF ELECTRICAL ENGINEERING
NATIONAL INSTITUTE OF TECHNOLOGY WARANGAL

Certificate

This is to certify that the thesis entitled **"Investigation on Control Strategies for Grid and Off-Grid Connected Inverters in Distributed Generation System"**, which is being submitted by **Mr. Ratna Rahul Tupakula** (Roll No. 714122), is a bonafide work submitted to National Institute of Technology Warangal in partial fulfilment of the requirements for the award of the degree of **Doctor of Philosophy** in Electrical Engineering. To the best of my knowledge, the work incorporated in this thesis has not been submitted elsewhere for the award of any degree.

Dr. D. M. Vinod Kumar
(Supervisor)
Professor
Department of Electrical Engineering
National Institute of Technology Warangal
Warangal – 506004

Date:

Place: Warangal

Declaration

This is to certify that the work presented in the thesis entitled **"Investigation on Control Strategies for Grid and Off-Grid Connected Inverters in Distributed Generation System"** is a bonafide work done by me under the supervision of **Dr. D. M. Vinod Kumar,** Professor, Department of Electrical Engineering, National Institute of Technology, Warangal, India and was not submitted elsewhere for the award of any degree.

I declare that this written submission represents my ideas in my own words and where others' ideas or words have been included; I have adequately cited and referenced the original sources. I also declare that I have adhered to all principles of academic honesty and integrity and have not misrepresented or fabricated or falsified any idea/date/fact/source in my submission. I understand that any violation of the above will be a cause for disciplinary action by the institute and can also evoke penal action from the sources which have thus not been properly cited or from whom proper permission has not been taken when needed.

Date:

Place: Warangal

Ratna Rahul Tupakula

(Roll No: 714122)

ACKNOWLEDGEMENTS

It gives me immense pleasure to express my deep sense of gratitude and thanks to my supervisor **Dr. D. M. Vinod Kumar**, Professor, Department of Electrical Engineering, National Institute of Technology Warangal, for his invaluable guidance, support, and suggestions. His encouragement helped me to overcome the difficulties encountered in my research as well in my life. I offer my special thanks to **Dr. P. Chandrasekhar**, Assistant Professor, School of Electrical Sciences, Indian Institute of Technology, Bhubaneshwar for his guidance. His knowledge, suggestions, and discussions helped me to become a capable researcher. He has shown me the interesting side of this wonderful and potential research area.

I am very much thankful to **Prof. S. Srinivasa Rao**, Head, Department of Electrical Engineering for his constant encouragement, support and cooperation.

I take this privilege to thank all my Doctoral Scrutiny Committee members, **Dr. B. L. Narasimharaju**, Associate Professor, Department of Electrical Engineering, **Dr. A. V. Giridhar**, Assistant Professor, Department of Electrical Engineering and **Dr. P. Muthu**, Associate Professor, Department of Mathematics for their detailed review, constructive suggestions and excellent advice during the progress of this research work. I would also like to thank Dr. M. Raja Vishwanathan, Assistant Professor, Department of Humanities and Social Science for the proof reading of papers and thesis.

I also appreciate the encouragement from teaching, non-teaching members, and fraternity of Department of Electrical Engineering of NIT Warangal. They have always been encouraging and supportive.

I wish to express my sincere thanks to **Prof. N. V. Ramana Rao**, Director, NIT Warangal for his official support and encouragement.

I convey my special thanks to contemporary Research Scholars Mr. Hareesh M, Dr. Kasi Ramakrishna Reddy, Dr. Venu Sonti, Mr. B Anil Kumar, Mr. Pranay Kumar A, Mr. Madhu Babu S, Mr. Sumon Dhara and Dr. Siva Prasad Nandyala (ECE) and also M.Tech student Mr. Srinivas Pandit (2015 Power Electronics and Drives).

I acknowledge my gratitude to all my teachers and colleagues at various places for supporting and co-operating me to complete the work.

My special, sincere acknowledge, heartfelt gratitude and indebtedness are due to my parents Shri. Venkata Subbaiah T & Smt. Venkata Subbarathnamma T and my elder brother Ratna Kranthi Kumar T for his sincere prayers, blessings, constant encouragement, shouldering the responsibilities and moral support rendered to me throughout my life, without which my research work would not have been possible. My hearty gratitude to my sister in law T. Surekha and my maternal uncle B. Ramakrishna. I heartily acknowledge all my relatives for their love and affection towards me.

Above all, I express my deepest regards and gratitude to “ALMIGHTY” whose divine light and warmth showered upon me the perseverance, inspiration, faith and enough strength to keep the momentum of work high even at tough moments of research work.

——— Ratna Rahul Tupakula

Ж

ABSTRACT

Globally, with the gradual exhaustion of fossil fuels, increase in carbon emissions and global warming, the quest for renewable energy sources has gained prominence. Among renewable sources, Photovoltaics (PV) has gained importance because of its easy deployment and considerable advantages over other renewable sources like wind, tidal etc. As all the renewable energy sources are intermittent in nature, it will be a noble idea if such distributed generators (DGs) are interconnected to elements like energy storage units and loads together to form a microgrid. Distributed generators are the heart of microgrid applications. The distributed generators need reliable and efficient methodologies for their controlled operation. The methodologies involved in their control depend on whether DGs operated in islanding mode for feeding loads or in grid connected mode feeding active and reactive powers to the grid. The main aim of the development of such control strategies is to increase the reliability and to enhance power quality. The thesis focuses mainly on developing such methodologies that are mainly helpful for microgrid applications. Many DGs are of small capacity with low power ratings are interfaced with single phase distribution systems. For example, roof-top based PV generation systems, which are gaining prominence in distribution systems, are in general interfaced with single phase power distribution networks. The interconnection of single phase DG inverter with utility grid becomes difficult due to the inherent pulsating nature of single phase powers at double the grid frequency. In this thesis, the control strategies involve two loops in which the inner control loop is used to establish the duty ratio/modulation index for the generation of sinusoidal output current that is in phase with the grid voltage; the outer loop is used to correct the error in real and reactive powers.

The two loop control strategies for grid interconnection is proposed in this thesis, comprises three current reference generations, namely, scalar control, modified scalar control and simplified active and reactive power control for generating the required active and reactive powers along with the separate modulation method employed, these being either asynchronous sigma delta modulation (ASDM) or model predictive control (MPC) based space vector modulation (SVM). The performance of MPC based SVM and ASDM for the control of active and reactive powers of single phase grid connected DG is verified with different current reference generation schemes. The scalar reference generation scheme results in steady state error. Though the modified scalar reference generation scheme renders zero steady state error, and it induces delay in power tracking. The MPC based SVM in combination with simplified active and reactive power control (SRPC) has the advantages of quick, accurate and stable

control when compared with ASDM. Although the modified scalar reference generation scheme and SRPC have error correction mechanisms, their performance with ASDM is very poor. Therefore, the MPC based SVM with SRPC is observed to be the best combination among reference generation and modulation schemes. Though the MPC based SVM with SRPC proved to be better, there is a need of reducing the two stage to single stage as cascade loops always reduce efficiency.

The development of single stage control strategy involves the powers to be generated as an objective function. Therefore, for the control of single phase DG to operate in grid connected mode, the powers are modeled using an MPC integrated with SVM. Further, for the operation of DG in islanding mode, the voltage is utilized as an objective function. A simple phase locked loop (PLL) free grid synchronization mechanism along with seamless transition control between grid connected mode and off-grid mode is developed. The developed MPC is integrated with SVM and examined for delivering the set-point powers in grid connection mode, supplying the local load at nominal voltage and frequency in off-grid mode and for smooth transition between these modes. The designated performance of the developed control scheme for single phase DG is confirmed through simulations, which are further validated on an experimental test bed.

Though the achieved objectives are found to work fine for single phase designated systems, for large scale power supply single phase DGs are not suitable. Therefore, three phase systems are controlled using the objectives presented in the single phase system. However, for the large scale power generations in grid connected mode, it is observed that there is no problem in feeding power to the grid. During the islanding mode of operation in a microgrid, there may be multiple DGs. Hence, there is a need to develop a control strategy which addresses the issue of maintaining the voltage and frequency operated at nominal values while feeding the load. Also there will be rotating interface in addition to the photovoltaic operated DGs. To address these issues, a control strategy is proposed for multiple DGs coordination with a simple pulse width modulation strategy comprising of primary and secondary control. The primary control comprises modified droop control which decides the power sharing between the DGs whereas the secondary control begins restoring the voltage and frequency to nominal values if the primary control fails. The performance of the proposed control strategy is validated through simulations and hardware-in-loop (HIL) implementations using OPAL-RT.

Table of Contents

List of Figures

List of Tables

Abbreviations

AC	Alternating current
ASDM	Asynchronous sigma delta modulation
CAN	Communication Area Network
CCC	Circular chain control
CCS	Continuous control set
CRG	Current reference generation
DB	Dead beat
DC	Direct current
DG	Distributed generator
DSO	Distribution system operator
FCS	Finite control set
HB	Hysteresis band
HCC	Hysteresis current control
HIL	Hardware in loop
IEEE	Institute of Electrical and Electronics Engineers
IAE	Integral absolute error
LBC	Low band-width communications
MG	Microgrid
MPC	Model predictive control
PC	Personal computer
PCC	Point of common coupling
PF	Power factor
PI	Proportional integral
PLL	Phase locked loop
PR	Proportional resonant
PV	Photovoltaic
PWM	Pulse width modulation
SDM	Sigma delta modulation
SMC	Sliding mode control
SOGI	Second order generalized integrator
SRPC	Simplified active and reactive power control

STATCOM	Static synchronous compensator
SVM	Space vector modulation
THD	Total harmonic distortion
s	Seconds

List of Symbols

ϕ	Power factor angle
δ	Power angle
$\Delta\delta$	Power angle compensation
θ	Phase angle
Ψ_1	Voltage phase angle
$\Delta\theta$	Perturb in phase angle
τ	Time constant of integrator
C_f	Filter capacitance
d	Duty ratio of ASDM
f_s	Switching frequency
f_{nom}	Nominal frequency
f	Frequency of grid voltage
g	Minimized objective function
g_i	Objective function for i^{th} vector
g_{sl}	Objective function with powers
g_v	Objective function with voltage
I	Current supplied by DG before filtering
I_{act}	Measured current
IAE_P	Integral absolute error in active power
IAE_Q	Integral absolute error in reactive power
I_L	Current supplied to load
I_m	Peak value of the current flowing into the grid
I_{mref}	Reference peak current
I_{PCC}	Current supplied to PCC
I_{ref}	Reference current
I_0	Current supplied by DG
ΔI	Perturb in current
K_{P1}, K_{I1}	Proportional and integral parameters of powers
K_{pv1}	Proportional value for primary voltage parameters
K_{Psv1}, K_{Isv1}	Proportional and integral parameters of secondary voltage parameters
K_{psf1}, K_{Isf1}	Proportional and integral parameters of secondary frequency parameters

L	Line inductance
L_f	Filter inductor
m	Modulation index
P	Active power
P_{DG}	Active power supplied by DG
P_{grid}	Active power supplied to grid
$P_{gridref}$	Grid reference active power
P_{load},	Active power supplied to load
Q	Reactive power
Q_{DG}	Reactive power supplied by DG
Q_{grid}	Reactive power supplied to grid
$Q_{gridref}$	Reference reactive power to grid
Q_{load}	Reactive power supplied to load
P_{ref}	Reference active power
ΔP_L	Hysteresis band lower limit for active power
ΔP_U	Hysteresis band upper limit for active power
Q_{ref}	Reference reactive power
ΔQ_L	Hysteresis band lower limit for reactive power
ΔQ_U	Hysteresis band upper limit for reactive power
R	Line resistance
R_f	Filter resistance
S_1- S_6	IGBT switches
S	Apparent power
S^-	Negative slope
S^+	Positive slope
S_{ref}	Reference apparent power
T	Time period of voltage signal
T_1	Turn on time
T_2	Turn off time
T_s	Sample time
V_{cc}	Pulsating voltage train
V_{dc}	DC link voltage
V_i	Inverter output voltage

V_g	Grid voltage
V_m	Peak value of the voltage at PCC
V_P	Instantaneous voltage at PCC
V_{PCC}	Voltage at loads
ω	Angular frequency
X	Inductive line reactance

Chapter 1

Introduction

Chapter 1

Introduction

1.1 General Overview

Rapid industrial development and exponential population growth in world demand increased need of energy sources. However, the limited capacity for regeneration and sustainability of energy sources becomes a challenging concern for the technological and industrial growth. In view of sustainability problems in the global scenario, the governments and committees are encouraging technology promoters to develop ways of promoting sustainable energy sources. From the renewable energy statistics 2018 [1], the power generation by non-renewable energy is 73.5%, whereas the power generation by renewable energy sources is 26.5%. Out of the power generation from renewable energy, the major share of power is contributed by Hydropower (16.4%) followed by Wind power (5.6%), Bio-power (2.2%), Solar PV (1.9%) and other sources (0.4%) i.e., combination of ocean, concentrating solar thermal power and geothermal power respectively as shown in Figure 1.1.

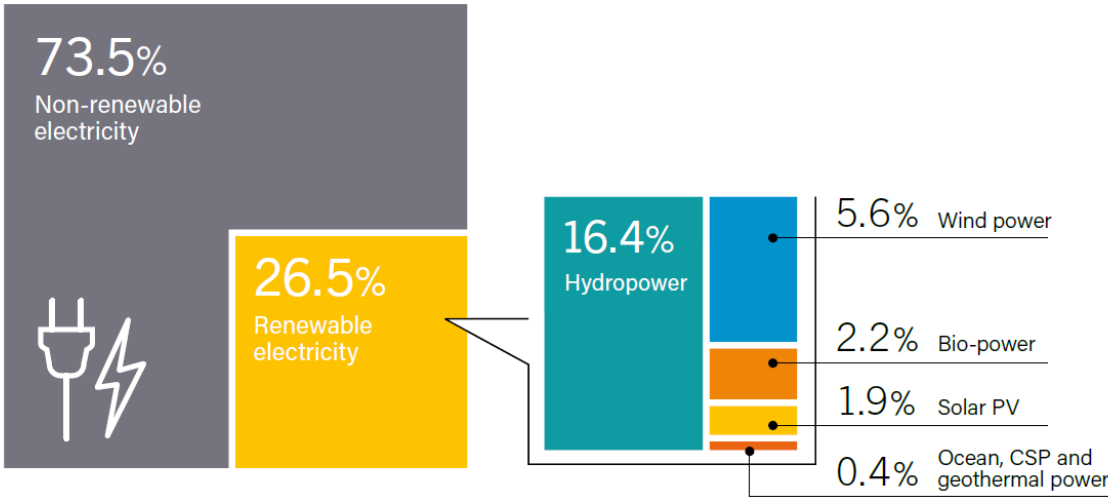

Figure 1.1 Global Energy generation using different renewable energy sources.

With wide ranging developments, reduction in panel cost, easy maintenance and relatively less capital cost, the governments of different countries have started investing heavily in PV considering them as the best viable source. The governments have even started providing the incentives for the installation and development of projects based on PVs. According to the statistics [1], the power generation shared by different countries in the world is provided in Figure 1.2. The statistics shown in Figure. 1.2 indicate that China leads the power generation

with 32% followed by Japan (12%), Germany (10%), India (5%). The Government of India has the target of increasing renewable energy capacity to 175 GW by the year 2022 which includes solar power of 100 GW, wind power of 60 GW, bio-power of 10 GW and 5 GW from small hydro-power. The target of 100 GW of solar power is set under the Jawaharlal Nehru National Solar Mission (JNNSM) will predominantly comprise 40 GW from Rooftop and 60 GW through Medium and Large Scale Grid Connected Solar Power Projects. In view of this high penetration of the solar energy sources, the state of art of the distributed generation has gained prominence.

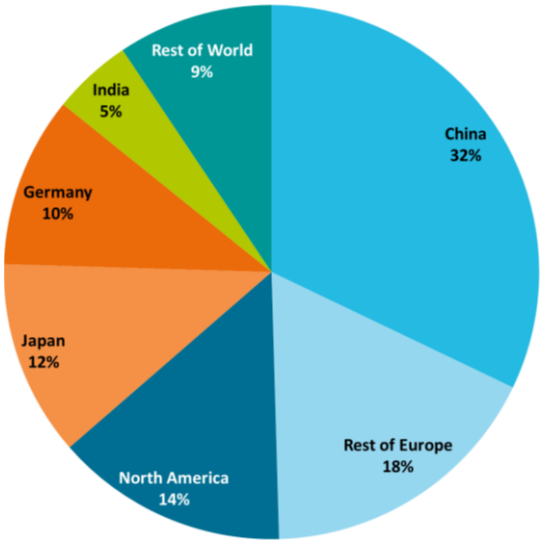

Figure 1.2 Solar power generation across the world.

A DG is power generation source that can be connected with any distribution network or simply to a standalone load operating similar to an uninterrupted power supply (UPS) system. As all the renewable energy sources are intermittent in nature, it will be a noble idea if such distributed generators (DGs) are interconnected to elements like energy storage units and loads together to form a microgrid. The advantages of distributed generation are as follows:

- High reliability in power supply.
- Flexibility in effectively utilizing the renewable energy sources.
- High power quality.
- Rural applications.

Despite the advantages offered under the distributed generation, there are also technical limitations such as:

- Significant transient voltages during connection/ disconnection from the grid.
- Fluctuation in DG output because of intermittent nature of the renewable sources.
- Impact on power system dynamics
- Safety concerns in islanding operation.

Due to the disadvantages stated above, the distributed generators need reliable and efficient methodologies for their controlled operation.

1.2 Overview of a Microgrid

The methodologies involved in the control of DG depend on whether their operation is in islanding mode for feeding loads or in grid connected mode feeding active and reactive powers to the grid. The block diagram of a DG connected to loads/ utility grid is shown in Figure 1.3.

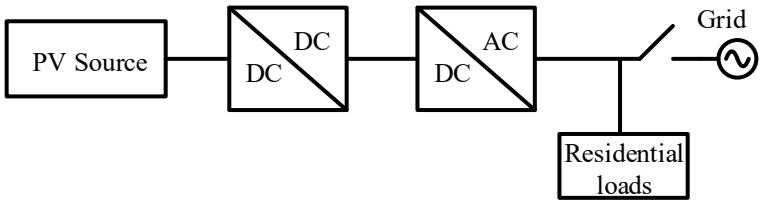

Figure 1.3 PV based DG connected to load / utility grid.

The photovoltaic based DG utilizes power electronic interfaces for the conversion process which provide greater flexibility between the energy sources and loads / utility grid is shown in Figure 1.3. Each DG has its own operation and method of control. The cluster of such DGs and local loads can be connected together to form a microgrid which offers various advantages of interconnection with the grid in terms of power injection and their ability to incorporate non-conventional energy sources with the existing conventional energy sources. In the grid-connected operation, the DGs are operated together with the utility grid supply power to the local loads connected. If the power generation from the microgrid is greater than the loads connected, the excess power is injected to the grid. Alternatively, if the power generation is lower compared to the load demand, the deficit power can always be imported from the grid. During the islanding operation, the DGs should be always able to provide a stable operating voltage at the point of common coupling (PCC) supplying active and reactive powers to loads. The microgrid should always have the ability to reconnect with the utility grid whenever, the

grid is available. An additional function that can be performed by utilizing the microgrids is that each microgrid can always serve the grid as an ancillary service providing the voltage support and improvement of power factor. Due to the increase in penetration of renewable sources into active distribution systems, there is a need of DGs to be equipped with their own capability of supplying reactive power in addition to active power. It will be very helpful for utilities to reduce investments on voltage regulation devices. The application of the voltage regulating devices like static synchronous compensator (STATCOM) at the distribution networks is not feasible owing to its high cost to the system.

In general, the main issues that are to be addressed for any renewable energy system to be interfaced with grid/ standalone system are power sharing, reliability with power quality, seamless transfer, protection and stability of the system.

1.3 Organization of the Thesis

The work carried out as part of the research is organized into seven chapters and presented as follows:

The **first Chapter** describes the introduction and a brief overview of the microgrid and the need for the development of control methodologies for microgrid applications is presented. The scope of the work has been highlighted and author's contribution in the research area has been summarized.

The second Chapter presents comprehensive literature review of the existing control techniques for the distributed generators and microgrid applications. Thus, the motivation and objectives for the research work carried out in this thesis is explained.

In **third Chapter**, three current reference generation schemes are developed for the control of grid connected DGs and the three current reference generation schemes are validated using two PWM methodologies using Asynchronous Sigma Delta Modulation (ASDM) and model predictive control (MPC) based space vector modulation (SVM). Simulation results of all three current reference generation schemes are presented with ASDM as well as MPC based SVM are performed and presented.

In **fourth Chapter**, a single-stage PLL free MPC based SVM for grid connected and islanding mode is developed. In addition, a simple synchronization process is proposed to

achieve the seamless transition between islanding and grid connected mode. The proposed control methodologies eliminate multi loop control. The modelling, design and analysis of the proposed MPC based SVM are presented. Simulation results of the proposed control methodology are performed and validated on a test-bed.

In **fifth Chapter**, the control strategy developed for single phase system is also applied for three phase system. The seamless transition is checked between the grid connected mode to islanding mode and vice versa. In the latter half of the chapter, for the parallel connected DGs, two control strategies viz; primary control as well as secondary control is proposed for the coordinated control operation of the DGs. The primary control is droop control that mimics the operation of synchronous generator and decides the power sharing between the two DGs. The secondary control restores the voltage and frequency to nominal values if the primary control fails. The simulation results of the different case studies are performed and validated with HIL using OPAL-RT.

In **sixth Chapter**, the dynamic performance of the controller is validated using the diesel generator and the control strategies are validated with HIL using OPAL-RT. The proposed control strategies are effective in maintaining the voltage and frequency to nominal values and the elimination of filters drastically improves the performance and the settling of the real and reactive powers and voltages are quick to settle down to their values as per the controller parameters. The primary control decides the power shared between two distributed generators along with the diesel generator, with voltage and frequency maintained at nominal values at the point of common coupling (PCC). The secondary control strategy allows the distributed generators to restore the voltage and frequency to nominal values if the primary control fails. The proposed control strategy is free of conventional d-q transformations which eliminates the discrete filters and thereby increases the speed of the controller. The effect of communication delays also do not relatively affect the controller and the controller is quick in bringing the voltage and frequency values settle to nominal values.

The **Chapter-7** highlights the summary of overall significant contributions of the thesis work and provides the scope for further research in this area.

Chapter 2

Literature Review on Control Methodologies of DGs

Chapter 2
Literature Review on Control Methodologies of DGs

2.1 Introduction

The essential requirement for the power conversion process is whether the DG sources are connected to the grid or operated in islanding mode supplying the power to the local loads are power electronic converters. These converters help in providing smart and flexible interface between the customers and non-conventional energy sources. Due to the high penetration in the utilization of renewable energy sources like wind energy, solar PV and tidal energy, it has marked the beginning for the interface of renewable sources with AC or DC buses connected to the utility grid. Due to the increase in the penetration of non-conventional energy sources, the rise in development of control methodologies also began for effective and efficient utilization thereby achieving the power quality and higher stability dynamics [2-3]. Different pulse-width modulation (PWM) strategies have been developed and substantial research is being carried out in this area to fulfill these requirements; however, there is a need of advanced control methodologies to attain the objectives.

Basically, the control methodologies developed are classified into two types.

- Control of DG in Grid-Connected Operation
- Control of DG in Islanding operation and Parallel connected operation of DGs

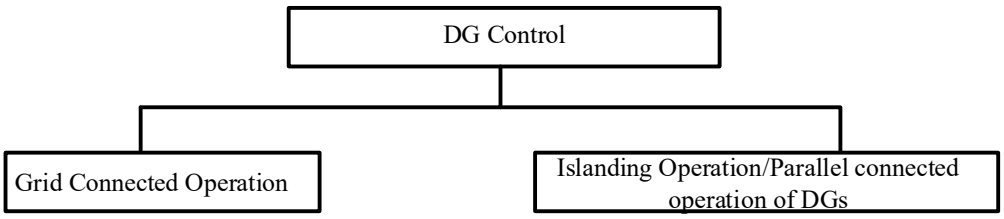

Figure 2.1 Control of DG.

The control of DG mainly depends on the operation of the DG which is presented in Figure 2.1. Based on the method of PWM and the method of control used, the control methodologies are classified as presented in Figure 2.2.

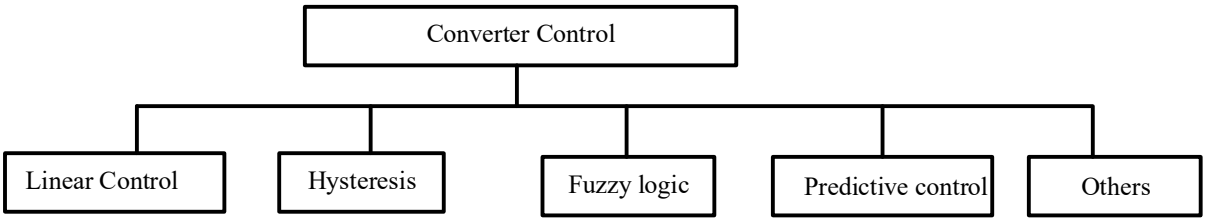

Figure 2.2 Control methodologies of power converters.

2.2 Control of DG in Grid Connected Operation

Several controllers were proposed in literature to operate the DG in grid connected operation. Out of these controllers, the conventional linear controllers with PWM schemes and nonlinear controllers based on hysteresis bands are most widely employed. Due to rapid increase in digital signal processing capability, complex control methodologies like sliding mode control, predictive control and fuzzy logic control were also developed. Due to the increase in PV penetration, the controllers should supply power to the grid based on grid requirements. Therefore, the controllers should have the capability to inject the required amount of active and reactive powers as demanded by the grid. Depending on the amount of power injection, the converters are classified into single phase and three phase as per grid regulations. For large scale power to be injected, the preferred converters are three phase and similarly for the small scale, the converters to be preferred are single phase. Due to the fact that the distributed sources of roof-top residential applications are of 5kW range, the most suitable converters are single phase in nature. DG systems are normally connected with the distribution system feeders along the line; reactive power is needed to support the load voltage, when loads are fed by the grid [4]. Due to the inherent reactive nature of modern domestic loads, continuous reactive power supply from DG side helps in meeting the reactive power demand when operated in islanding mode and reduce the load burden on the feeders when the load is grid connected [5]. With these features, it is evident that a single phase DG should possess the reactive power supplying capability as demanded by the grid.

The interconnection of the single phase DG becomes difficult with the grid because of the inherent pulsating nature of the single phase active and reactive powers at double the signal frequency. The amount of active and reactive powers is regulated by controlling the current synchronized with utility. A proper current control scheme for the generation of real and reactive powers is necessary subject to its stability, speed and accuracy. The basic block diagram of the single/three phase grid connected DG is presented in Figure 2.3. The block

diagram mainly consists of DC source as it is assumed that the voltage from PV source is fixed. In this thesis, developing the control methodologies to grid connected DG is focused. So, the conversion process starts assuming the voltage as a fixed DC source. The combination of a DC source, single/three phase inverter and filter is considered as DG. The filter can be either *L* or *LC* or *LCL* depending on the requirement. The DG can be connected to the grid by the use of transformer which can be a normal utility transformer. For the interface of DG with grid, synchronization process is essential for the interface with grid. The power and current control structure basically develops the reference currents that are used to inject the required amount of active and reactive powers to the grid whereas the PWM generator generates the switching pulses to the inverter. The combination of the current control and PWM generator can be any of the control methodologies shown in Figure 2.2.

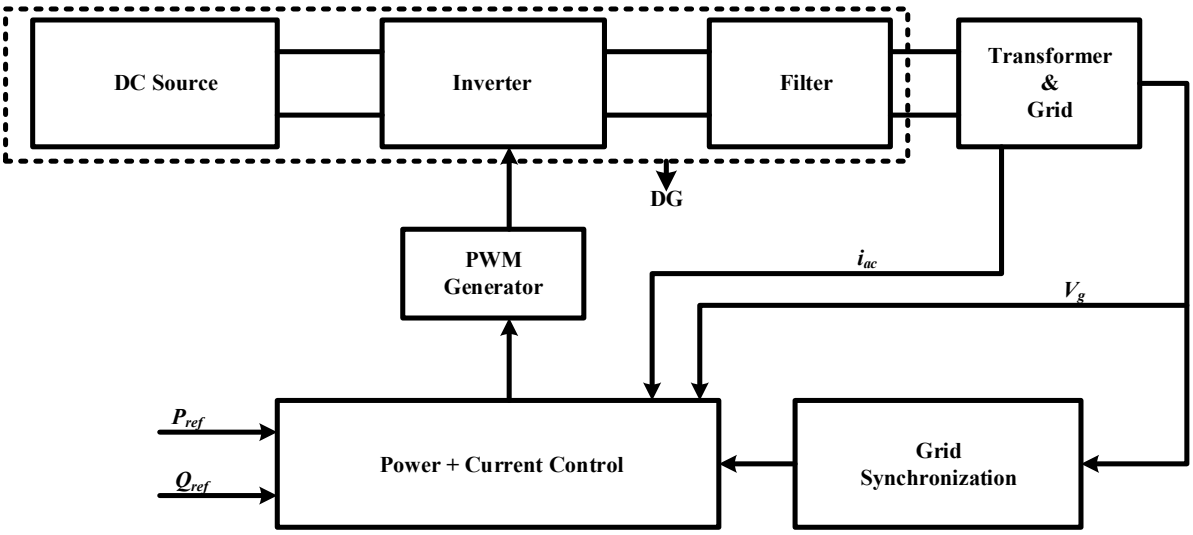

Figure 2.3 Generalized block diagram of single phase/three phase grid connected DG.

2.2.1 Control Methodology with PI Controller

The PI controller is considered to be the best choice but due to its inherent inability to work with the single phase double frequency error signal, its control fails. To overcome this problem, the synchronous sinusoidal currents can be transformed into α, β domain so as to obtain reference and actual current stationary with respect to each other However, the conversion process utilizes the conventional (α-β) [6] transforms which induces the time delays in the circuit thereby affecting the overall time in the system dynamics. The schematic diagram in Figure 2.4 shows a single phase voltage source inverter connected to the grid by an *L* filter. The PLL is used to synchronize the single phase inverter to the grid. Depending upon the current generation scheme adopted, measured grid current (i_{ac}) and voltage (V_g) are fed to

current generation block, to calculate the instantaneous active and reactive powers needed to generate reference current. The generated reference current (i_{ref}) is then transformed into α, β frame to generate currents $i_{ref\alpha}$ and $i_{ref\beta}$ which are compared with transformed grid current $i_{ac\alpha}$ and $i_{ac\beta}$ respectively to generate errors in respective currents as shown in Figure 2.4. The errors developed in reference current and measured grid current, two PI controllers are required, that give rise to reference voltages $V_{ref\alpha}$ and $V_{ref\beta}$ which are then transformed into sinusoidal reference voltage synchronized with the grid. The reference voltage can be compared to triangular wave in order to generate sinusoidal PWM signals. SPWM can be unipolar or bipolar in nature. In order to reduce the filter size, the switching frequency must be kept high. But too high switching frequency can result in higher cost, derating of IGBT and higher switching losses. So a tradeoff must be made to determine the suitable switching frequency of the inverter.

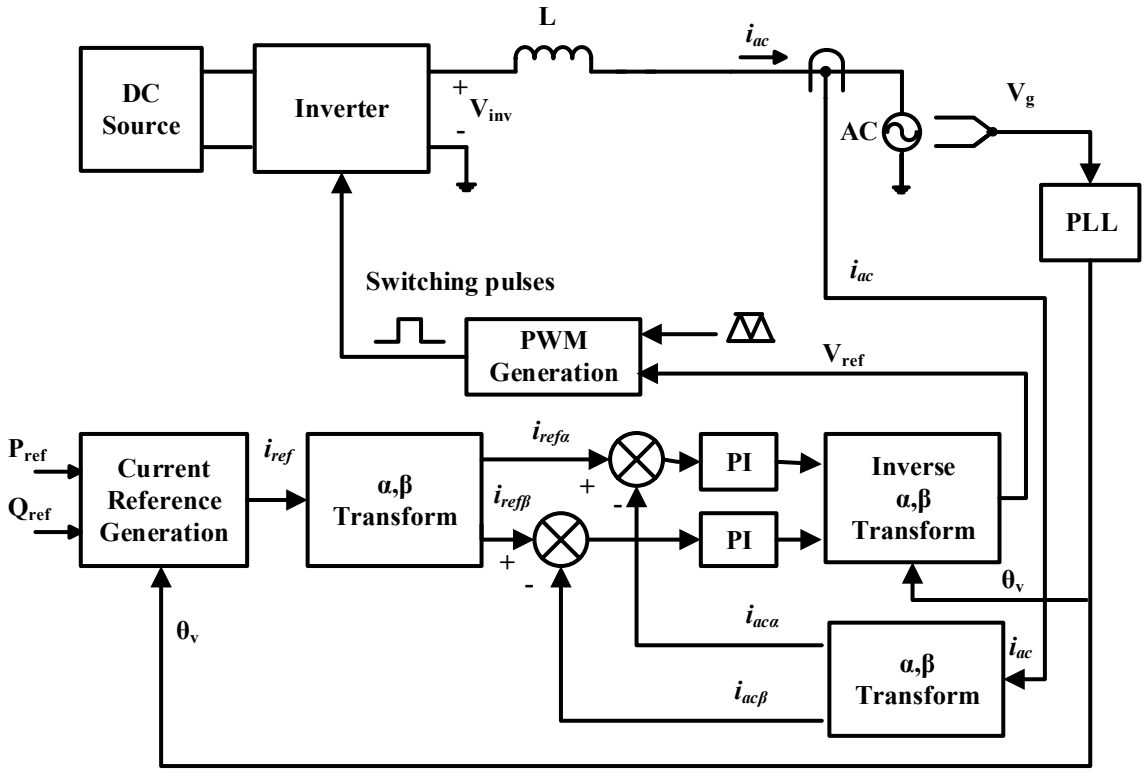

Figure 2.4 Control methodology using PI controller.

2.2.2 Control Methodology with Proportional Resonant (PR) Controller

PR controller offers an inherent advantage of filter to a sinusoidal current reference that can track both the magnitude and phase of reference current with fair accuracy. PR controllers are mainly used as an inner loop for the control of output of grid connected inverters. In PR control methodology, the dc link capacitor needs to be properly designed for the approximation of the output inverter stage as linear and hence dependent on source side dynamics. The PR

controller design procedure is discussed in [7-8]. The control of active and reactive powers with proportional and resonant (PR) controller is shown in Figure 2.5. It can be observed that the current control loop includes only one controller as compared to two controllers as in the case of PI control techniques. It includes the same single phase inverter connected to utility grid by L filter. The current reference generation unit produces a reference current i_{ref} that is compared with the measured grid current i_{ac} in order to produce an error which is applied to the PR controller. The PR controller is tuned at the fundamental grid frequency that results in a distorted sinusoidal reference voltage. Further, it can be provided with some damping. The output of PR controller is fed to the PWM generation unit in order to produce unipolar PWM pulses to the switches.

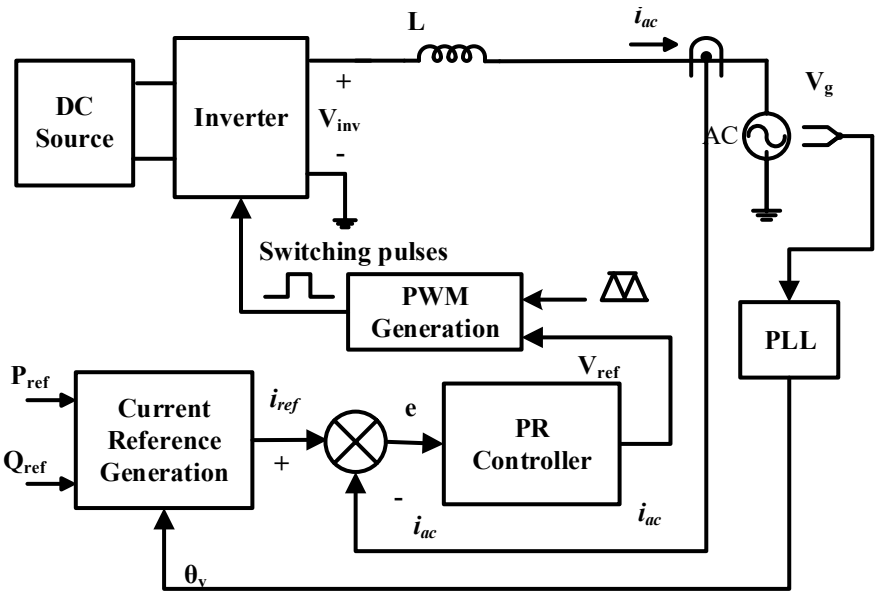

Figure 2.5 Control methodology using PR controller.

2.2.3 Control Methodology with Hysteresis Controller

Hysteresis current control (HCC) method [9-12] is based on the instantaneous comparison between the required reference current and the measured current. For the generation of switching pulses to the DG there will be two bands present i.e., upper hysteresis band (UHB) and lower hysteresis band (LHB). Based on the difference between the reference current and the measured current if the inverter falls in either of the bands, the switching pulses to the DG are generated.

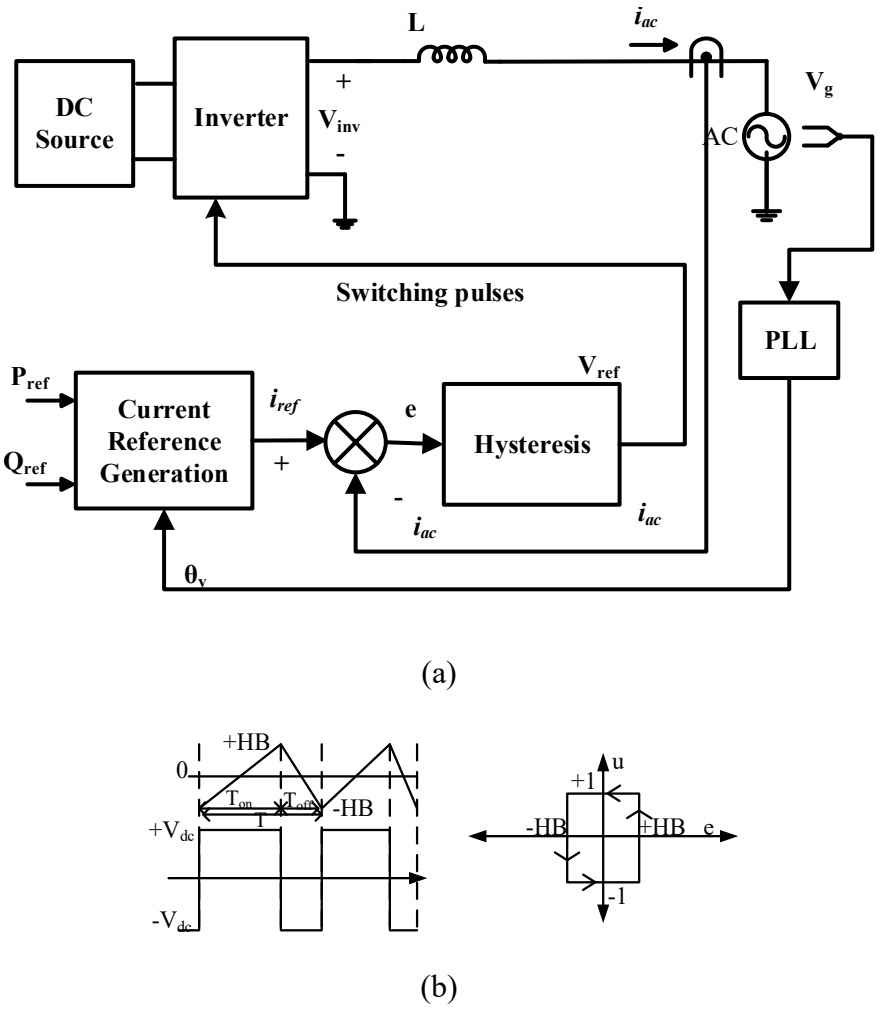

Figure 2.6 (a) Control methodology using hysteresis controller (b) Hysteresis controller inner view.

2.2.4 Nonlinear Controller using Lyapunov's approach

Linear controllers for nonlinear PV systems can provide satisfactory results only over a set of operating points, since the designed system will be linearized at the point of equilibrium. The restrictions in such operating points can be avoided by the design of suitable nonlinear controllers for nonlinear PV systems. The nonlinear controller is very powerful controller due to its ability to make the overall system asymptotically stable. It requires some set of governing laws that makes system to work subjected to variation in reference quantity. A nonlinear controller scheme based on Lyapunov's stability criterion for single phase grid connected inverter is shown in Figure 2.7. The above scheme shows a single phase grid connected inverter with the same components as already explained in the case of PI controller based technique [7-8]. With same reference current generating unit, the reference current i_{ref} and measured current i_{ac} are compared and the difference between i_{ref} and i_{ac} yields error e. To design the controller in order to eliminate error e, a governing law has to be developed as originally done in [13-14] employing Lyapunov's criterion for absolute stability, which can be

deduced from the state equation of grid connected inverter. The switching pulses to the DG are generated by using a PWM modulator with a function of duty ratio *u* generated by the nonlinear controller.

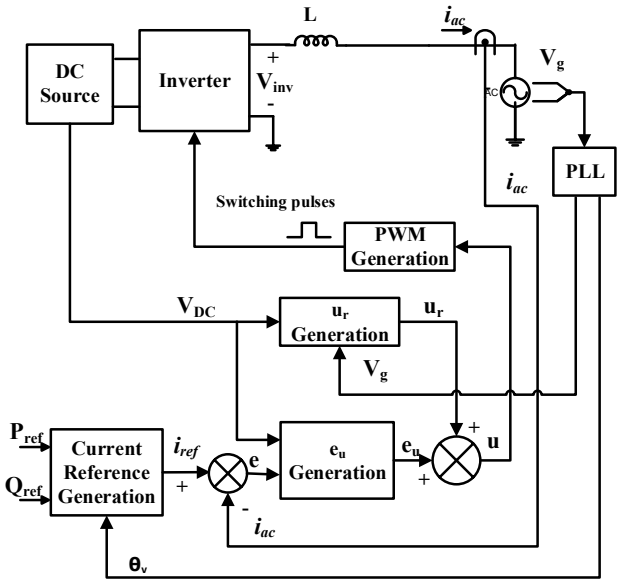

Figure 2.7 Control Methodology using Lyapunov approach.

From Figure 2.7, Applying KVL

$$L\frac{di_{ac}}{dt} = u.V_{dc} - V_g \tag{2.1}$$

Similarly, the state equation for reference u_r can be expressed as:

$$L\frac{di_{ref}}{dt} = u_r.V_{dc} - V_g \tag{2.2}$$

Where u and u_r are the actual and reference duty ratio functions respectively. From the above equations u & u_r can be given by:

$$u = \frac{L\frac{di_{ac}}{dt} + V_g}{V_{dc}}; u_r = \frac{L\frac{di_{ref}}{dt} + V_g}{V_{dc}} \tag{2.3}$$

The desired closed loop behavior from the system error dynamics can be obtained by synthesizing the control signal. Mainly the control signal u consists of two variables namely u_r and e_u designed for the elimination of system error. Now, perturbing the equation (2.1)

$$u = \left(e_u + u_r\right); i_{ac} = (e + i_{ref}) \tag{2.4}$$

$$L\frac{d\left(e + i_{ref}\right)}{dt} = \left(e_u + u_r\right).V_{dc} - V_g \tag{2.5}$$

The error dynamics can be obtained by equation (2.5) comparing with equation (2.2) as:

$$L\frac{de}{dt} = e_u.V_{dc} \tag{2.6}$$

In order to synthesize e_u and prove the stability of the control, a Lyapunov's function F may be defined as:

$$F = \frac{1}{2}Le^2 \tag{2.7}$$

Differentiating above equation along the system trajectories, we get

$$\frac{dF}{dt} = Le\frac{de}{dt} = ee_uV_{dc} \tag{2.8}$$

The closed-loop system will be globally asymptotically stable if the above expression is negative definite, i.e.$dF/\,dt$, if for all values of e different from zero. To make F positive definite function, $dF/\,dt$ must be negative definite. This can be realized for all e_u if:

$$e_u = -K\left(eV_{dc}\right) \tag{2.9}$$

Where K >0 is a control parameter. By tuning the values of K, the controller can be designed to track the reference current. In this way, the non-linear controller for the grid connected inverter using Lyapunov's approach is designed. However, the demerits of the non-linear controller using Lyapunov's approach are system complexity and high variable switching frequency.

2.2.5 Control Methodology with Fuzzy Logic Control

Fuzzy logic control has the feature of adaptability and can achieve robust response to a system even under parameter variations, uncertainties and load disturbance. Figure 2.8 presents the fuzzy logic control applied to single phase grid connected inverter DG.

Compared with the nonlinear control using Lyapunov's approach, the fuzzy logic control adapts to the parameter variations by using the fuzzy logic rules applied to the instantaneous error correction of reference currents and the evaluated grid current to be injected. At every sampling time instant, the error (e) is converted to corresponding fuzzy variable for the optimal switching state evaluation [15-16].

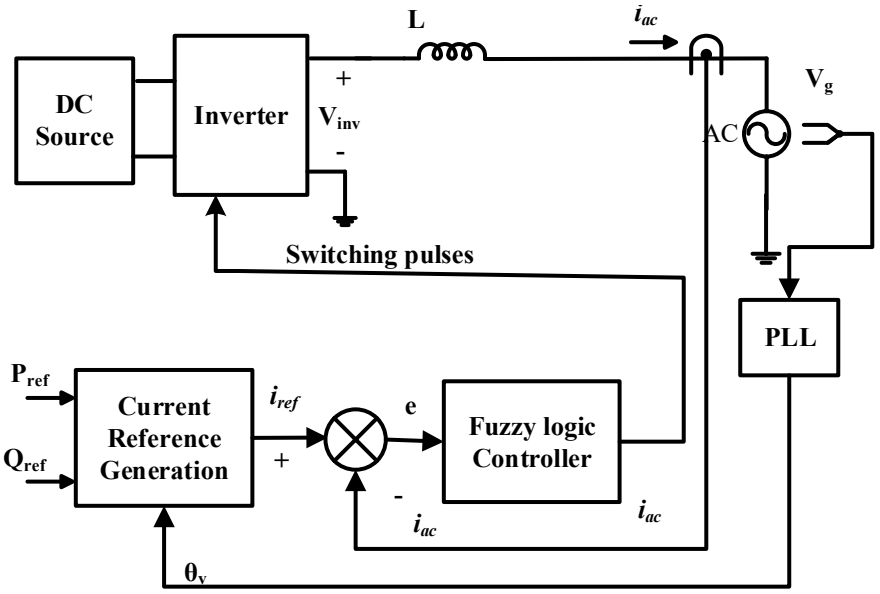

Figure 2.8 Control methodology with Fuzzy logic control.

2.2.6 Control methodology with Sliding Mode Control

Sliding mode control (SMC) when adapted with the feedback linearization eliminates the parameter dependencies and uncertainties. Figure 2.9 shows the sliding mode control methodology adapted to the grid connected DG. The sliding mode control methodology consists of a sliding surface. The demerit of SMC is it leads to chattering (Higher Order SMC is better). Also, if the switching gain is not chosen properly, it may lead to limit cycle. The error between the generated and evaluated reference currents is given to SMC. In order to uphold the transient response and reduce the steady state errors, the sliding surfaces are chosen in the integral forms. Alternatively, these surfaces can also be designed by using back stepping as well as nonlinear damping methods. A Lyapunov's approach is generally followed for obtaining the conditions that will force the evaluated to reference values. [17-19].

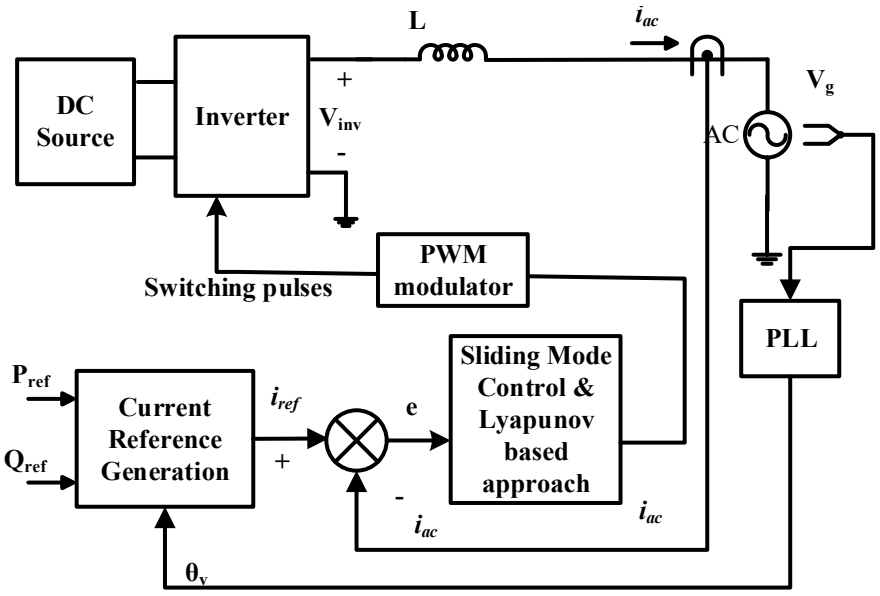

Figure 2.9 Control methodology with Sliding mode control.

2.2.7 Control methodology with Predictive Control

The concept of predictive control gained prominence and is emerging as an attractive solution for the control of power electronic based converters and drives. There are different types of control proposed under predictive control. The most important types of control are dead beat, model predictive control (MPC) and vector based predictive control. The deadbeat control adopts a system model for prediction of the reference voltage at each instant of sampling period. The voltage is mainly generated using any modulator [20-28]. A system model is utilized for predicting the behavior of the system variables over a time horizon and the objective function is developed for the selection of the optimal switching states [29-34]. In case of the vector based predictive control, the system variables are forced to follow the pre-evaluated trajectories where the voltage vectors are used within each sampling period and different direct power control strategies are discussed in [35-44]. A summary of the control methodologies is presented in Table 2.1. Though the literature discussed several problems, the control of powers with single phase is a problem to be addressed and the controller should be PLL free and the grid synchronization algorithm should be simple and effective.

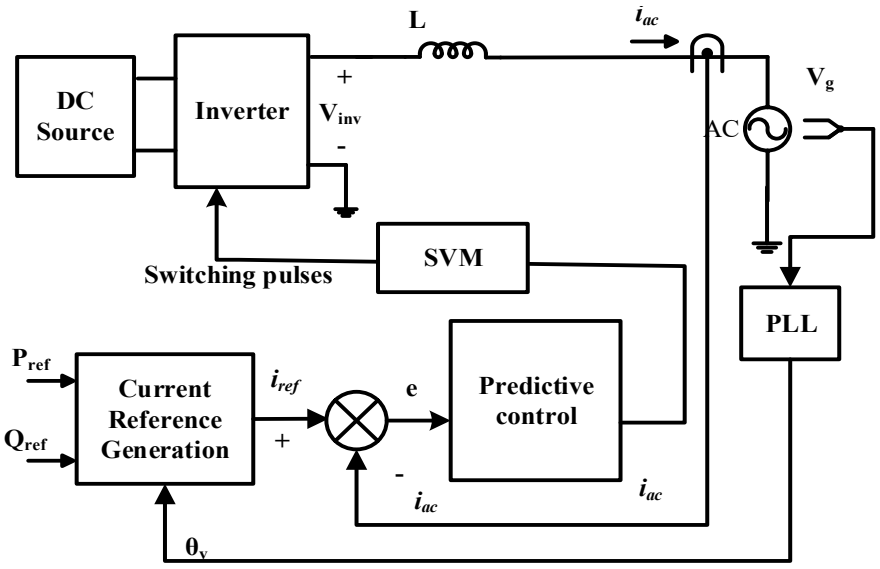

Figure 2.10 Schematic of predictive control.

Table 2.1 Merits and Demerits of control methodologies

Control technique	Merits	Demerits
Classical PI control	• Simple control structure and easy implementation and zero steady-state error in dq frame	• Performance degradation during disturbances and Steady-state error in an unbalance system.
Proportional Resonant (PR)	• Improved performance with a robust inner current controller. • Almost zero steady-state error. • Low computational burden and implementation complexity	• Sensitive to frequency variation. • Difficulty in controlling harmonics. • Require accurate tuning.
Dead beat controller	• Suitable for harmonics control. • Fast transient response with low THD and sampling frequency.	• Require accurate filter model. • Sensitive to network parameters
Hysteresis control	• Easy implementation. • Fast transient response. • Inherent current protection.	• Resonance problems. • Limited to lower power levels. • Error in current tracking and harmonic issues.
Fuzzy control	• Cannot be influenced by parameter variations and operational points. • Suitable for a large-scale non-linear system with easy design.	• Slow control method.
Sliding mode control	• Reliable performance during transients. • Control over THD based on design. • Good disturbance rejection.	• Chattering Phenomenon in discrete implementation. • Difficulty in designing procedure.
Predictive Control	• Suitable for use in non-linear system • Require less switching frequency. • Accurate current control with lower THD and harmonic noise.	• Require extensive calculations.

2.3 Control of DGs in Islanding mode / Parallel Operation

In islanding mode of operation, the control objectives are mainly to maintain the voltage and frequency at nominal values and supply the required amount of power to the loads. For a single DG, it will be easy to control and supply the loads to operate at nominal values of voltage and frequency whereas for multiple DGs there are different aspects that need to be addressed. The main aspect is to maintain the voltage and frequency at nominal values thereby catering the loads with required amount of active and reactive powers. The other important aspect is to minimize the circulating current by ensuring proper load sharing between multiple DGs. The control techniques adapted for the parallel operation of DGs are classified as: i) Droop control schemes and ii) active load sharing methods.

2.3.1 Droop Control Schemes

Droop control is a well-established methodology adapted for the large scale power system consisting of the synchronous generator. Among the droop control [45,46] schemes, the most commonly adapted scheme for parallel operation is voltage and frequency droop. This method mimics the parallel operation of the synchronous generators where there is increase in load, the frequency dips. The required power sharing is achieved by the tight adjustments over the inverter's voltage amplitude as well as frequency. In literature, researchers have proposed different droop control techniques for DG applications, namely modified droop [47-54], adaptive droop [55-60], combined droop [61-63], networked droop [64,65] and hierarchical droop [66-69] control schemes. The droop techniques are summarized in Table 2.2.

2.3.1.1 Conventional Droop

Conventional droop control strategy [45,46] is mainly based on the assumption that a purely inductive line reactance (X_L) is connected from the point of interface of DG to the point of common coupling (PCC). The single line diagram of DG to PCC and its phasor diagram is presented in Figure 2.11 (a) and (b) respectively. The active and reactive powers (P and Q) injected from the DG end to the PCC bus can be represented as:

$$P = \frac{EV}{X}\sin\delta;\ Q = \frac{V\left(E\cos\delta - V\right)}{X} \tag{2.10}$$

In equation (2.10), if the power angle (δ) is assumed to be very small ($sin\delta \approx \delta$ and $cos\delta = 1$), then the active power injected from the DG mainly depends on δ. Since, $cos\delta$

=1, the reactive power injected is dependent on the difference in voltage magnitudes. The conventional droop control schematic presented in a block diagram is shown in Figure 2.12 (a). Figures 2.12 (b) and (c) indicate the droop characteristics of the P-ω and Q-E. The droop characteristic for each inverter can be expressed as:

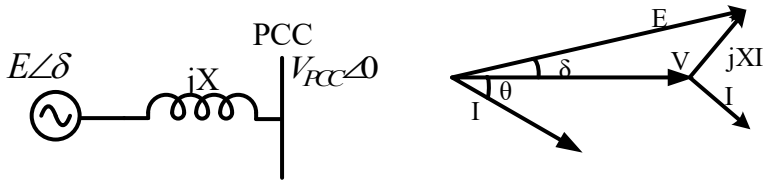

(a) (b)

Figure 2.11 DG connected to PCC bus (a) Equivalent single line diagram (b) Phasor diagram.

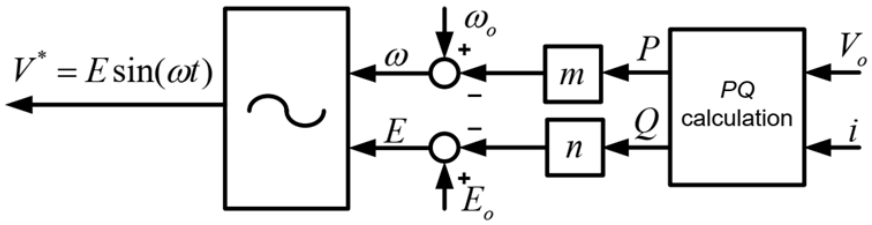

(a)

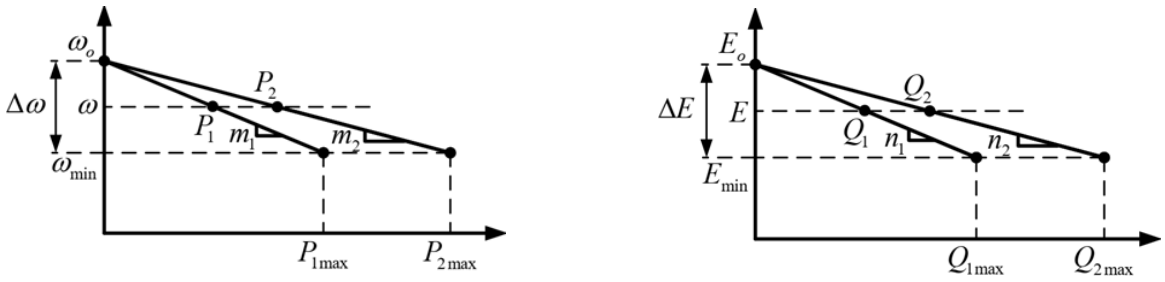

(b) (c)

Figure 2.12 Schematic of Conventional droop (a) block diagram (b) P-ω droop and (c) Q-E droop.

$$\omega_i = \omega_0 - m_i P_i \tag{2.11}$$

$$E_i = E_0 - n_i Q_i \tag{2.12}$$

Where P_i and Q_i are the active real and reactive power outputs, ω_i and ω_0 are the frequency of the inverter and rated nominal frequencies, E_i *and* E_0 are the inverter output voltage and rated nominal voltage and m_i and n_i are the positive droop constants of i^{th} unit.

$$m_i = \frac{\Delta\omega}{P_{i\max}}; n_i = \frac{\Delta E}{Q_{i\max}} \tag{2.13}$$

Where P_{imax} and Q_{imax} are the maximum active power and reactive power supplied by the inverter of i^{th} unit. $\Delta\omega$ and ΔE are the maximum deviations allowed for the frequency and voltage magnitude respectively. From Figure 2.12 (b) and (c), it can be observed that at steady state, when $\omega_1=\omega_2$ and $E_1=E_2$, DG1 is supplying P1 and Q1 while DG2 supplies P2 and Q2 to PCC. Therefore, if the droop coefficients are increased, better power sharing can be accomplished; however, the voltage regulation is observed to be poor. Therefore, while designing the droop coefficient, a tradeoff between voltage and frequency is to be considered. The main advantage of the droop mechanism is that, no communication is required between the parallel connected inverters thereby high modularity and reliability can be achieved. The drawbacks of the conventional droop are:

- Load dependent frequency and amplitude deviations induce poor load voltage regulation.
- Impedance mismatch affects sharing of powers.
- Poor transient performance.

2.3.1.2 Modified Droop

To enhance the dynamic performance of parallel connected DGs, the authors [47] have proposed modified droop scheme by adding an extra transient to the conventional scheme. Though the control scheme achieves good transient response, it has the drawback of choosing a suitable value for the derivative term. In [51], the droop equation is modified and adapted virtual impedance concept adopted to nullify the effect of line impedance. Though the adapted scheme provides good sharing of currents and reduction in circulating current harmonics, the sharing of Q is not discussed. The droop control adapted with a derivative control is presented in [52]. Though the power dynamics is significantly improved, for the simulation as well as experimentation, transient cases are not considered. In [53], the authors have proposed a modified droop equation by the subtraction of the rms voltage of the measured value from the nominal voltage rms. This method helps in compensating the voltage drop due to the load and the droop effect. Q versus rate of change of V with respect to time is discussed along with a voltage restoration function [54]. The voltage regulation is improved along with the reactive

power sharing. The schematic representation of some modified droop techniques is presented in Figure 2.13.

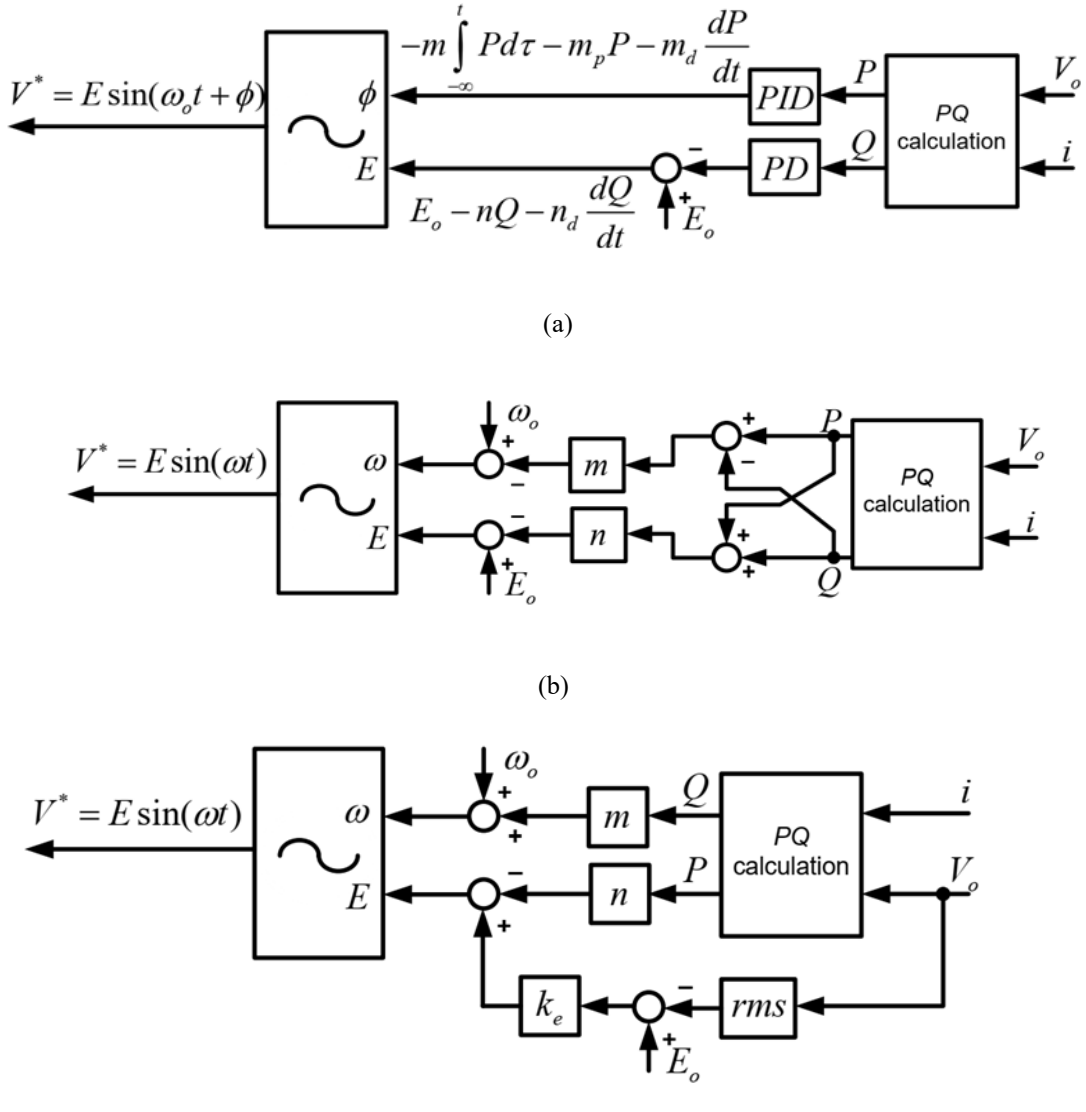

Figure 2.13 Modified droop control: (a) supplemental transient droop [47], (b) complex line impedance droop [51], and (c) robust droop [53].

2.3.1.3 Networked Droop Schemes

Networked droop schemes are employed for sharing the information among multiple DGs connected in parallel to improve the performance of the conventional droop control schemes. In [64], the authors developed an angle droop based methodology with the use of web based low bandwidth communications (shown in Figure 2.14 (a)) for the sharing of power. The power angle information from other DGs is utilized to make the adjustments

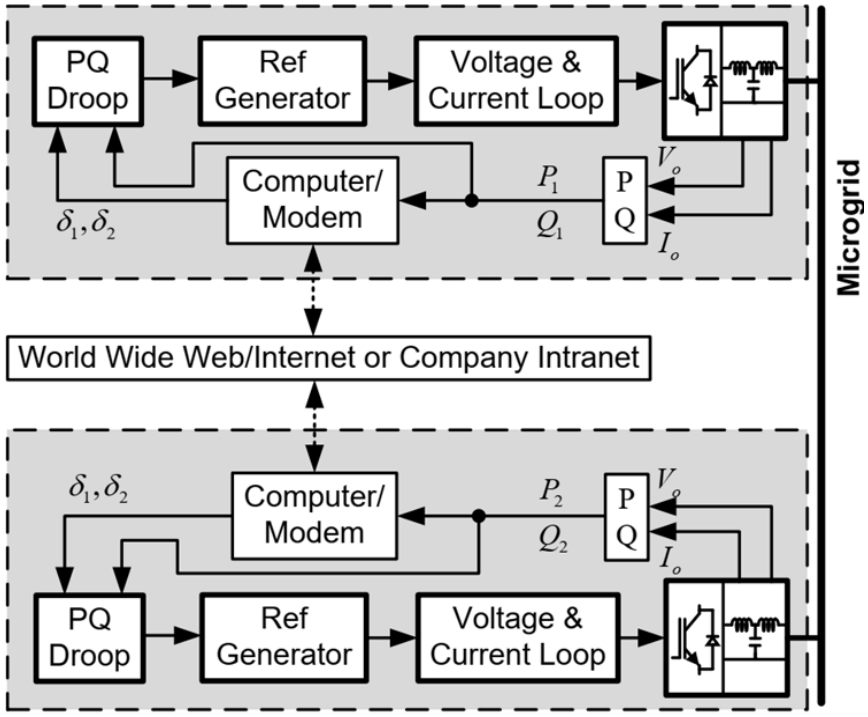

(a)

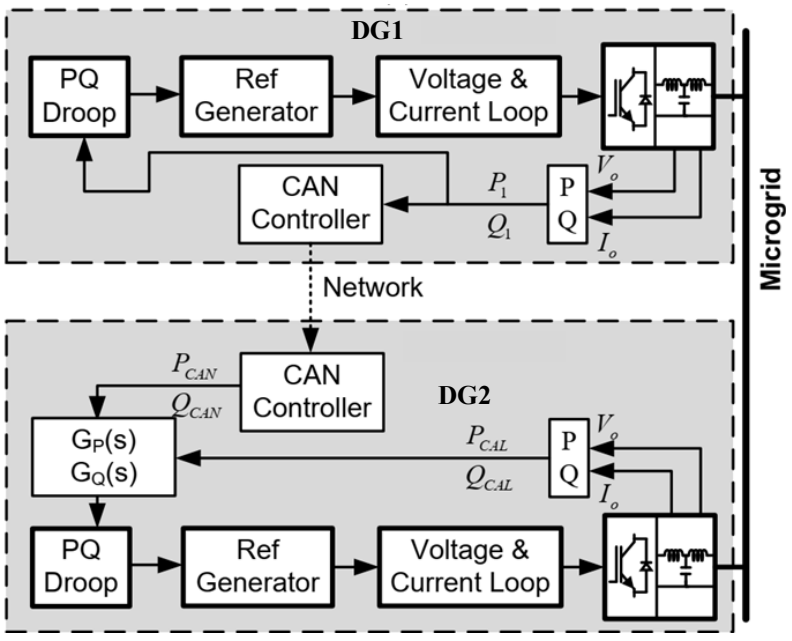

(b)

Figure 2.14 Schematic of Networked droop (a) networked droop with web based application [64] and (b) networked data based with weighted power function[65].

in DGs droop coefficients. Though the method achieves good sharing of P, the sharing of Q is not discussed. In [65], the authors proposed a weighted power function with the data sent through distribution network for improving the sharing of powers. DG1 sends the information

of powers shared to DG2 through a communication area network (CAN). DG2 further processes the information of powers and evaluates the power to be supplied as weighted powers. Though the authors claimed the methodology has superior load sharing but still the plots of P and Q sharing have not been presented as evidence.

2.3.1.4 Hierarchical Droop Scheme

Hierarchical control strategies are proposed by different authors for improving the P and Q sharing and voltage regulation of conventional droop schemes. The hierarchical control scheme consists of three layers. The first layer i.e., primary layer consists of the droop control with regulated voltage and frequency. Secondary and tertiary controls were proposed in [66] to restore the deviations that are caused in voltage and frequency due to the change in loads. The control scheme can be employed on ac as well as dc microgrids providing good power sharing and voltage regulation. Communication is required between each inverter and the secondary controller.

A schematic picture of the controller is presented in Figure 2.15 (a). In [67], the authors proposed another hierarchical control strategy. Primary control consists of droop control and there is a compensation function designed for the deviations in voltage for secondary control. In the tertiary control, there is a synchronization mechanism adapted which ensures the DG's voltage magnitude and phase to be the same as that of the PCC's voltage and phase. The adapted method involves the measurement of the microgrid voltage for secondary and tertiary layers. Though there is good sharing of active power between DGs, the reactive power is not discussed.

A schematic representation of this controller is shown in Figure 2.15 (b). In [68], the secondary control is adapted to compensate the load voltage unbalance as well as harmonics. The proposed method enhances power quality and the load sharing performance is improved. In [69], the authors proposed a two-layer with the primary control consisting of droop and secondary control comprising a mechanism to restore the voltage and frequencies to nominal values. Low bandwidth communication is employed between the DG and load. Though this method presents a good sharing of powers along with voltage amplitude and frequency regulation, the communication delays to the controller are not considered.

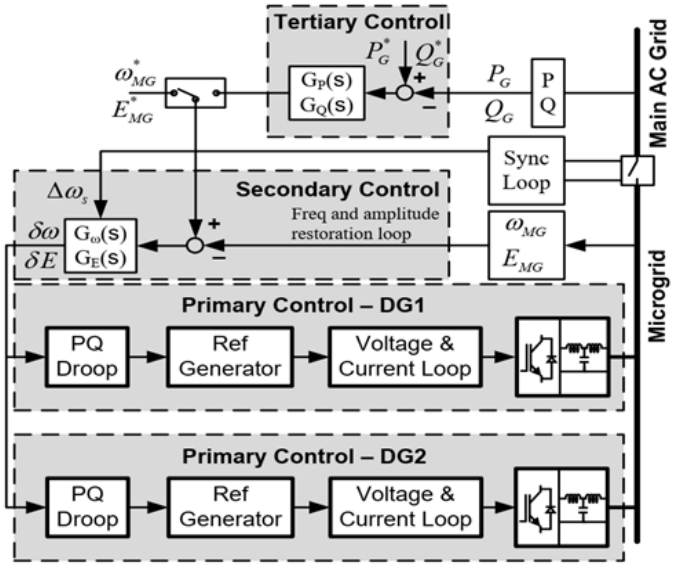

(a)

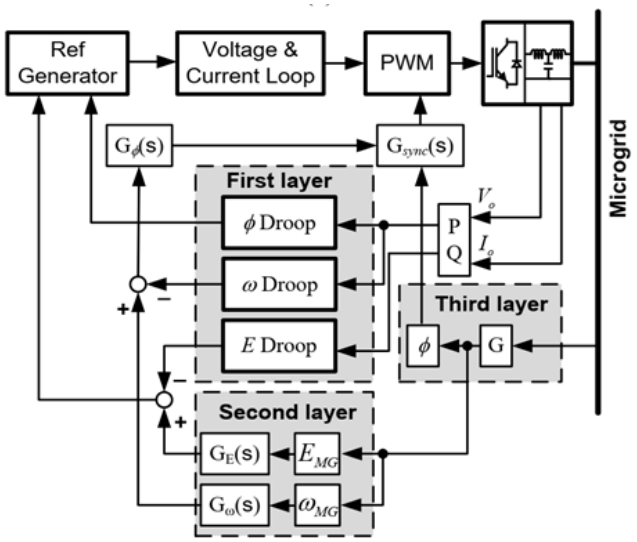

(b)

Figure 2.15 Hierarchical droop (a) hierarchical control presented in [66] and (b) three layer control technique [67].

2.3.2 Active Load Sharing Schemes

In order to achieve current sharing and voltage regulation among multiple DGs connected to microgrid, information should be shared between the DGs. The second mode of control scheme employed for the DGs connected in parallel is named as active load sharing scheme [70]. These schemes employ different methods of sharing information among the multiple DGs. The most cited active load sharing methods in literature are categorized as: master slave control [71-75], circular chain control [76], centralized control [77-78], average current sharing control [79-81], and average power sharing control [82-84].

2.3.2.1 Master Slave Control

In master slave control shown in Figure 2.16, the master inverter plays a vital role in regulating the voltage as well as frequency while the other inverters act as slaves. In other words, it can be seen that the master inverter module serves as a voltage source inverter while the slave inverters act as the current sources. The control scheme achieves very good current sharing and also maintains stability. Some variants are present in the developed control scheme, which depend on the choice of the master module. One fixed module is to be chosen as master unit. Also there is a scheme in which the master unit is arbitrarily selected. In another variant, a module producing the maximum rms current is selected as the master module [70].

In [71], the reference current for slave inverter was source from the power distribution centre while in [72] output current from the master module was used as reference current for the slave module. The authors in [73] proposed master–slave control strategy, which allows plug-and-play integration of DGs thereby ensuring efficient and reliable operation under different operating conditions. However, it has the drawback of communication between different DGs which may result in entire system failure. Another approach of master slave control is proposed in [74]. The results presented show that the control strategy exhibits good dynamic features and is able to reject the power disturbances but the slave and master should be coordinated properly; or else there will be huge spikes in the power and currents resulting in damage to the loads. Another variant of the master control strategy is current limitation control using a hybrid PLL [75]. In this technique, there is a master module that controls the load voltage and the slave modules only supply and share the load current with the master module. A slave module receives a reference current command from the previous module which has limited amplitude, resulting in non-sinusoidal output current from each inverter. The technical difficulty and risk of master–slave control is relatively low compared to the other control. The failure of the master controller results in the damage to the whole MG.

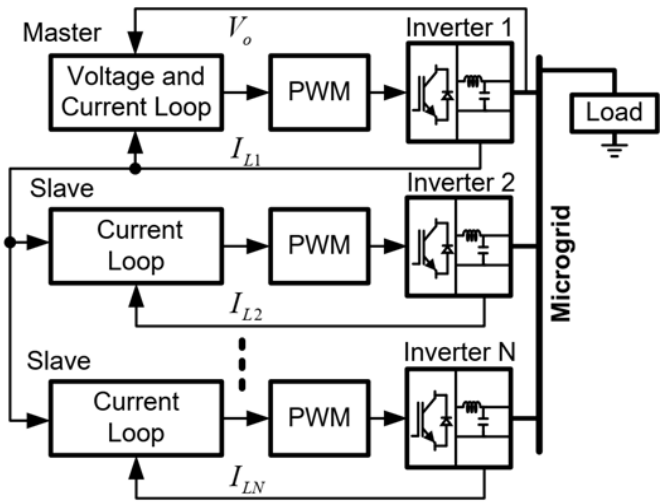

Figure 2.16 Schematic of Master Slave Control.

2.3.2.2 Circular Chain Control (3C)

The 3C schematic is presented in Figure 2.17 [76]. Different inverter modules track the current of the consecutive inverter modules for achieving equal distribution of current. A circular chain connection is formed by forming the closed loop by the track of the last inverter module to the first. Based on the common reference voltage, the inverter modules regulate their own voltage. However, if a problem occurs i.e., any module gets damaged or failed inverter in the loop there will be an effect on voltage regulation. In case the problem is not detected and the inverter modules are not isolated, the performance of the entire system gets affected and may result in the entire system failure. Therefore, two communication lines are utilized for achieving the bidirectional data and increasing the reliability.

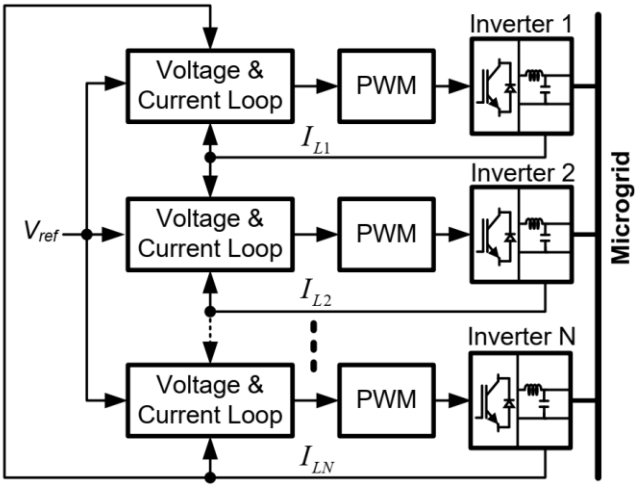

Figure 2.17 Schematic of 3C methodology.

2.3.2.3 Centralized Control

A schematic representation of centralized control scheme [77-78] is shown in Figure 2.18. A central controller is present which regulates the load voltage in an outer loop and sends the reference value of current to each inverter. The reference current to each inverter is determined by the addition of output voltage and the average load current i.e., the total load current divided by the total number of inverter modules. The controller present in each inverter module evaluates the difference between the reference current and the output current. Though this control scheme provides good current sharing, it lacks redundancy and reliability. The measure of load current makes the control strategy inappropriate for a system with distributed loads.

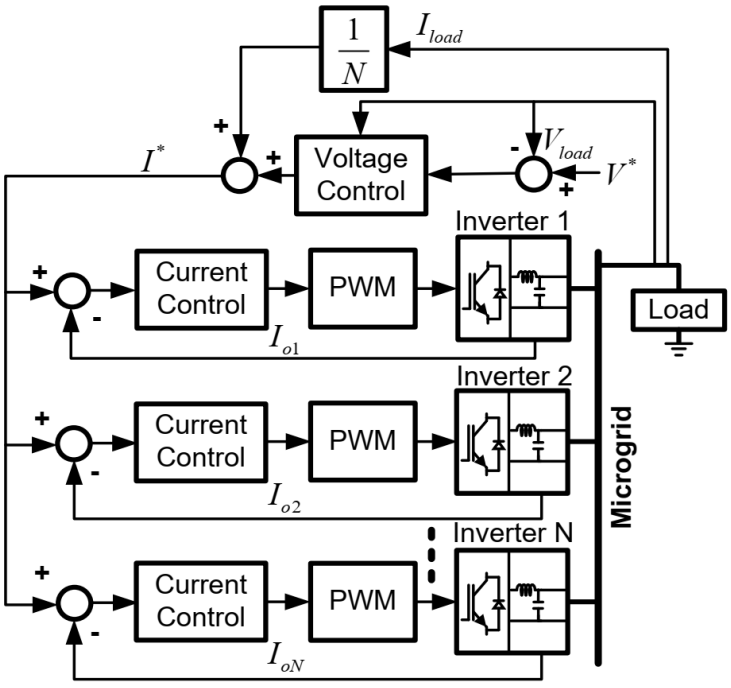

Figure 2.18 Centralized Control scheme.

2.3.2.4 Average Current Sharing Control

The average current sharing scheme utilizes the concept of the parallel connected dc/dc converters to DC microgrid. A common sharing bus will be present which indicates the system average current information. The average current to be dispatched is evaluated by connecting each current sensor of the inverter through a resistor to current bus. The central controller can also be utilized to evaluate the average current values before transmitting the data to each inverter module. This developed value of average current will be used as a reference current and the controller present in each inverter evaluates the difference between the reference and

average current and is implemented in the inner scheme of control. In this scheme, all the inverters present in the microgrid participate in the voltage, frequency and current regulation. The control schematic is shown in Figure 2.19. A current sharing bus with an instantaneous output voltage control with current deviation and cancellation control of such current deviation is presented [79]. A robust design of voltage and current controllers is presented [80] for improving the current sharing and voltage regulation. An average current sharing scheme by using GPS is presented in [81] using three shared buses (inverter reference, sensed load current, and feedback voltage) connecting all the parallel connected modules. The control scheme yields a fast dynamic response but the addition of an extra communication node makes it complex.

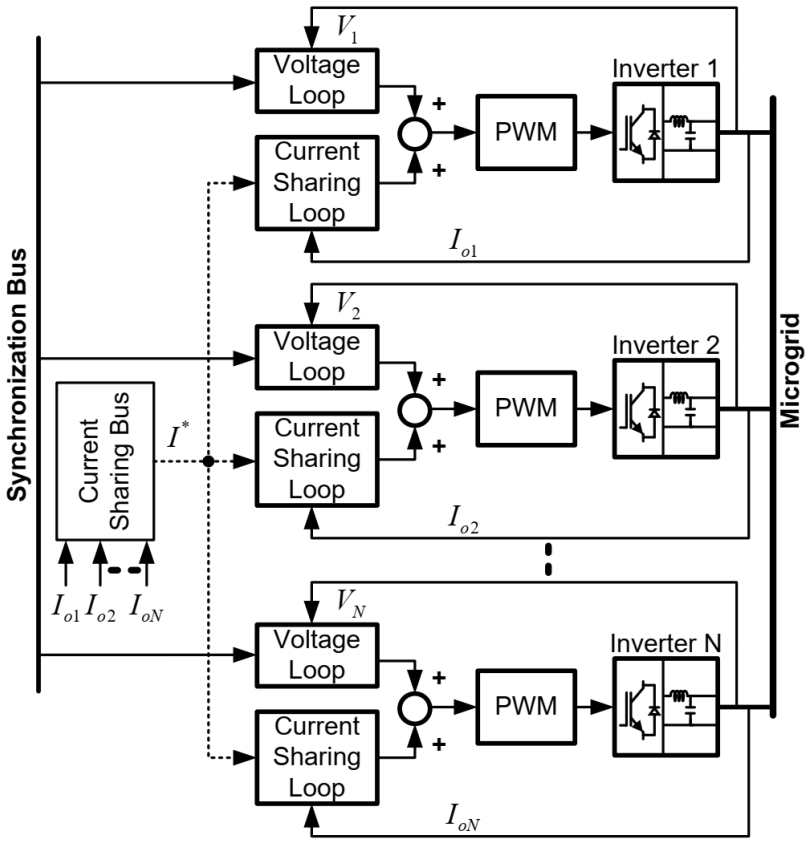

Figure 2.19 Average Current Sharing methodology.

2.3.2.5 Average Power Sharing Control

A technique similar to current sharing is developed, while the power [82-84] is averaged. As a result of this, only low bandwidth will be enough in comparison with the high bandwidth signal required for average current sharing. Every inverter controls P and Q sharing by using voltage regulator and phase locked loop. The scheme adopted achieves good power

sharing but is only suitable for a balanced system. A summary of the control techniques for parallel connected DGs is presented in Table 2.2.

Table 2.2 Control techniques for parallel connected DGs

Control techniques	**Advantages**	**Disadvantages**
Conventional droop	• No communication • High modularity • Good reliability	• Load dependent frequency and amplitude deviations that induce poor performance in load voltage regulation • Impedance mismatch will affect P and Q sharing Only based on predominantly inductive line impedance. • Poor transient and hot swap performance
Modified droop	• Fast transient response	• Difficult to select the suitable coefficients for derivative term that ensures stable operation
Combined droop	• Improved load sharing capability. • Compensation of voltage unbalance. • Compensation effort is properly shared between DGs.	• Requires communication and system is complex.
Networked droop	• Good active power sharing.	• Requires communication • Performance under impedance mismatch is unknown • Q sharing cannot be analysed properly.
Hierarchical droop	• Good active power sharing. • Improved voltage amplitude and frequency regulation.	• Q sharing performance is unknown. • Requires communication.
Master Slave control	• Current is shared based on rating.	• Total system failure may occur if master fails.
Circular Chain control	• Good current sharing performance.	• Total system failure may occur if communication fails.
Centralized control	• Good current sharing performance.	• Lacks redundancy and reliability.
Average Current Sharing	• Excellent current sharing and fast dynamic response.	• Communication signal for current, Voltage and frequency.
Average Power Sharing Control	• Low bandwidth signal compared to current sharing.	• Suitable for only balanced system.

2.4 Motivation

Based on the literature review, following inferences were made for the control of grid and off grid connected inverters.

i. Most of the control methodologies discussed in the literature on grid connected inverters require current reference generation schemes for the control of active and reactive powers as demanded by the load dispatch center. A current reference generation scheme in combination with the control methodology which is simple and free of the system parameters should be proposed.
ii. Most of the control methodologies presented in literature, use PLL for the grid synchronization process and a multi loop approach for the grid and off grid connected operation which is not economically viable and further the control is complex. A PLL free synchronization mechanism should be proposed and the controller should be a single loop avoiding the multi loop methodology.
iii. In case of the parallel connected operation of DGs, the literature presented various schemes which have their own merits and demerits. For schemes already available, the control strategies proposed are either complex or suitable for specific balanced systems. A control strategy should be proposed considering the objective of low band width communication and it should be applicable for all systems i.e., balanced or unbalanced systems.
iv. The solar PV control strategies proposed in the literature do not consider the rotating interface. A strategy should be proposed which should be applicable for all kinds of interfaces.

2.5 Objectives

The objectives of the research work presented in the thesis are as follows:

i. The interconnection of the single phase DG becomes difficult with the grid because of the inherent pulsating nature of the active and reactive powers at double the signal frequency. So for this, three current reference generation schemes are to be developed and their suitability for the application to grid connected inverters is investigated using MPC based SVM as well as ASDM method. However, the proposed scheme consists

of two loops i.e., outer loop for current reference generation and inner loop for the development of modulation index to generate sinusoidal output current.

ii. A model predictive controller is proposed for single phase distributed generator with seamless transition between grid and off-grid modes of operation. In addition, a simple synchronization mechanism is developed to achieve the smooth transition between the grid and off-grid modes, thereby avoiding the complex multi-loop controls. The voltage vectors, hence the switching pulses are generated by using space vector modulation technique based on the minimization of the cost function of the predictive model. The two cost functions considered are instantaneous power error and instantaneous voltage error, respectively, for the grid and islanding operation of the single phase generator. The performance of the developed controller for feeding the set-point powers in grid connected mode and serving the load at nominal voltage and frequency in off-grid mode is verified using simulations. The simulation results are experimentally validated on a prototype. This can be further extended to the three phase systems as well. Though the proposed system performs very good for the control in grid and off grid connected operation, the system had drawbacks when multiple DGs are operated in islanding operation.

iii. To overcome this drawback, a control strategy is proposed for the coordinated control operation of multiple distributed generators. A simple control strategy for primary as well as secondary control is proposed in this thesis. The primary control consists of droop control which is analogous to the synchronous generator control. The primary control decides the power to be shared between two distributed generators and regulates the voltage and frequency to nominal values at the point of common coupling, where loads are present. The secondary control strategy allows the distributed generators to restore the frequency and voltage to the nominal values, if the primary control fails. The developed controller possesses the features of adaptability for smart grid interconnection. The performance of the proposed control strategy is validated through numerical simulations and real-time implementation. However, the control strategy needs to be further validated dynamically.

iv. To validate the dynamic performance of the controller, a diesel generator is considered along with the distributed generators. The proposed control strategy is free of conventional d-q transformations, which eliminates the filters and increases the speed of

controller. The performance of proposed control strategies is validated through different case studies of simulation and hardware-in-loop using OPAL-RT.

2.6 Summary

In this chapter, the first part consists of a brief overview of the DG. The second part of the chapter consists of the different control methodologies adopted for the control of grid connected DGs and their merits and demerits. The third part of the chapter reviewed different control schemes adopted for the control of parallel connected multiple DGs. All the presented control schemes can be adopted for both single phase as well as three phase systems. Their characteristics, applications, advantages and disadvantages are briefly discussed.

From the literature review on grid connected inverters, it can be seen that the interconnection of the single phase DG becomes difficult with the grid because of the inherent pulsating nature of the active and reactive powers at double the signal frequency. So in the chapter 3, three current reference generation schemes are developed and their suitability for the application to grid connected inverters is investigated using MPC based SVM as well as ASDM. However, the developed scheme consists of two loops i.e., outer loop for current reference generation and inner loop for the development of modulation index to generate sinusoidal output current.

Chapter 3

Current Reference Schemes for Control of Single Phase Inverter using Model Predictive Control and Asynchronous Sigma Delta Modulation

Chapter 3
Current Reference Schemes for Control of Single Phase Inverter using Model Predictive Control and Asynchronous Sigma Delta Modulation

3.1 Introduction

This chapter investigates three different current reference generation schemes developed for the control of single phase inverter based distributed generator with i) model predictive control based space vector modulation and ii) asynchronous sigma delta modulation (ASDM) schemes. The current references for the developed controller has been deduced from three different schemes, known as scalar, modified scalar and simplified active and reactive power control. A clear analysis of the three different current reference generation schemes along with the ASDM as well as the model predictive control is presented.

Simulations were performed in Matlab / Simulink environment. The performance of the developed controllers with considered current reference generation schemes are examined for different real and reactive power feedings from the single phase generator to the grid.

3.2 Modeling of Inverter with ASDM

The block diagram of the single phase grid connected inverter along with ASDM switching scheme is shown in Figure 3.1. The DG is interfaced to the grid through inverter after filtering out the harmonics as depicted in Figure 3.1. The P_{ref} and Q_{ref} are the two set point powers for which the reference current i_{ref} is generated by the respective current generation techniques. The i_{ref} is compared with the actual current fed by the inverter, i_{ac} to generate the current error, i_{err}. This i_{err} is fed to the first order current controller to generate reference voltage V_{ref}. The basic operation of ASDM to modulate the current and produce PWM signals for the inverter switches is depicted in Figure 3.2. The ASDM consists of an integrator with error amplifier and a band comparator. The error signal, V_{err}, is the difference (Delta) between the input reference V_{ref} and the output pulsating voltage train. The integrated signal V_{int} is the sum (Sigma) of error signal which will be processed by the comparator in order to generate the output pulsating voltage train for inverter switches. To understand the operation of ASDM, the reference signal is assumed to be constant during a switching period as the reference voltage frequency is very small as compared to the switching frequency. The waveforms of V_{ref} , V_{err} and train of ASDM pulses can be shown in Figure. 3.3 for a particular frame of time.

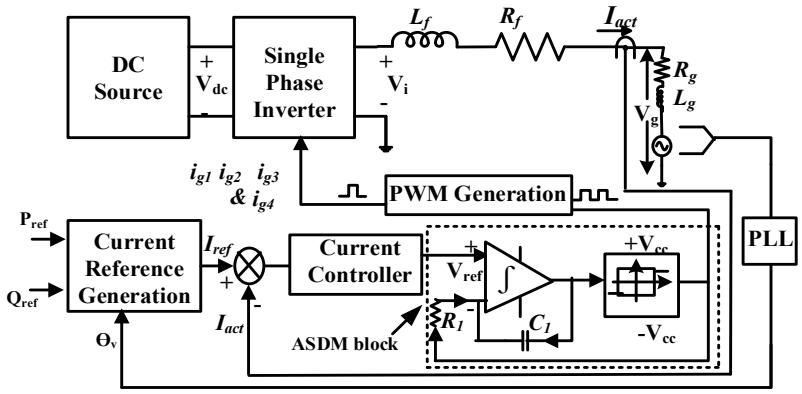

Figure 3.1 Block diagram of single phase grid connected inverter with ASDM.

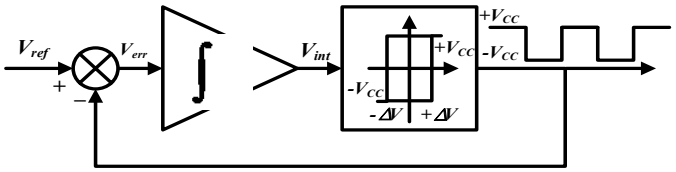

Figure 3.2 Block Diagram of ASDM.

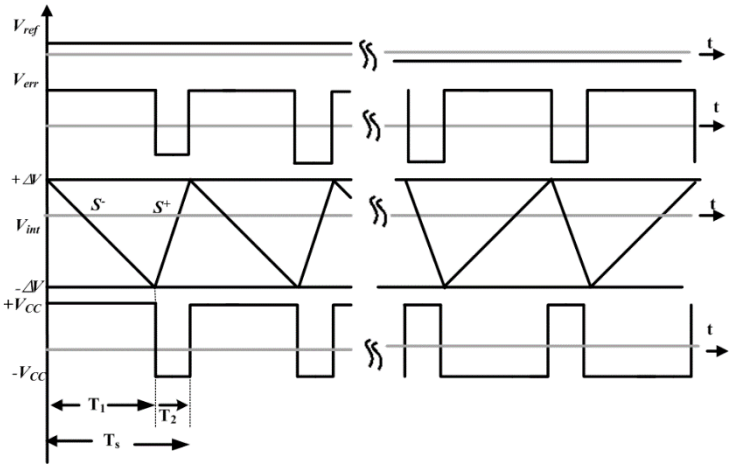

Figure 3.3 Switching pulse generation in ASDM.

At the end of the time period T_1 and just before the starting of the time period T_2, it can be seen that V_{err} is a negative constant because of which the integral signal V_{int} will decrease with a negative slope, S_{int}^-. The S_{int}^- and T_1 can be expressed as in (3.1).

$$\left.\begin{aligned} S_{int}^{-} &= \frac{V_{ref} - V_{cc}}{\tau} \\ T_1 &= \frac{-2\Delta V}{S_{int}^{-}} \end{aligned}\right\} \tag{3.1}$$

where $\tau = R_1C_1$ is the time constant of the integrator. As V_{int} reaches the lower limit of hysteresis band $-\Delta V$, the output of ASDM is changed from $+V_{cc}$ to $-V_{cc}$ changing the V_{err} from negative to positive value. With this, the slope will be changed from negative to positive. The slope S_{in}^{+} and T_2 can be expressed as (3.2)

$$\left.\begin{aligned} S_{int}^{+} &= \frac{V_{ref} + V_{cc}}{\tau} \\ T_2 &= \frac{2\Delta V}{S_{int}^{+}} \end{aligned}\right\} \tag{3.2}$$

As soon as the V_{int} with positive slope reaches the upper limit of hysteresis band $+\Delta V$ the output of ASDM will be changed from $-V_{cc}$ to $+V_{cc}$, thus completing one switching cycle. The duty ratio and switching frequency can be expressed in (3.3).

$$\left.\begin{aligned} d &= \frac{1}{2} + \frac{V_{ref}}{2V_{cc}} \\ f_s &= \frac{(V_{cc})^2 - (V_{ref})^2}{4R_1C_1\Delta V V_{cc}} \end{aligned}\right\} \tag{3.3}$$

where V_{cc} is the DC train voltage of the op-amps, ΔV is the hysteresis voltage window of the band-band comparator, and τ is the time constant of the integrator. It can be observed that the duty ratio d of the PWM signal is linearly proportional to the reference signal and is irrelevant to circuit parameters, such as ΔV or τ. It implies that the ASDM can achieve very good controllability. Secondly, ASDM operates at various switching frequencies which can spread switching noise over a wider frequency spectrum. It has the merit of low electromagnetic interference.

3.3 Modeling of Inverter using MPC based SVM

The block diagram of single phase DG connected to grid using MPC based SVM and the block diagram of MPC based SVM are presented in Figures 3.4 and 3.5 respectively.

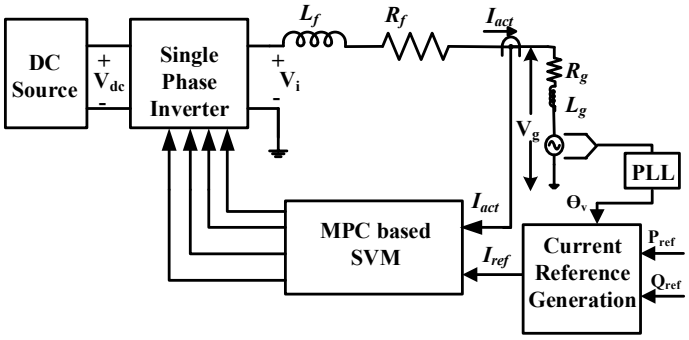

Figure 3.4 Single phase grid connected inverter with MPC based SVM.

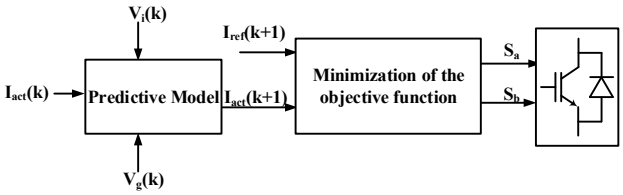

Figure 3.5 Block diagram of MPC based SVM.

$$V_i = I_{act}R_f + L_f \frac{dI_{act}}{dt} + V_g \tag{3.4}$$

After simplification, (3.4) can be written as

$$\frac{dI_{act}}{dt} = \frac{V_i - V_g - I_{act}R_f}{L_f} \tag{3.5}$$

On discretizing (3.5),

$$\frac{I_{act}\,(k+1) - I_{act}\,(k)}{T_s} = \frac{V_i(k) - V_g(k) - I_{act}\,(k)R_f}{L_f} \tag{3.6}$$

$$I_{act}\,(k+1) - I_{act}\,(k) = \left(\frac{V_i(k) - V_g(k) - I_{act}\,(k)R_f}{L_f}\right)T_s \tag{3.7}$$

Simplifying and rearranging (3.7),

$$I_{act}\,(k+1) = \left(V_i\,(k) - V_g\,(k)\right)\frac{T_s}{L_f} + I_{act}\,(k)(1 - R_f\frac{T_s}{L_f}) \tag{3.8}$$

where I_{act} (k+1) is the predicted current for the next sampling instant. After the evaluation of the current for the next state is done, this current is compared with the generated reference current to evaluate the objective function as defined in (3.9).

$$g_i = \left| I_{act}(k+1) - I_{ref}(k+1) \right| \tag{3.9}$$

Where $I_{ref}(k+1)$ is the reference current generated by using the current reference generation schemes developed in section 3.4 for the next sampling instant. As the system under study is a single-phase system, the inverter has four possible switching states/vectors. Out of four switching states, two are null states and for the remaining two states, the minimum of objective function is evaluated as in (3.10). The next switching state is selected such that the state should result in minimum value of the objective function. Based on the selected switching state, the MPC based SVM generates switching pulses as depicted in Figure 3.5.

$$g = \min\ (g_i);\ \ \mathrm{i} = 1, 2. \tag{3.10}$$

3.4 Current Reference Generation Schemes

Three different current reference generation schemes, namely, scalar control, modified scalar control and simplified active and reactive power control are considered for the validation of ASDM and MPC based SVM. A brief discussion of these schemes is given as below:

3.4.1 Scalar Current Reference Generation Scheme

The simplest among the three current reference generation schemes developed is scalar control, as it involves the direct conversion of the power reference into current reference based on the instantaneous active and reactive power theory. The reference active and reactive powers can be written in complex form as shown in (3.11). The powers are converted into polar form as shown in (3.12) and (3.13). The magnitude value is divided by the peak value of the grid voltage obtained from PLL to obtain the peak value of current reference as in (3.14). Figure 3.6 depicts the principle of scalar current reference generation scheme. Though the current reference generation scheme is simple and converts the power references quickly, it can result in non-zero steady state error due to the absence of error correction mechanism.

$$S_{ref} = P_{ref} + jQ_{ref} \tag{3.11}$$

$$\phi = \tan^{-1}\left(\frac{Q_{ref}}{P_{ref}}\right) \tag{3.12}$$

$$S_{ref} = \frac{V_m \, \mathrm{I}_{\mathrm{m}ref}}{2} = \sqrt{\left(P_{ref}{}^2 + Q_{ref}{}^2\right)} \tag{3.13}$$

$$\mathrm{I}_{mref} = 2\sqrt{\left(\left(\frac{P_{ref}}{V_m}\right)^2 + \left(\frac{Q_{ref}}{V_m}\right)^2\right)} \tag{3.14}$$

In Figure 3.6, $X = \frac{P_{ref}}{V_m}$; $Y = \frac{Q_{ref}}{V_m}$, V_m is the peak value of grid voltage

The limitation of scalar current reference generation scheme is that it may result in nonzero steady state error which can be addressed by modifying the reference generation scheme as shown in Figure 3.7.

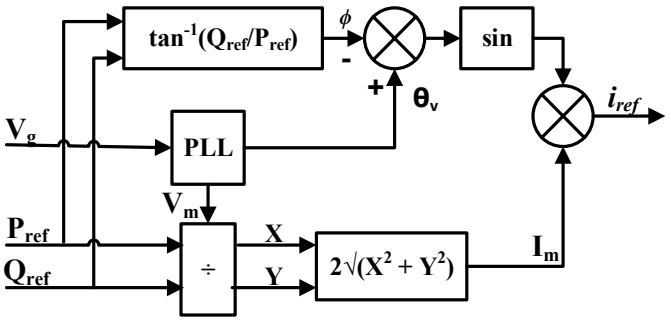

Figure 3.6 Scalar current reference scheme.

3.4.2 Modified scalar current reference generation scheme

The errors obtained after the comparison of the reference powers with the delivered powers will be processed by PI controllers to ensure the steady state errors be reduced to zero as shown in Figure 3.7. However, as this scheme involves PI controllers for reference current generation, dynamics of the system is influenced by the gains of the controllers. The scalar scheme is compared with modified scalar scheme reveals that the response induces delay, resulting from non-zero integral value of the PI controller. Hence, the current dynamics will be slower than the scalar current reference scheme. Moreover, the PI controller need to be tuned carefully to meet the control objectives, like overshoots, rise time and settling time, etc.

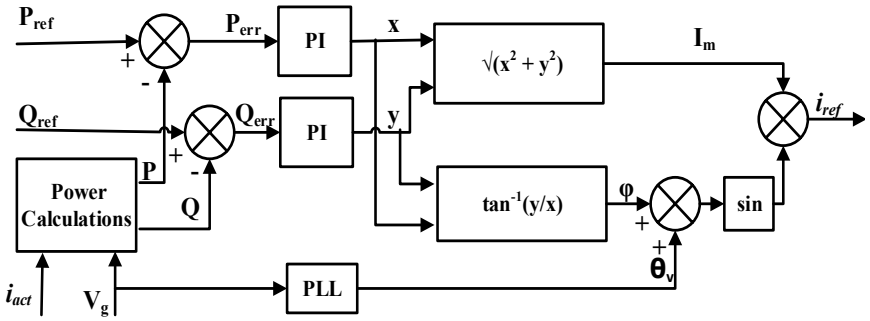

Figure 3.7 Modified scalar reference current generation scheme.

3.4.3 SRPC current reference generation scheme

In this scheme, the errors obtained from the comparison of the actual and reference powers are modulated as the reference current with the help of two hysteresis controllers. The hysteresis controllers are further used to deduce the reference current magnitude and the phase angle shown in Figure 3.8. As (*X/R)* ratio is low for the distribution systems, active power can be regulated by controlling the magnitude of injected current while reactive power can be regulated by controlling the phase angle of injected current. The current and phase angle references are generated as in (3.15) and (3.16), in which the subscript indices *U* and *L* denote the upper and lower bounds of the hysteresis band.

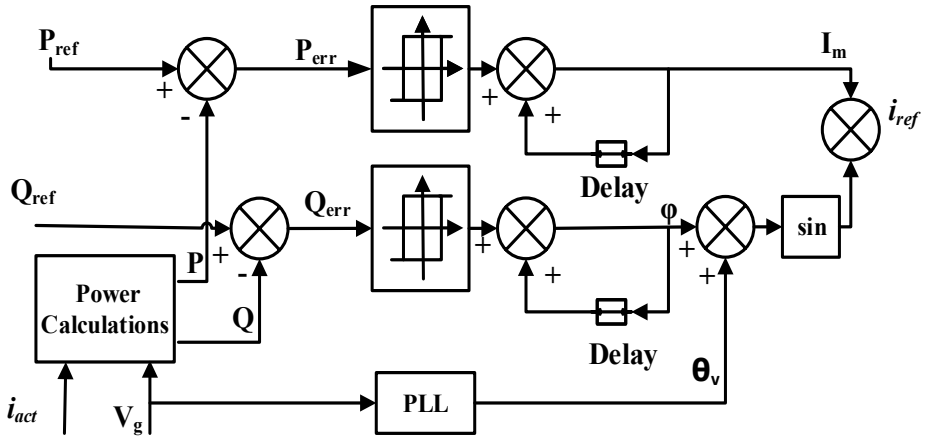

Figure 3.8 SRPC reference generation scheme for current.

$$\left.\begin{aligned} &if\ P_{err} > \Delta P_U\ then\ n = 1; \\ &else\ if\ P_{err} < \Delta P_L\ then\ n = -1; \\ &else\ n = 0; \\ &I_m(k+1) = I_m(k) + n\Delta I \end{aligned}\right\} \tag{3.15}$$

$$\left.\begin{array}{l} if\ Q_{err} > \Delta Q_U\ then\ \mathrm{n} = 1; \\ else\ if\ Q_{err} < \Delta Q_L\ then\ \mathrm{n} = -1; \\ else\ \mathrm{n} = 0; \\ \theta(k+1) = \theta(k) + \mathrm{n}\Delta\theta \end{array}\right\} \quad (3.16)$$

As this method involves iterative changes in the phase angle and current magnitude, I_m and θ are modulated such that the steady state error is made zero. However, one should take care while choosing the magnitudes of perturbs, ΔI and $\Delta\theta$, otherwise sustained oscillations in the powers will degrade the performance of the DG. The system parameters are presented in Table 3.1.

Table 3.1 System parameters

Parameters	Values
V_{dc}	400 V
V_g	230 V (RMS)
f_g	50 Hz
R_f	0.2 Ω
L_f	5 mH
K_p	0.1 Ω
K_I	50
R_g	0.1
L_g	0.318 mH
V_{cc}	15 V
T_s	20 μs

3.5 Results and Discussion

The performances of ASDM and MPC based SVM for single phase DG are examined with the three considered reference current generation schemes. The set-point real and reactive powers are considered as 2,500W and 1,250VAr (0.9 p.f.) until 1 s as shown in Figures 3.9 to 3.12. The tracking of active powers with ASDM for different current reference generation schemes is shown in Figure 3.9 while Figure 3.10 depicts the tracking performance of MPC based SVM. To validate the performance of the controller, the set-point active power is changed from 2,500W to 3,000W at 1s. From Figures 3.9 and 3.10, it can be observed that among the three reference generation schemes, scalar scheme is the quickest with minimum settling time. However, the scalar scheme using ASDM suffers from relatively large steady state errors with respect to the set-point active powers than scalar scheme using MPC based SVM. This is due to fact that the optimal MPC based SVM has the higher accuracy and faster convergence.

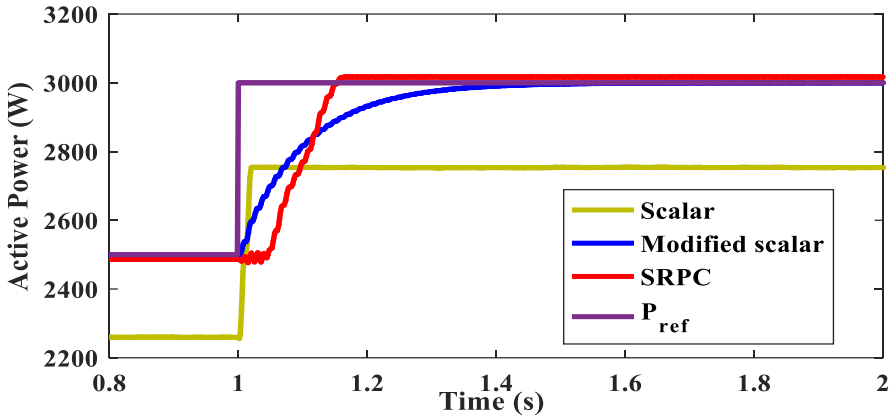

Figure 3.9 Active powers with ASDM for different schemes.

The settling time for the active powers with MPC based SVM for the set-point powers using modified scalar and SRPC methods is low when compared with the ASDM scheme with the same parameters. This can be understood as a consequence of finite control set optimization in the MPC based SVM against ASDM which uses the hysteresis controller to obtain switching pulses. Hence, for the set-point powers, MPC based SVM shows superior performance when compared with ASDM method. Whereas the current reference generation scheme such as the modified scalar reference scheme consists of PI controller and the power evaluation blocks, the response is comparatively sluggish with respect to the scalar scheme. From Figures 3.9 and 3.10, the SRPC scheme is almost as quick as modified scalar control scheme. However, it could reduce the steady state error to zero without using PI controller.

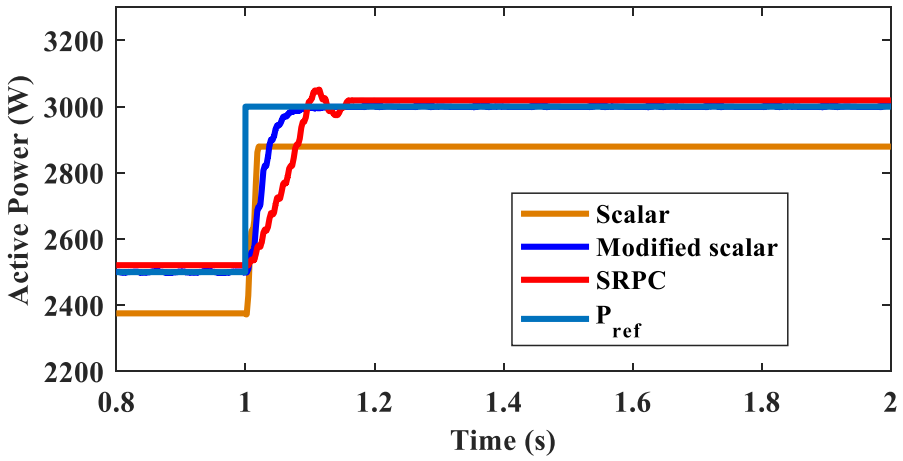

Figure 3.10 Active powers with MPC based SVM for different schemes.

To validate performance of the controller for the reactive power control, the set-point reactive power is changed from 1,250VAr to 1,500VAr at 1 s to maintain 0.9 p.f. As in the case of real powers, the scalar scheme is quickest for the reactive power control and lacks power correction mechanism. However, for the control schemes with power correction

mechanism, like SRPC and modified scalar control schemes, the MPC based SVM delivers superior performance compared to ASDM. Figures 3.11 and 3.12, shows that the SRPC scheme when controlled with MPC based SVM renders superior performance than the modified scalar scheme employed with either ASDM or MPC based SVM without using PI controller.

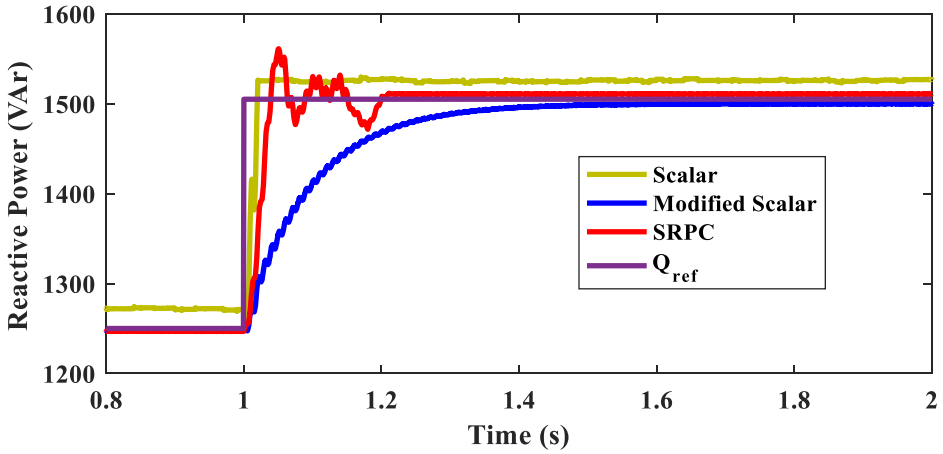

Figure 3.11 Reactive powers with ASDM for different schemes.

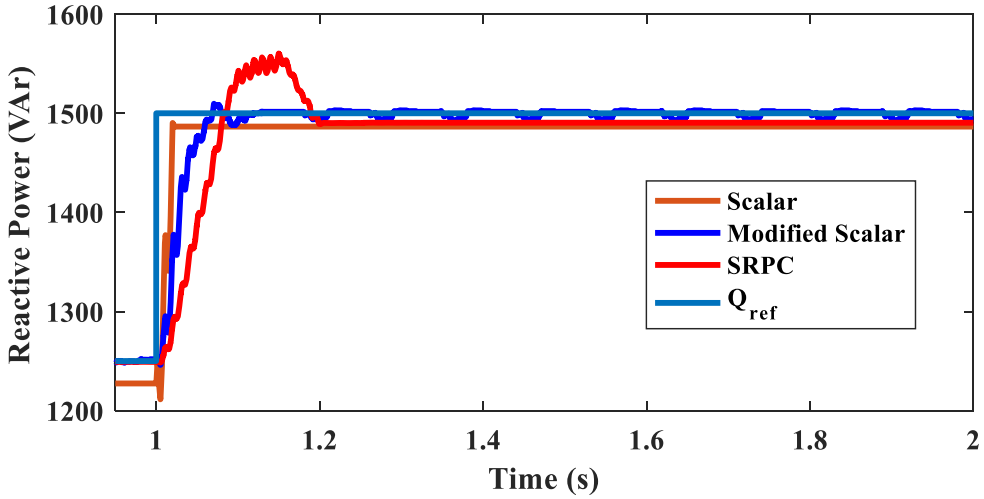

Figure 3.12 Reactive powers with MPC based SVM for different schemes.

It can be seen that the SRPC is the best among reference generation schemes, since it is examined for the parameter variation using ASDM as well as MPC based SVM. The Figures 3.13 and 3.14 show the SRPC scheme performance of single phase DG with 0.1A current perturb and 0.01rad phase perturb (ΔI, $\Delta\theta$) and with (i) hysteresis bands of 30W and 30VAr in real and reactive powers as Set-1 and (ii) hysteresis bands of 20W and 20VAr in real and reactive powers as Set-2. From Figure 3.13, it can be seen that the change in the hysteresis

band results in high ripples in power tracking if the switching pulses are derived from ASDM, which is undesirable.

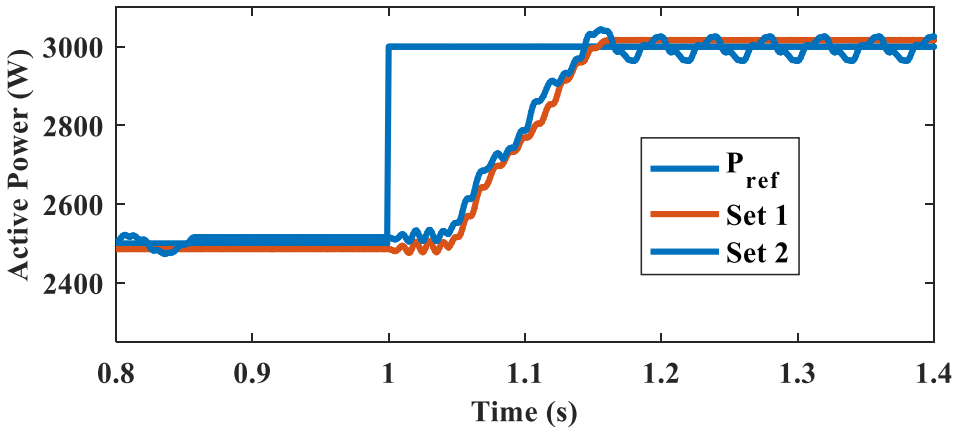

Figure 3.13 Real power tracking with change in control parameters using SRPC with ASDM.

From Figure 3.14, it can be inferred that the MPC based SVM is delivering smooth, ripple free tracking with zero steady state errors. Therefore, it can be concluded that the choice of the control parameters will affect the performance of the SRPC scheme when employed with ASDM as well as the DG output; however, the SRPC scheme employed with MPC based SVM promises excellent performance irrespective of control parameters. Moreover, its operation is independent of grid disturbances, operating points and set-point boundaries.

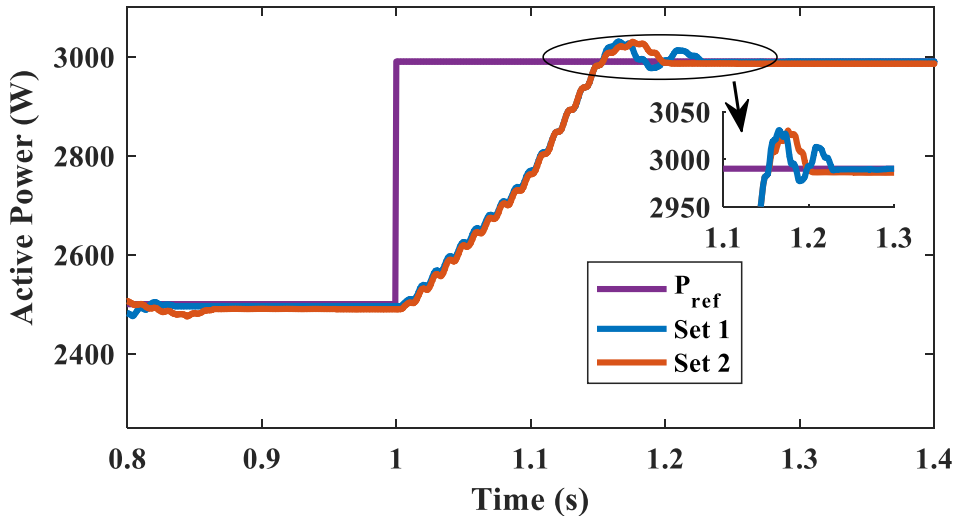

Figure 3.14 Real power tracking with change in control parameters using SRPC with MPC based SVM.

Figures 3.15 and 3.16 show the SRPC scheme performance with different upper and lower hysteresis bands in reactive powers as considered in real power control (30VAr as set-1 and 20VAr as set-2) and with same perturbs (i.e., 0.1 A, 0.01 rad). The tracking performance in Figures 3.15 and 3.16 reconfirms the superiority of SRPC with MPC based SVM.

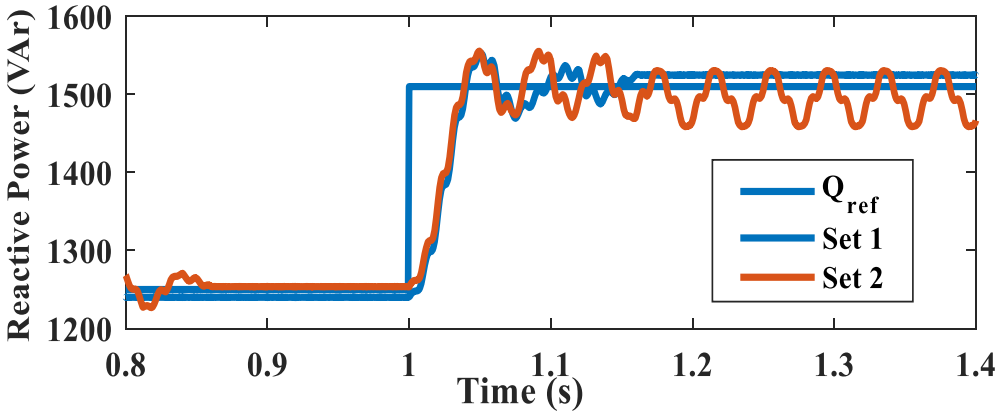

Figure 3.15 Reactive power tracking with change in control parameters using SRPC with ASDM.

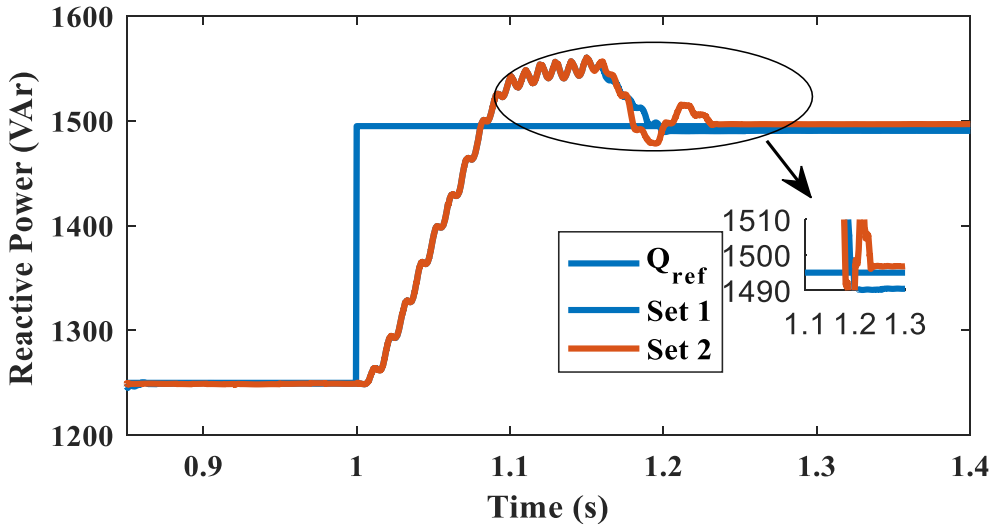

Figure 3.16 Reactive power tracking with change in control parameters using SRPC with MPC based SVM.

From the discussions, it is evident that the control and performance of the single phase DG when employed with MPC based SVM shows superior performance, compared with ASDM for all the current reference generation schemes. To validate the efficacy of the proposed schemes, Integral Absolute Error (IAE) is considered for evaluating active and reactive powers as presented in (3.17).

$$\left.\begin{aligned} IAE_P &= \int_0^T (\mathrm{P}_{ref} - P)dt \\ IAE_Q &= \int_0^T (Q_{ref} - Q)dt \end{aligned}\right\} \tag{3.17}$$

The performance of the current reference generation schemes with ASDM and MPC based SVM are evaluated using performance index IAE, as presented in Table 3.1. It can be

confirmed from Table 3.1 that the MPC based SVM exhibits excellent performance when compared with ASDM for all current reference generation schemes.

Table 3.2 IAE for different schemes using MPC based SVM and ASDM

Current reference Scheme	ASDM		Proposed MPC based SVM	
	IAE_P (W)	IAE_Q (VAr)	IAE_P (W)	IAE_Q (VAr)
Scalar control	251.8561	22.2565	126.2347	16.8391
Modified scalar	65.2871	19.3769	55.9503	7.1216
SRPC	55.2652	16.1998	49.8903	6.1691

3.6 Summary

The performance of MPC based SVM and ASDM for control of active and reactive powers of single phase grid connected DG is verified with different current reference generation schemes. The scalar reference generation scheme results in steady state error. Though, the modified scalar reference generation scheme renders zero steady state error, it induces delay in the power tracking.

The MPC based SVM method in combination with SRPC scheme has the advantages of quick, accurate and stable control when compared with ASDM method. Although, the modified scalar reference generation scheme and SRPC scheme have error correction mechanisms, their performance compared with ASDM is very poor. Therefore, it is concluded that that MPC based SVM with SRPC is the best combination among reference generation and modulation schemes considered in the study.

Though the SRPC using MPC based SVM proved to be a better method when compared with ASDM, an effective method needs to be designed with a single stage conversion i.e., the elimination of the current reference generation scheme. A control strategy must be designed for both grid and islanding modes avoiding the multi-loop control. A strategy must be developed to achieve grid synchronization without the use of any PLL and to achieve a seamless transition between grid connected and islanding modes.

Chapter 4

Model Predictive Controller based Single Phase Distributed Generator with Seamless Transition between Grid and Off-Grid Modes

Chapter 4
Model Predictive Controller based Single Phase Distributed Generator with Seamless Transition between Grid and Off-Grid Modes

4.1 Introduction

The primary objective of the inverter based DG is to supply the local loads continuously while feeding excess power to the grid. If the DG is operating in grid connected mode, it has to be controlled for specified real and reactive power feedings [85]. To achieve the successful integration with the grid thereby specified power feedings, the DG has to be synchronized with the grid. To accomplish successful synchronization, the voltage magnitude and its phase along with frequency of the incoming DG should match with that of the grid's voltage, frequency and phase. The task of synthesizing the required voltage can be achieved by adopting zero crossing detection method. However, this methodology may yield unsatisfactory synchronization in case of distorted grid voltages, which is very common in weak grids. This limitation can be alleviated by filtering the grid voltage as proposed in [86-87]. However, with these methodologies, the inherent delay resulting from filtering circuits in control loop cannot be avoided. Whereas, the adaptive vectorial filter is proposed in [88], can be employed. However, this methodology involves complex coefficient filters and necessitates careful design. To address this limitation, phase-locked loop (PLL) based synchronization schemes have been developed and their detailed discussion is presented [89-91]. As concluded in [90], the second order generalized integrator (SOGI) based PLL, inverse park transform based PLL and adaptive transfer delay based PLL have superior performance when compared with other PLLs, in terms of dynamic response, filtering capability and computational complexity. However, PLL involves PI controllers, which requires rigorous tuning. Since the PI is a fixed gain controller, the performance of the PLL and hence the synchronization phenomenon will be affected by unavoidable nonlinearities in the system. Moreover, PLL based synchronization involves multiple control loops of voltage (magnitude, frequency and phase loops) which makes the control complex. Therefore, a robust controller that address the aforesaid issues with minimized control loops is to be developed for grid synchronization of the DG.

Different seamless transition control strategies are discussed [92-94]. In [94], MPC based seamless control strategy is proposed; however, the control methodology adopted involves different weighting factors, acceptable tracking error ranges and initial weights which

necessitate careful design. In addition, the grid synchronization mechanism [94] involves the look-up table approach to find the right phase angle information using four zones of operation in one fundamental period.

In this connection, this chapter presents a PLL free, single loop, instantaneous voltage based synchronization scheme, which is free of weighting factors and look-up tables, for the control of single phase DG using SOGI based MPC. SOGI is preferred over adaptive vectorial filter as it is simple to design, easy to implement and has been used only for orthogonal signal generation [95]. Though SOGI extracts the fundamental components by filtering all other components, it does not induce any delay into the signals that have been processed. The developed MPC is integrated with the SVM, to realize a FCS-MPC which gives robust performance even under system frequency variation. In addition, a simple scheme for seamless transition between grid and off-grid modes of single phase DG is developed. The developed controller along with the seamless transition scheme is examined through simulations and has been validated on a proto type.

4.2 System Modeling in Grid Connected Mode

A single phase inverter based DG system supplying the local loads and grid is shown in Figure 4.1.

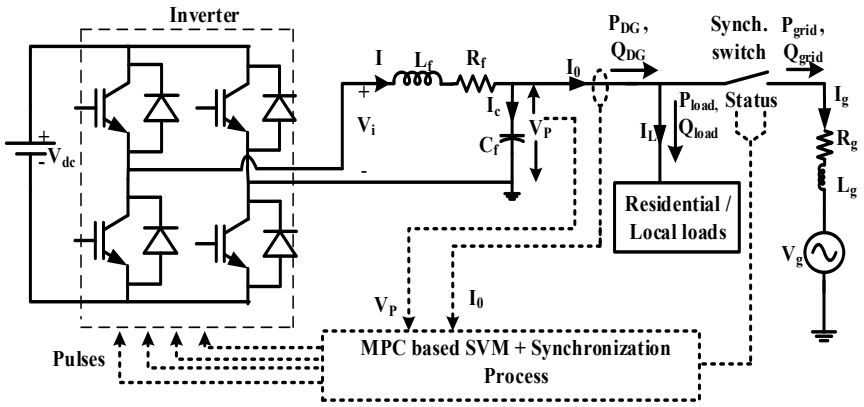

Figure 4.1 MPC based SVM controlled single phase Inverter with residential loads and grid interface.

The DG output voltage V_P and current $I_{0,}$ sensed after filtering, are given to the MPC based SVM. Based on the status of the synchronization switch, the DG is operated in either off grid mode or grid connected mode. The synchronization process for the interconnection of DG with the grid is implemented as per the methodology proposed in Section 4.4. The DG output power (P_{DG}, Q_{DG}) is equal to the sum of power absorbed by local load (P_{load}, Q_{load}) and the grid

feeding (P_{grid}, Q_{grid}). The system from the inverter end to the point of common coupling (PCC) can be represented as (4.1).

$$V_i = IR_f + L_f \frac{dI}{dt} + V_P \tag{4.1}$$

Considering grid connected mode of operation along with residential loads, the currents can be written as

$$\left.\begin{aligned} I_0 &= I_L + I_g \\ I &= I_c + I_0 \end{aligned}\right\} \tag{4.2}$$

Differentiating latter part of (4.2) with respect to t

$$\left.\begin{aligned} \frac{dI}{dt} &= \frac{dI_c}{dt} + \frac{dI_0}{dt} \\ I_c &= C_f \frac{dV_P}{dt} \end{aligned}\right\} \tag{4.3}$$

The PCC voltages and currents can be transformed into α-β domain using SOGI [11] methodology as $V_{P\alpha}$, $V_{P\beta}$, $I_{0\alpha}$, $I_{0\beta}$.

$$\left.\begin{aligned} V_{P\alpha} &= V_m \cos \omega t \\ V_{P\beta} &= V_m \sin \omega t \end{aligned}\right\} \tag{4.4}$$

Differentiating (4.4) with respect to 't'

$$\left.\begin{aligned} \frac{dV_{P\alpha}}{dt} &= -V_m \omega \sin \omega t = -\omega V_{P\beta} \\ \frac{dV_{P\beta}}{dt} &= V_m \omega \cos \omega t = \omega V_{P\alpha} \end{aligned}\right\} \tag{4.5}$$

Substituting (4.4) & (4.5) in latter part of (4.3),

$$\left.\begin{aligned} I_{c\alpha} &= -C_f \omega V_{P\beta} \\ I_{c\beta} &= C_f \omega V_{P\alpha} \end{aligned}\right\} \tag{4.6}$$

Differentiating (4.6) with respect to t,

$$\left.\begin{aligned}\frac{dI_{c\alpha}}{dt} &= -\omega^2 C_f V_{P\alpha} \\ \frac{dI_{c\beta}}{dt} &= -\omega^2 C_f V_{P\beta}\end{aligned}\right\} \tag{4.7}$$

Therefore, writing (4.1) and (4.2) in α-β domain

$$\left.\begin{aligned}V_{i\alpha} &= I_\alpha R_f + L_f \frac{dI_\alpha}{dt} + V_{P\alpha} \\ V_{i\beta} &= I_\beta R_f + L_f \frac{dI_\beta}{dt} + V_{P\beta}\end{aligned}\right\} \tag{4.8}$$

$$\left.\begin{aligned}I_\alpha &= I_{c\alpha} + I_{0\alpha} \\ I_\beta &= I_{c\beta} + I_{0\beta}\end{aligned}\right\} \tag{4.9}$$

Since the objective of the control is to achieve the desired real and reactive powers in grid connected mode, the switching decisions for the converter are made based on the error between the actual and set point powers. In general, the power can be written as

$$\left.\begin{aligned}S &= VI_0^* \\ S &= \left(V_{P\alpha} + jV_{P\beta}\right)\left(I_{0\alpha} - jI_{0\beta}\right)\end{aligned}\right\} \tag{4.10}$$

$$\left.\begin{aligned}P &= \left(V_{P\alpha} I_{0\alpha} + V_{P\beta} I_{0\beta}\right) \\ Q &= \left(V_{P\beta} I_{0\alpha} - V_{P\alpha} I_{0\beta}\right)\end{aligned}\right\} \tag{4.11}$$

Differentiating with respect to *t*, (4.11) will be

$$\frac{dP}{dt} = \left(\frac{dV_{P\alpha}}{dt} I_{0\alpha} + \frac{dI_{0\alpha}}{dt} V_{P\alpha} + \frac{dV_{P\beta}}{dt} I_{0\beta} + \frac{dI_{0\beta}}{dt} V_{P\beta}\right) \tag{4.12}$$

$$\frac{dQ}{dt} = \left(\frac{dV_{P\beta}}{dt} I_{0\alpha} + \frac{dI_{0\alpha}}{dt} V_{P\beta} - \frac{dV_{P\alpha}}{dt} I_{0\beta} - \frac{dI_{0\beta}}{dt} V_{P\alpha}\right) \tag{4.13}$$

For the evaluation of (4.12) & (4.13), $\dot{I}_{0\alpha}$ and $\dot{I}_{0\beta}$ are necessary

$$\begin{aligned} \dot{I}_{0\alpha} &= \dot{I}_{\alpha} - \dot{I}_{c\alpha} \\ \dot{I}_{0\beta} &= \dot{I}_{\beta} - \dot{I}_{c\beta} \end{aligned} \tag{4.14}$$

where dot operator represents differential of respective terms. Substituting (4.8) & (4.9) in (4.14) and on simplifying, the resultant $\dot{I}_{0\alpha}$ and $\dot{I}_{0\beta}$ will be

$$\dot{I}_{0\alpha} = \frac{i_{\alpha} + V_{P\alpha}\left(\omega^2 L_f C_f - 1\right) - \omega R_f C_f V_{P\beta} - I_{0\alpha} R_f}{L_f} \tag{4.15}$$

$$\dot{I}_{0\beta} = \frac{i_{\beta} + V_{P\beta}\left(\omega^2 L_f C_f - 1\right) - \omega R_f C_f V_{P\alpha} - I_{0\beta} R_f}{L_f} \tag{4.16}$$

After substituting (4.5), (4.9), (4.15), (4.16) in (4.12) and (4.13), the powers in state space representation is given as

$$\begin{bmatrix} \dot{P} \\ \dot{Q} \end{bmatrix} = -\frac{1}{L_f}\begin{pmatrix} -R_f & -\omega L_f \\ \omega L_f & -R_f \end{pmatrix}\begin{bmatrix} P \\ Q \end{bmatrix} + \frac{1}{L_f}\begin{pmatrix} V_{P\alpha} & V_{P\beta} \\ V_{P\beta} & -V_{P\alpha} \end{pmatrix}\begin{bmatrix} V_{i\alpha} \\ V_{i\beta} \end{bmatrix} + \frac{1}{L_f} * \begin{bmatrix} \left(\omega^2 L_f C_f - 1\right)V_{P\alpha} - \omega R_f C_f V_{P\beta} & \left(\omega^2 L_f C_f - 1\right)V_{P\beta} - \omega R_f C_f V_{P\alpha} \\ -\left(\omega^2 L_f C_f - 1\right)V_{P\beta} + \omega R_f C_f V_{P\alpha} & -\left(\omega^2 L_f C_f - 1\right)V_{P\alpha} - \omega R_f C_f V_{P\beta} \end{bmatrix} * \begin{bmatrix} V_{P\alpha} \\ V_{P\beta} \end{bmatrix} \tag{4.17}$$

where $\dot{P} = \frac{dP}{dt}, \dot{Q} = \frac{dQ}{dt}$

Taking the powers as state variables and considering V_i as inputs, (4.17) can be re-written as follows.

$$\dot{X}_l = A_l X_l + B_l V_w + C_l V_{Pl} \tag{4.18}$$

Where

$$V_w = \begin{bmatrix} V_{i\alpha} \\ V_{i\beta} \end{bmatrix};\ V_{Pl} = \begin{bmatrix} V_{P\alpha} \\ V_{P\beta} \end{bmatrix} \tag{4.19}$$

$$C_l = \frac{1}{L_f}\begin{bmatrix} \left(\omega^2 L_f C_f - 1\right)V_{P\alpha} - \omega R_f C_f V_{P\beta} & \left(\omega^2 L_f C_f - 1\right)V_{P\beta} - \omega R_f C_f V_{P\alpha} \\ -\left(\omega^2 L_f C_f - 1\right)V_{P\beta} + \omega R_f C_f V_{P\alpha} & -\left(\omega^2 L_f C_f - 1\right)V_{P\alpha} - \omega R_f C_f V_{P\beta} \end{bmatrix}$$
$$A_l = \frac{1}{L_f}\begin{pmatrix} -R_f & -\omega L_f \\ \omega L_f & -R_f \end{pmatrix}; B_l = \frac{1}{L_f}\begin{pmatrix} V_{P\alpha} & V_{P\beta} \\ V_{P\beta} & -V_{P\alpha} \end{pmatrix} \quad (4.20)$$

The equation (4.18) can be written as (4.21)

$$\frac{X_l(k+1) - X_l(k)}{T_s} = A_l X_l(k) + B_l V_w + C_l V_{Pl} \quad (4.21)$$

$$X_l(k+1) = \left(I + A_l T_s\right) X_l(k) + B_l V_w T_s + C_l V_{Pl} T_s \quad (4.22)$$

However,

$$e^{A_l T_s} = I + A_l Ts + \frac{(A_l Ts)^2}{2!} + .. + \frac{(A_l Ts)^n}{\text{n!}} + .. \approx I + A_l Ts \quad (4.23)$$

Hence, (4.22) can be written as

$$X_l(k+1) = X_l(k) A_{ld} + B_d V_w + C_d V_{Pl} \quad (4.24)$$

where $A_{ld} = e^{A_l T_s}$; $B_d = B_l T_s$; $C_d = C_l T_s$;

With this, powers are taken as control variables to implement the model predictive methodology for the control of grid connected inverters. The cost function, g_s for the model predictive control is taken as the Euclidean distance of the predicted powers and reference powers as

$$g_s = \sqrt{\left(\left(P_l(k+1) - P_{ref}\right)^2 + \left(Q_l(k+1) - Q_{ref}\right)^2\right)} \quad (4.25)$$

Where g_s is the objective function or cost function. The cost function represented in (4.25) is evaluated for all possible switching sets of inverter switching operation for which the voltage vectors are calculated based on SVM. As it is a single phase system, with four switches, the number of switching states will be four (00, 01, 11 and 10). Out of which only two are effective

states (01, 10), as the other two (00, 11) are null states. Hence, at any time the prediction states are limited to only two, resulting in decreased computational burden with quick control actions. Among the two effective states, the switching set will be selected such that for the given state, the cost function will result in minimum value for the considered sampling duration (4.26). The switches are controlled according to the derived switching set; the corresponding voltage vector will appear as inverter voltage. The control block diagram of the developed MPC with power as control variable is shown in Figure 4.2.

$$g = \min\left(g_{sl}\right), \text{ for } l = 1,2 \tag{4.26}$$

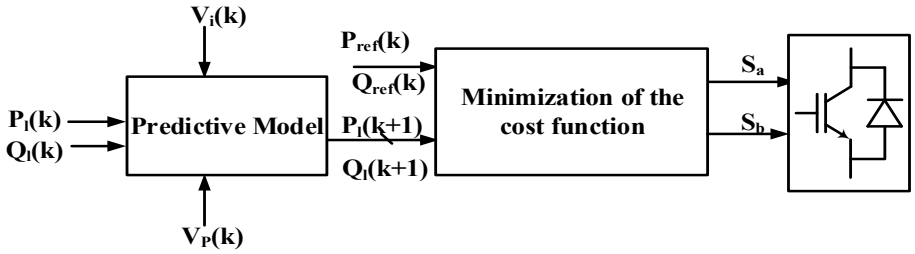

Figure 4.2 Block diagram of model predictive control for grid connected mode.

4.3 System Modeling for Off Grid Operation

Considering the inverter for off-grid operation, the current dynamics can be represented as

$$\frac{dI}{dt} = \frac{V_i - IR_f - V_P}{L_f}; I_c = I - I_L ; \frac{dV_P}{dt} = \frac{I - I_L}{C_f} \tag{4.27}$$

For the off-grid operation, the control variables are the load (PCC) voltage and frequency. Hence, considering the voltage V_P and I as state variables, the state space representation of the inverter is

$$\begin{bmatrix} \dot{I} \\ \dot{V}_P \end{bmatrix} = \frac{1}{f}\begin{pmatrix} -R_f & -1 \\ \frac{L_f}{C_f} & 0 \end{pmatrix}\begin{bmatrix} I \\ V_P \end{bmatrix} + \begin{bmatrix} \frac{1}{L_f} \\ 0 \end{bmatrix} V_i + \begin{bmatrix} 0 \\ \frac{-1}{C_f} \end{bmatrix} I_L \tag{4.28}$$

The above equation is of the form

$$\dot{X}_d = AX_d + BV_i + CI_L \tag{4.29}$$

The second row of (4.28) determines the controlled voltage vector for the off-grid operation.

where
$$A = \frac{1}{L_f}\begin{pmatrix} -R_f & -1 \\ \frac{L_f}{C_f} & 0 \end{pmatrix} B = \begin{bmatrix} \frac{1}{L_f} \\ 0 \end{bmatrix}; C = \begin{bmatrix} 0 \\ \frac{-1}{C_f} \end{bmatrix} \tag{4.30}$$

After discretization, the latter part in (4.27) can be written as:

$$\frac{V_P(k+1) - V_P(k)}{T_s} = \frac{I(k) - I_L(k)}{C_f} \tag{4.31}$$

$$V_P(k+1) - V_P(k) = \left(\frac{I(k) - I_L(k)}{C_f}\right) T_s \tag{4.32}$$

$$V_P(k+1) - V_P(k) = \frac{I(k)T_s}{C_f} - \frac{I_L(k)T_s}{C_f} \tag{4.33}$$

Simplifying and rearranging of (4.33) results in

$$V_P(k+1) = V_P(k) + \frac{I(k)T_s}{C_f} - \frac{I_L(k)T_s}{C_f} \tag{4.34}$$

In (4.34), $V_P\ (k+1)$ is dependent on I which further depends on V_i. Discretizing former part of (4.27) by using Euler's forward method, and on simplifying

$$\frac{I(k+1) - I(k)}{Ts} = \frac{V_i(k)}{L_f} - \frac{I(k)R_f}{L_f} - \frac{V_P(k)}{L_f} \tag{4.35}$$

$$I(k+1) - I(k) = \frac{V_i(k)}{L_f} Ts - \frac{I(k)R_f}{L_f} Ts - \frac{V_P(k)}{L_f} Ts \tag{4.36}$$

$$I(k+1) = I(k) + \frac{V_i(k)Ts}{L_f} - \frac{I(k)R_f Ts}{L_f} - \frac{V_P(k)Ts}{L_f} \tag{4.37}$$

For (4.34), $I(k)$ is essential for the evaluation of the voltage vector. For evaluating $I(k)$, $I(k+1)$ is shifted to $I(k)$ as (4.38)

$$I(k) = I(k-1) + \frac{V_i(k-1)Ts}{L_f} - \frac{I(k-1)R_f Ts}{L_f} - \frac{V_P(k-1)Ts}{L_f} \tag{4.38}$$

On simplification, (4.38) can be rewritten as

$$I(k) = I(k-1)(1 - \frac{R_f Ts}{L_f}) + \frac{V_i(k-1)Ts}{L_f} - \frac{V_P(k-1)Ts}{L_f} \tag{4.39}$$

Substituting (4.39) in (4.34) and on rearranging,

$$V_P(k+1) = V_P(k) + I(k-1)(\frac{1}{C_f} - \frac{R_f Ts}{L_f C_f})Ts + \frac{V_i(k-1)Ts^2}{L_f C_f} - \frac{V_P(k-1)Ts^2}{L_f C_f} - \frac{I_L(k)Ts}{C_f} \tag{4.40}$$

Considering the instantaneous voltage vector V_P as the control variable and the instantaneous reference voltage V_{ref} as the reference variable, the cost function is defined as the Euclidean distance between the predicted voltage vectors and reference voltage vector (4.41). For every instant, voltage is predicted and is compared with the reference value.

$$g_v = \sqrt{\left(V_{P\alpha}(k+1) - V_{ref\alpha}\right)^2 + \left(V_{P\beta}(k+1) - V_{ref\beta}\right)^2} \tag{4.41}$$

Where g_v is the cost function or objective function for off-grid connected operation. The switching vector corresponding to minimum g_v, as in (4.42), is selected and is given for the next sampling instant T_s to generate the voltage templates. Therefore, in steady state the voltage vector V_P will resemble the reference voltage at the set-point frequency. The block diagram of the developed MPC in off-grid mode of operation is shown in Figure 4.3.

$$g = \min\left(g_{vl}\right), \; for \; l = 1,2 \tag{4.42}$$

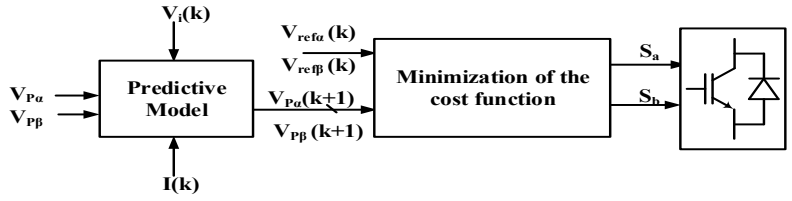

Figure 4.3 Block diagram of model predictive control for off grid mode.

4.4 Methodology of Grid Synchronization

The grid synchronization methods can be classified as zero crossing detection, open loop and closed loop techniques. Given its merits, the closed loop grid synchronization method is applied. In this method, the reference and actual voltages are compared after transforming the instantaneous symmetrical components into orthogonal components (α-β). Figure 4.4 illustrates the steps to be followed for grid synchronization. Prior to the synchronization or resynchronization with the grid, the inverter will be operating in islanding mode.

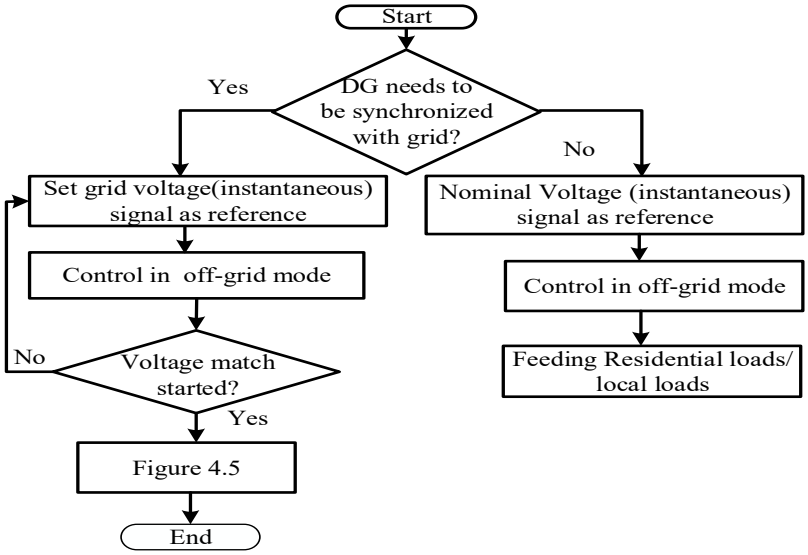

Figure 4.4 Flow chart of grid synchronization process.

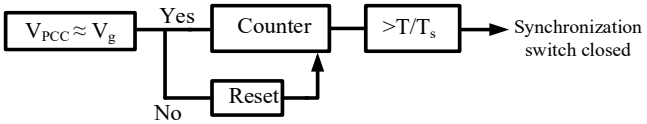

Figure 4.5 Decision making mechanism for instantaneous voltage match.

However, the objective of grid synchronization is to supply the set point real and reactive powers to the grid at the voltage and frequency as defined by the grid. Hence, the controller reference values are toggled from the nominal reference voltage and frequency to the frequency and voltage of the grid. Hence the grid voltage is sensed and is given to the controller. The synchronization switch should be closed only when the incoming DG's voltage magnitude, frequency and phase are matched with that of the grid's voltage magnitude, frequency and phase. However, in the proposed methodology, all the three parameters can be verified by comparing instantaneous values of voltages. Even though the instantaneous voltages match at

one time instant, they may deviate at the next instant. However, to have safe synchronization, one has to have an assurance that there is sustained synchronization of instantaneous voltages. Hence, in this study the instantaneous voltages are observed for the duration of one complete cycle. The counter will be initialized once the instantaneous voltages start matching and the number of matching instants is counted. If the count reaches the set value (T/T_s), indicating that the instantaneous voltages of incoming DG and the grid are matched for a complete cycle, the synchronization switch will be closed while toggling the MPC to grid connected mode. If the instantaneous voltages deviate from each other before the counter reaches its set value, the counter will be reset to zero as shown in Figure 4.5. The counter will restart only after the voltages start matching again. This procedure is adopted to assure sustained matching of instantaneous voltages and ensure safe synchronization. The user can wait for more than one complete cycle for assured smooth synchronization, however it delays the process of synchronization.

4.5 Simulation Results

To verify the performance of the proposed MPC integrated with SVM, along with the seamless transition mechanism for single phase DG system, a simulation test bed is developed using Matlab. Different case studies with all the possible operating conditions and modes are formulated, discussed in detail as Case-1 to 4, in the following subsections. The parameters considered for simulation and experimentation are presented in Table 4.1.

Table 4.1 Simulation and Experimental parameters

Parameters	**Simulation**	**Experiment**
V_{dc}	400 V	261 V
V_P	(230-240) V (RMS)	150 V (RMS)
V_{ref}	230 V	(130-150) V (RMS)
f_p	(49-50) Hz	(48-50) Hz
R_f, L_f	0.2 Ω, 5 mH	0.2 Ω, 5 mH
C_f	50 μF	50 μF
P	(2-7) kW	(0-1.5) kw
Q	(1-3.5) kVAr	-

4.5.1 Case -1: Grid connected mode

In this case, the DG is operated in grid connected mode with initial set-point real and reactive powers ($P_{gridref}$ and $Q_{gridref}$) as 5,000W and 2,500VAr (0.9pf) respectively. The $P_{gridref}$

is changed to 7,500W (0.9pf) at 1 s, to examine the capability of the controller in tracking the changes in reference powers. It can be seen from Figure 4.6 that the developed controller is very effective in tracking the new reference powers within 0.02 s (one cycle) with zero steady state error and without any appreciable oscillations (i.e., over/undershoots).

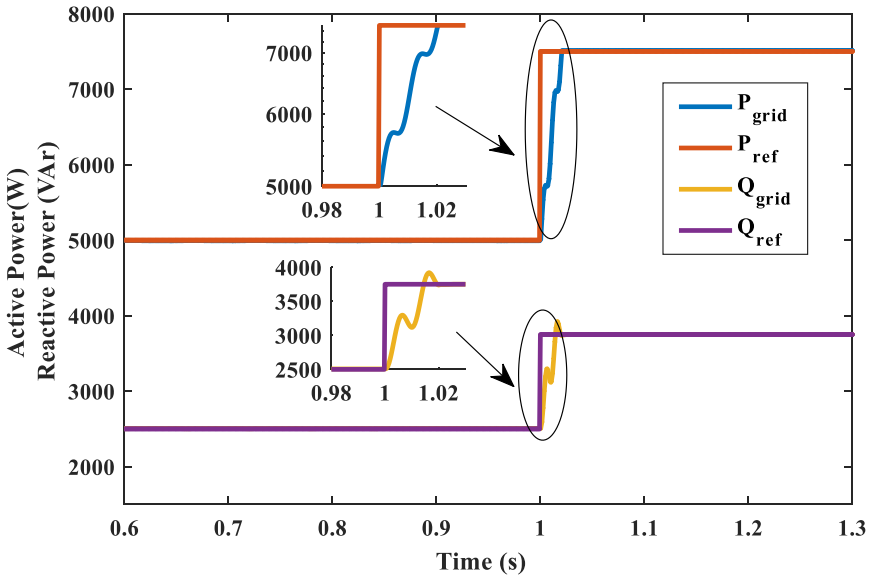

Figure 4.6 Active power and reactive power for grid-connected operation.

4.5.2 Case-2: Off grid mode

In this case, the DG is operated in islanding mode with initial load of real and reactive powers (P_{load} and Q_{load} of Figure 4.1) of 2,000W and 1,000VAr (0.9pf) respectively. Since the DG is operating in off-grid mode, P_{grid} and Q_{grid} are zero. The P_{load} and Q_{load} are changed to 3,500W and 1,750VAr at 1 s, and the performance of the designed controller in serving the varying load is as shown in Figure 4.7.

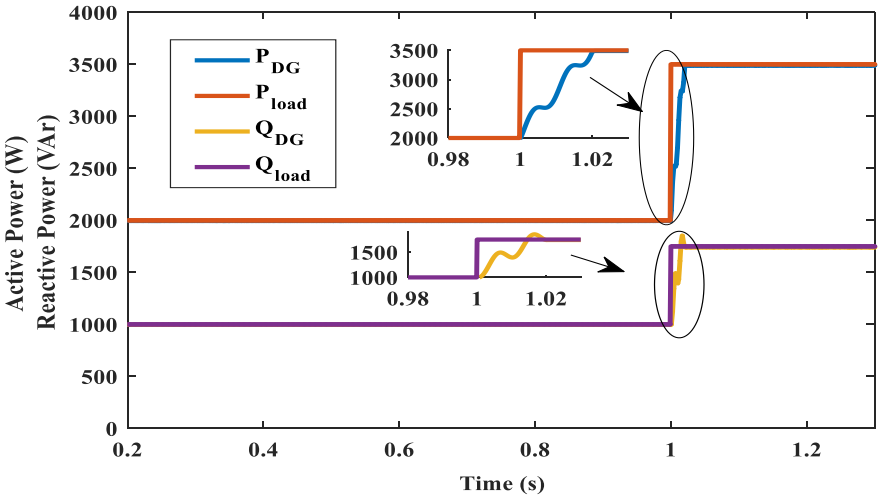

Figure 4.7 Active power and reactive power of residential loads supplied by DG.

As it is an islanding operation, to ascertain that the DG is operating at nominal voltage and frequency (230V rms, 50Hz), the output voltage, current and their total harmonic distortions (THDs) are plotted and shown in Figures 4.8 to 4.11.

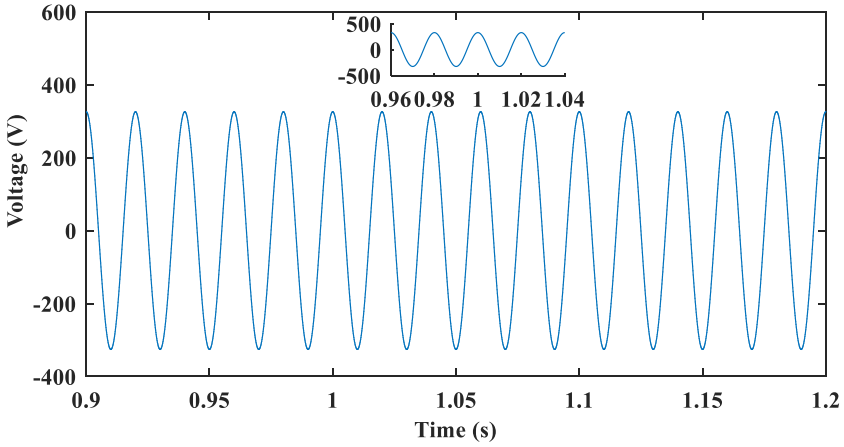

Figure 4.8 DG output voltage (V_P), feeding only residential loads.

The efficacy of the designed MPC for single phase DG system operating in islanding mode, while feeding the changing local loads at nominal voltage and frequency with very minimum THDs, can be ascertained from Figures 4.7 to 4.11. It can be observed from Figures 4.7, 4.8 and 4.10 that despite the change in connected load (P_{load} and Q_{load}) at 1s, the inverter output voltage (V_P) is unaffected and remains at nominal value all the time.

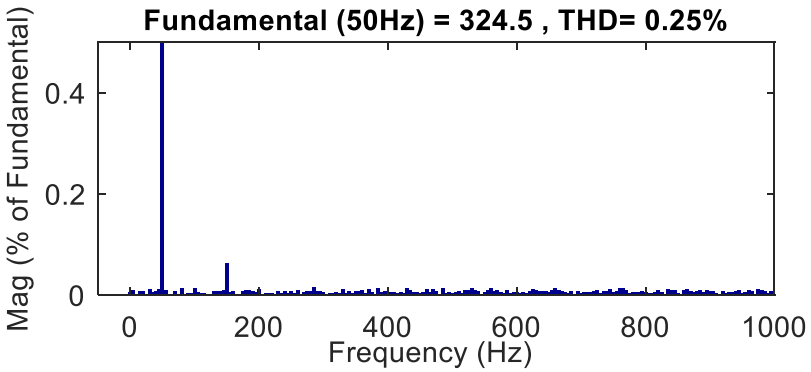

Figure 4.9 THD in voltage under off-grid mode, supplying only residential loads.

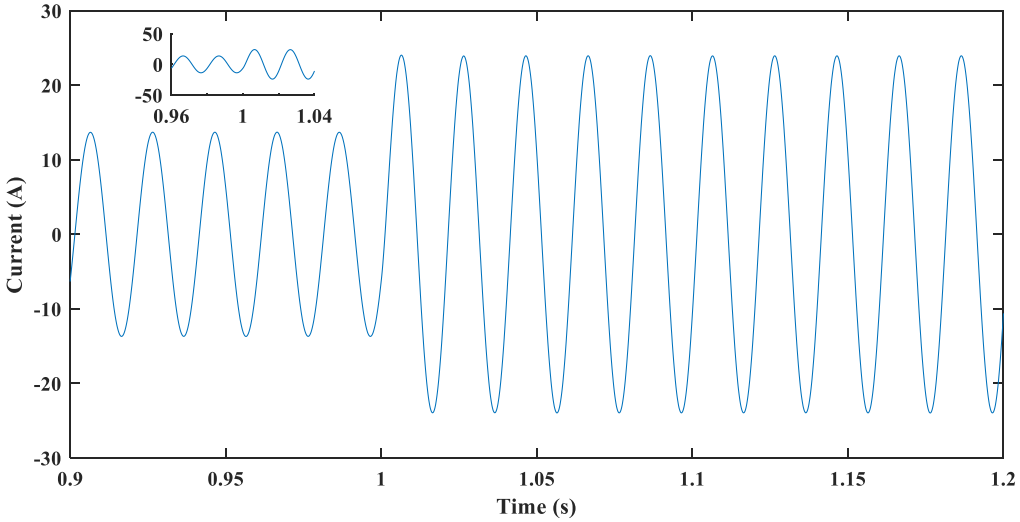

Figure 4.10 DG current in islanded mode, supplying only residential loads.

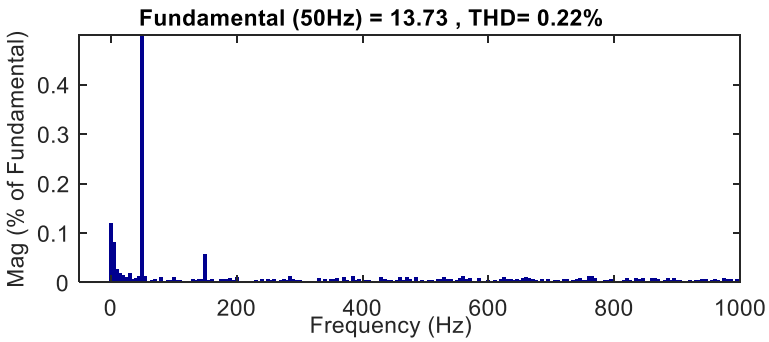

Figure 4.11 THD in current under off-grid mode, supplying only residential loads.

4.5.3 Case-3: Transition from grid to off grid mode

In this case, the DG is supplying real and reactive powers (P_{grid}, Q_{grid}) of 5,000W and 2,500VAr (0.9pf), initially to the grid. The residential loads (P_{load} and Q_{load}) connected in the systems are considered to be 2,000W and 1,000VAr respectively as shown in Figures 4.12 and 4.13.

At 1 s, it is considered that grid is isolated; hence the DG has to maintain its stability while feeding only the residential loads. Since the DG got isolated from grid at 1s, the grid feeding (P_{grid}, Q_{grid}) is becoming zero at 1s, as depicted in Figures 4.12 and 4.13. Even though the grid feeding has become zero at 1s, the DG output remains at 2,000W and 1,000VAr, which exhibits the superior seamless transition performance of the developed controller from grid connected mode to islanding mode.

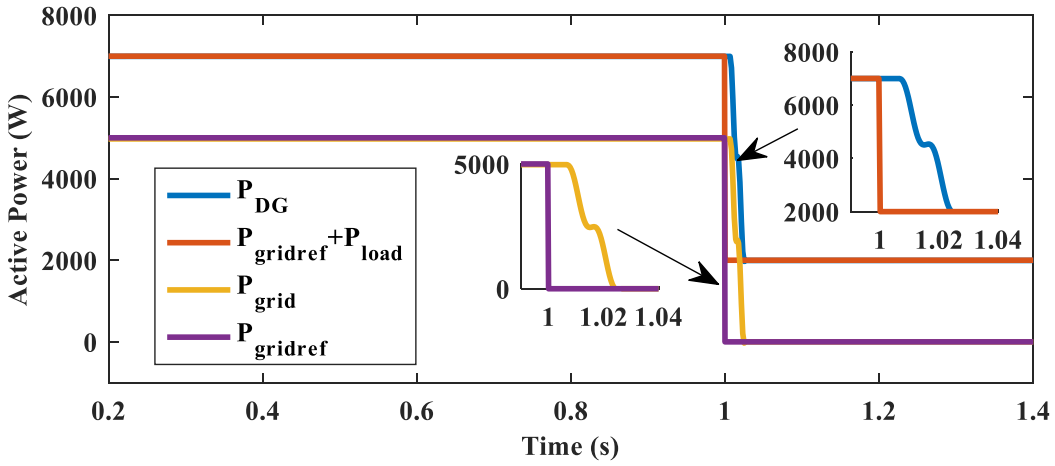

Figure 4.12 Active power during transition from grid mode to islanding mode.

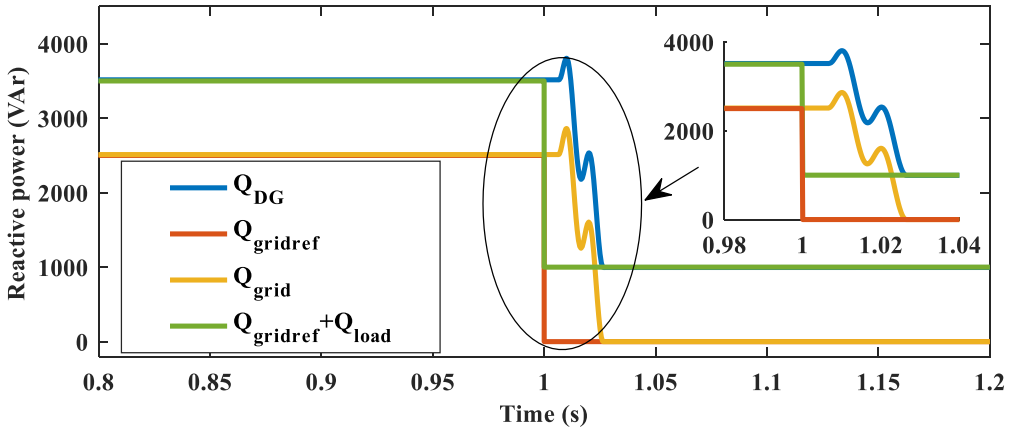

Figure 4.13 Reactive powers during transition from grid mode to islanding mode.

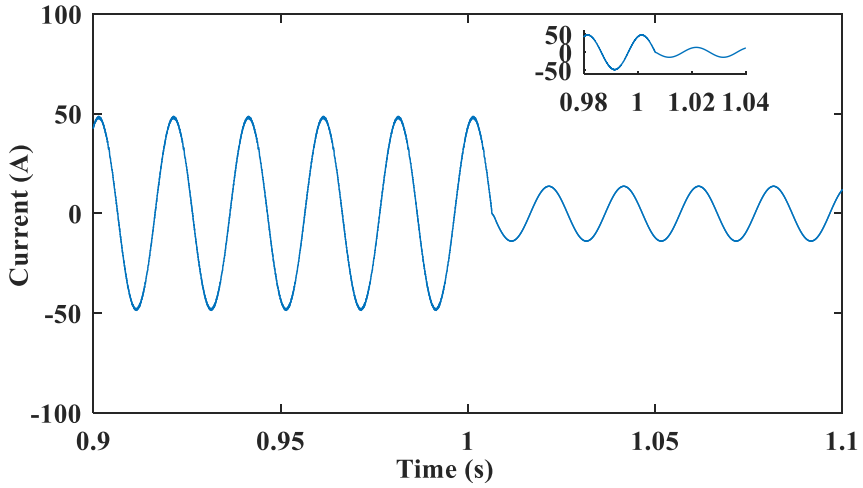

Figure 4.14 Current waveform for transition from grid to off-grid mode.

Figure 4.14 shows the DG output current which exhibits the chattering/oscillations free response during, before and after the transition from grid connected mode to islanding mode in spite of change in system parameters resulting from isolation. Therefore, confirms the extraordinary performance of the designed controller in achieving seamless transition. The Figure 4.11 shows the current THD in islanding mode and Figure 4.15 infers the current THD in grid connected mode.

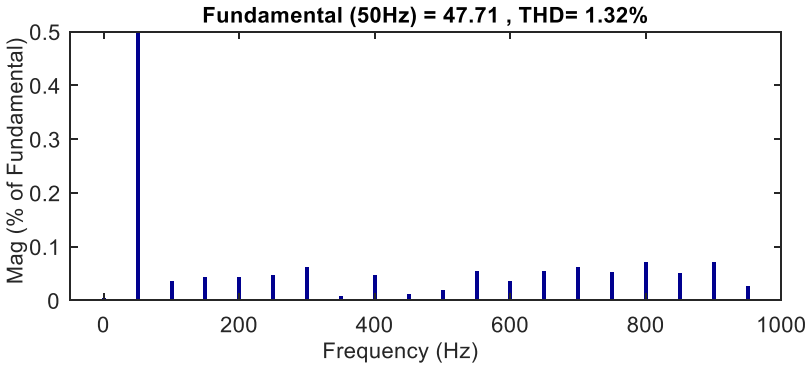

Figure 4.15 THD in current under grid connected mode.

4.5.4 Case-4: Transition from off grid to grid connected mode

The performance of the controller for resynchronization of DG with grid is studied in this case. As discussed in section 4.4, the DG is supplying its load initially at nominal voltage and frequency (230V (rms), 50Hz). At the same time the grid is operating at 240V (rms), 49Hz. It is decided that the DG which is operating in islanding mode is to be synchronized with the grid at 0.5 s. The grid synchronization algorithm (Figure. 4.4) will be initiated at 0.5s. It can be seen from Figure 4.16 that the DG voltage is having a magnitude difference of 10V (rms) and is

almost 180° out of phase with respect to the grid voltage at 0.5s, that is, the instant at which the grid synchronization algorithm is initiated. However, once the algorithm is initiated, the DG has quickly adapted its voltage magnitude and frequency along with phase so as to match the grid references, which is shown in Figure 4.16.

The counter (shown in Figure 4.5) is initiated at 0.501 s. To ensure the successful synchronization of DG with the grid, the counter is allowed to reach 1,000 (= 20ms/20μs). As and when the counter reaches 1,000, the MPC is toggled from off-grid mode to grid connected mode and the synchronization switch is turned ON. The power outputs of DG in this case study are shown in Figure 4.17. Since the DG is operating in islanding mode till 0.501 s, it is supplying the local load of 2,000W. As the DG reference voltage has changed from nominal voltage (230V) to grid voltage (240V) at 0.5 s, the local loads start absorbing an extra power of 177.69 W ($P = V^2/R$) from 0.5 s onwards as shown in Figure 4.17. Even after synchronization at 0.501 s, the DG power remains the same as the grid feeding references are kept zero till 0.9s., As the grid feeding references are changed to 1,000W and 500VAr at 0.9 s respectively, the DG supplies power of 3,177.69 W (local load + grid feeding) and 500VAr (0.988pf) as depicted in Figure 4.17.

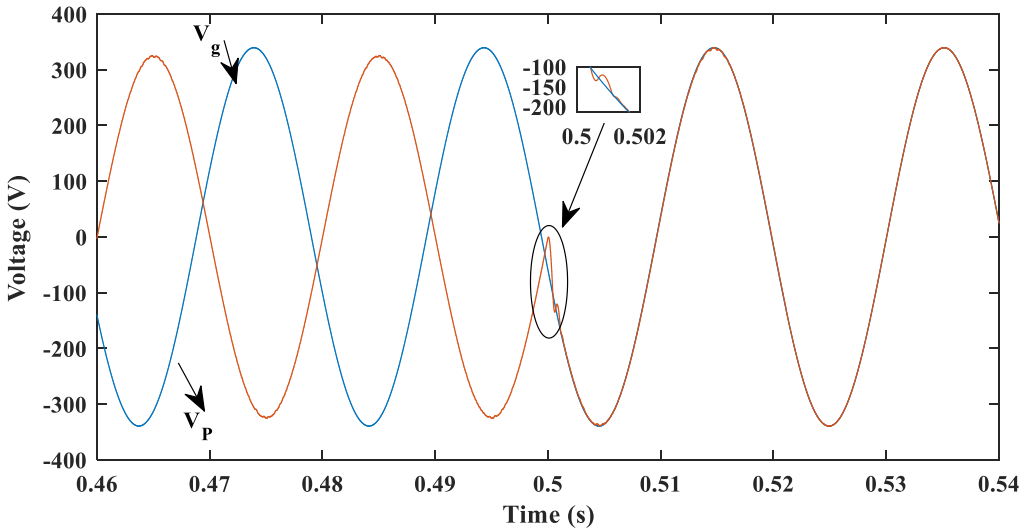

Figure 4.16 PCC and grid voltages before and after synchronization.

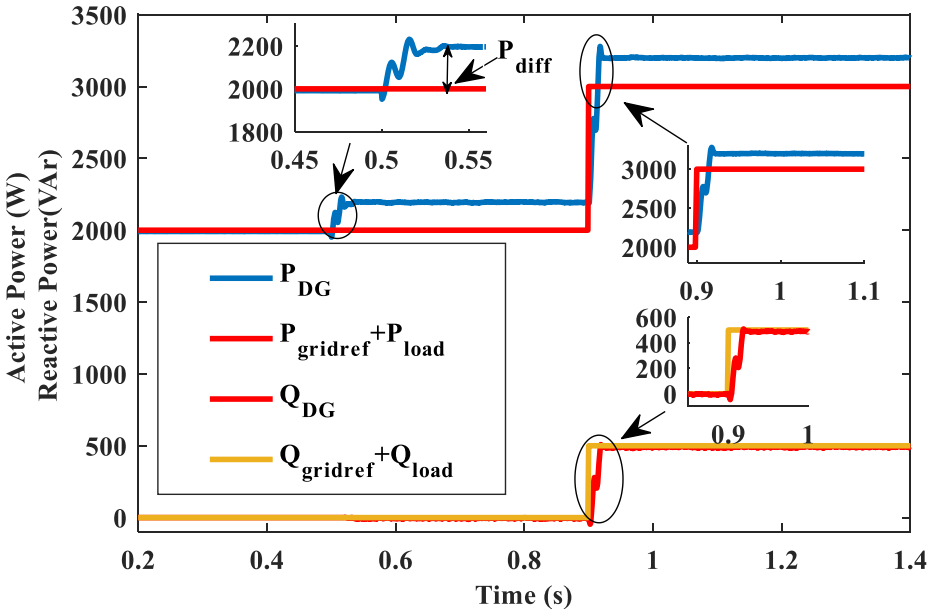

Figure 4.17 Active and reactive powers for transition from off-grid to grid mode.

The DG current during different operating conditions of this case study is shown in Figure 4.18. It can be seen in Figures 4.16 and 4.18 that the moment the DG references are changed to grid references, the DG output voltage and current are changing their magnitude, frequency as well as phase according to the grid references from 0.5s. Altogether, the proposed MPC is exhibiting an excellent performance in all the operating conditions and is also delivering extraordinary seamless response during the transitions between different modes of operation.

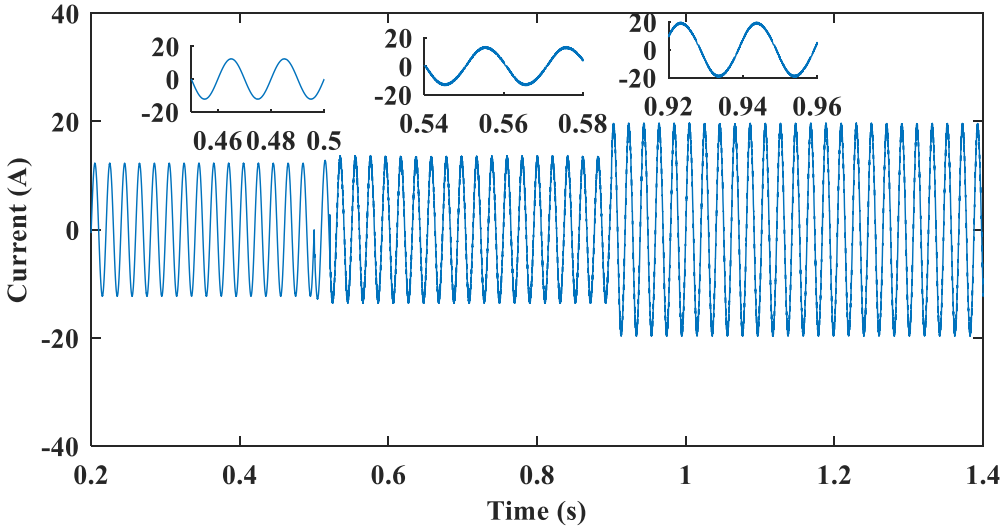

Figure 4.18 Current waveform for transition from off-grid to grid mode.

4.6 Experimental Validations

An experimental set up is shown in Figure 4.19 with different components, to examine and validate the performance of the proposed SVM based MPC for the control of single phase DG under different operating conditions. Different case studies have been carried out to validate the proposed seamless transition mechanism.

Using dSPACE DS1104 as control interface, the single phase DG is realized to achieve the defined objectives. The Figure 4.20 shows that the DG is supplying the local load at the specified nominal voltage of 150V rms (peak value of 210V). Due to the limitation in measuring infrastructure, which cannot measure reactive power averaged over a moving window, only a resistive load is considered during this experimentation. Since the considered load is of resistive nature, the phase difference between the voltage and current is zero, as shown in Figure 4.20. The THD in the experimental output voltage is recorded as 0.6% which is shown in Figure 4.21. The THDs in voltage as well as in current are well below the maximum allowable value of 5%.

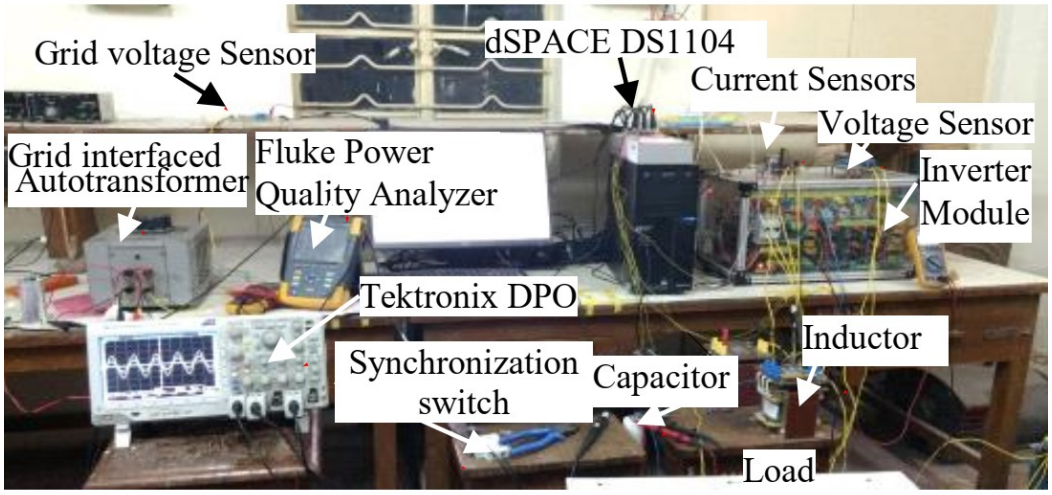

Figure 4.19 Experimental set-up of grid/off grid connected DG.

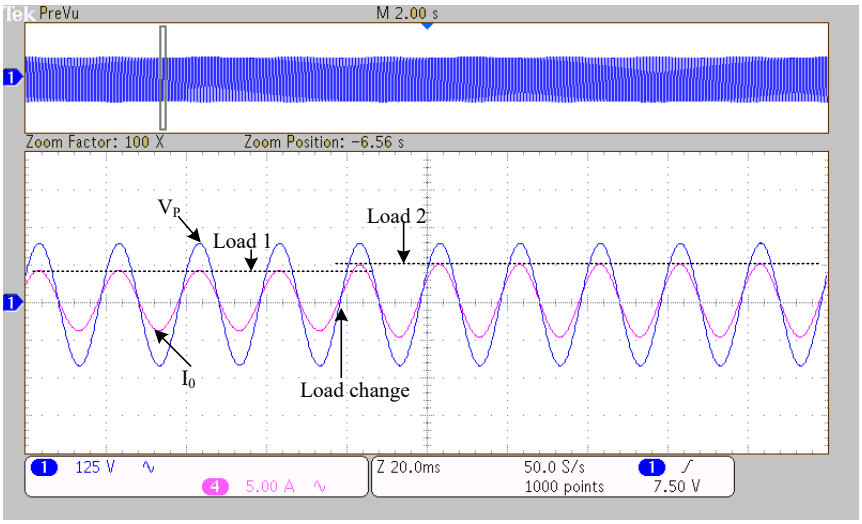

Figure 4.20 Voltage and current waveforms of off-grid with increased Resistive load.

For the successful integration of DG, the voltage magnitude, frequency and phase at the PCC must be matched with that of the grid's voltage, frequency and phase. To accomplish this, grid voltage is sensed by voltage sensor and is given to the controller which is operating in islanding mode. For the experimental validation, the magnitude of voltage at PCC which is supplied from DG, is kept as 130V (rms) at 48Hz, while the grid voltage is 150V (rms) at 50Hz, to validate the capability of the designed controller in synchronizing the DG which is operating at a voltage, frequency and phase that is different from the grid's voltage, frequency and phase. As the grid frequency cannot be controlled by converter, the DG is controlled to operate at 48Hz prior to synchronization.

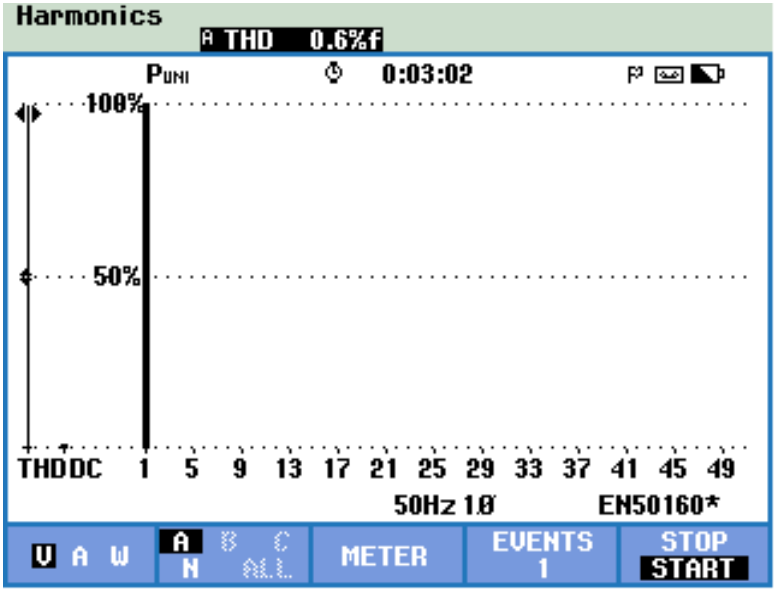

Figure 4.21 Voltage THD plot of off grid for Resistive load.

The performance of grid synchronization mechanism and the designed SVM based MPC scheme for seamless transition can be seen in Figure 4.22. The DG is operating in islanding mode till T_0 as shown in Figure 4.22. It is decided to synchronize the DG with the grid at the end of T_0, hence the synchronization mechanism will be activated at T_0.

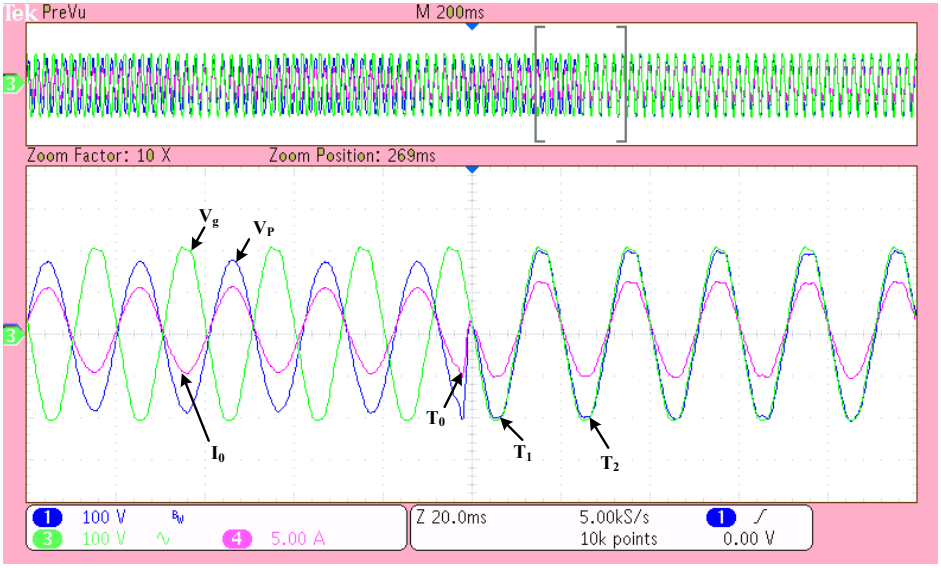

Figure 4.22 Voltage and current waveforms before and after grid synchronization.

The designed SVM based MPC scheme along with synchronization mechanism is trying to match the DG voltage, frequency and phase with that of the grid's voltage, frequency and phase between T_0 and T_1. Figure 4.22 shows that at T_1, the controller is able to synthesize a voltage at PCC so that the DG can be synchronized with the grid. However, to secure successful synchronization, the synchronizing switch is closed at T_2, as discussed in section 4.4. As the grid voltage (150V) is greater than the DG voltage (130V), there is slight increase in power (immediately after T_1) compared to power before synchronization as discussed in case-4 of section 4.5, which can be seen in Figure 4.23.

The power output of the single phase DG is depicted in Figure 4.23. At T_3, the $P_{gridref}$ is changed from 0W to 500W. Now the DG is feeding 500W to the residential load and 500W to grid. Figure 4.24 presents the inverter voltage and current waveforms for this variation of DG power from 500W to 1,000W. The current THD in grid connected mode (after T_3) is shown in Figure 4.25. The power output of the DG for further increase in $P_{gridref}$ by 500W at T_4 is as shown in Figure 4.26. As demonstrated in Figure 4.26, the proposed controller is very effective in tracking the defined powers without any steady state errors and transient oscillations.

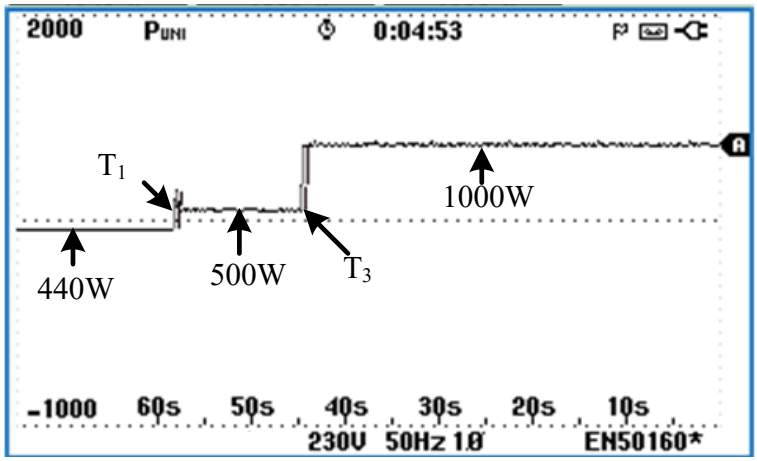

Figure 4.23 Power supplied by DG (P_{load}+P_{grid}) during transition.

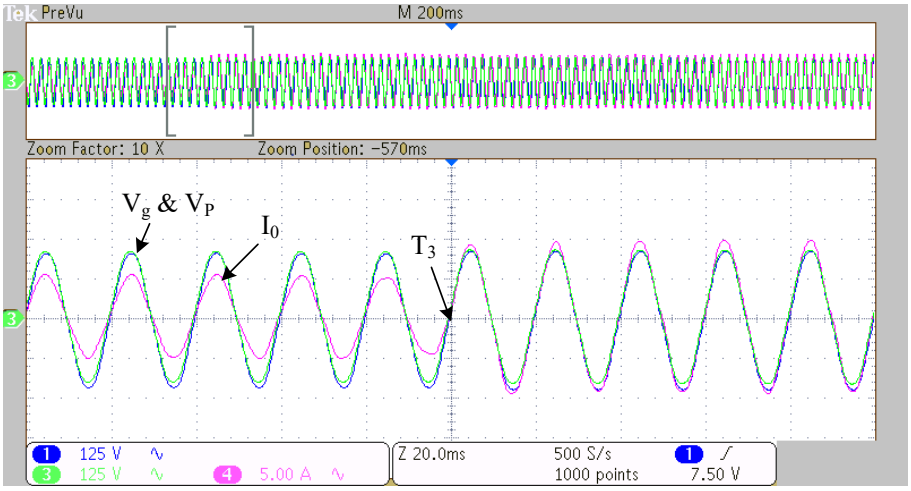

Figure 4.24 Voltage and current waveforms in grid connection mode with residential loads.

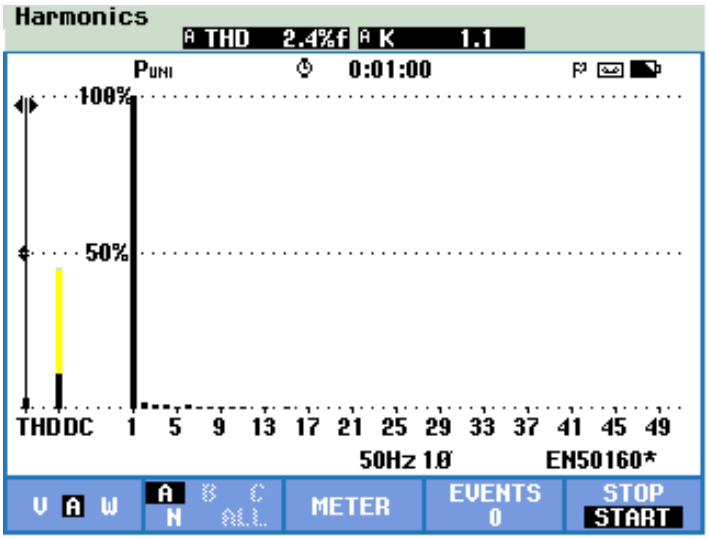

Figure 4.25 Current THD at DG supplying 500W to grid and residential load.

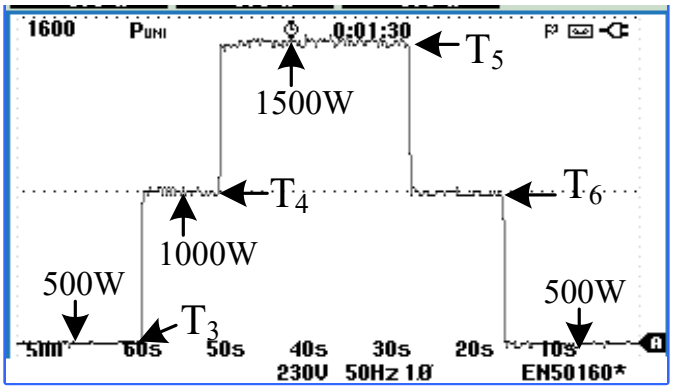

Figure 4.26 Power supplied by DG (P_{load}+P_{grid}).

Similarly, the grid power feeding is reduced by 500W at both the instants T_5 and T_6. After T_6, DG is supplying 0W to grid; however, it remains in grid connected mode while feeding only residential loads. At T_6, it is decided to bring back the DG into islanding mode, and it is controlled to deliver the residential loads at 130V. The inverter power output during the transition from grid connected mode to islanding mode is shown in Figure 4.27. Beyond T_7, as the DG is subjected to operate at 130V in islanding mode, against the grid voltage of 150V, there is a slight decrease in power fed by DG to the residential load as shown in Figure 4.27.

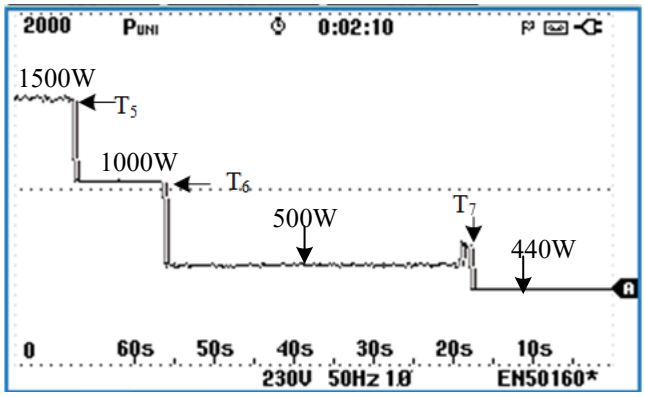

Figure 4.27 Transition of power from grid connected mode to islanding mode**.**

The voltage and current waveforms of DG prior to isolation are shown in Figure 4.28. At T_6 the power feeding to the grid is made zero, hence the DG is supplying only residential loads. However, the synchronization switch is still in closed position. Beyond T_6, once the grid feeding became zero, the synchronization switch is opened, hence islanding the DG. Figure 4.29 presents the DG voltage and current after it has been islanded. At T_7, the DG reference is changed to nominal voltage (130V, 48Hz) from grid voltage (150V, 50Hz).

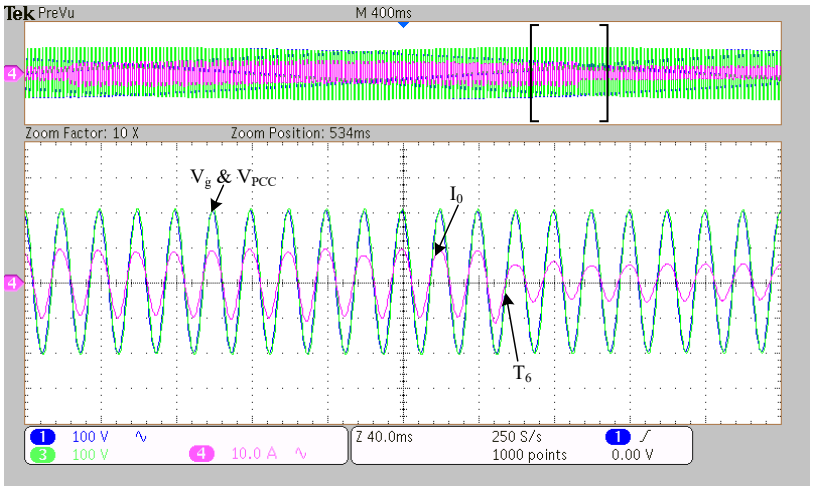

Figure 4.28 Voltage and current waveforms of DG prior to isolation.

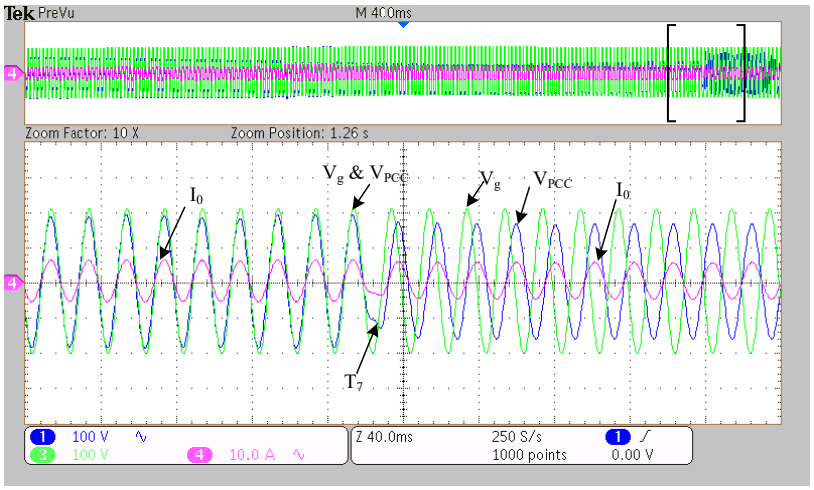

Figure 4.29 Voltages and current waveforms with DG supplying load at nominal voltage signal as reference.

The validated experimental results confirm the seamless transition of single phase DG between grid and off-grid modes while delivering the required powers, thereby achieving an extraordinary performance.

4.7 Summary

The proposed MPC integrated with SVM for the control of single phase DG to operate in grid connected mode as well as in off-grid modes is discussed in this chapter. A simple PLL free grid synchronization mechanism along with seamless transition control between grid connected mode and off-grid mode is developed. The developed MPC integrated with SVM is examined for delivering the set-point powers in grid connected mode, supplying the local load at the nominal voltage and frequency in off-grid mode and for smooth transitions between these modes. The designated performance of the developed control scheme for single phase DG is

confirmed through simulations, which are further validated on an experimental test bed. The performance of the controller proved to be very efficient in both the grid as well as off grid connected modes and the proposed methodology is free of weighting factors unlike seamless transition strategies using MPC references [34-43] [94].

The developed mechanism can be applied to the three phase DGs as well. The concept applied to three phase DG is discussed in the next chapter along with the parallel connected DGs.

Chapter 5

Model Predictive Control Based SVM Applied to Three Phase Distributed Generation System and Parallel Connected Distributed Generators

Chapter 5
Model Predictive Control Based SVM Applied to Three Phase Distributed Generation System and Parallel Connected Distributed Generators.

5.1 Introduction

Different seamless control strategies are discussed in literature; however, they either need multiple loops for grid synchronization or utilize weighting factors based methodology for the reduction of the steady state errors. However, a PLL free based mechanism is to be developed without the use of any weighting factors to reduce the computational burden as well as the complexity in tuning. The modeling of the three phase DG operated in grid connected mode along with the islanding mode is not discussed as the modeling will be the same as the DG discussed in the fourth chapter of the thesis.

In the latter half of this chapter, the DG operating in islanding mode with the proposed control strategy is applied to three phase multiple DGs and the operation is discussed with the simulation results. The problems that are presented due to their operation are addressed by a new control strategy with the simulation results followed by HIL results. The results are verified for seamless operation, adaptability and suitability when applied with the introduction of communication delays.

5.2 System Schematic Representation of the Three Phase DG

The detailed modeling is presented in chapter 4. Figure 5.1 presents a three phase DG connected with the grid based on the synchronization process discussed in chapter 4. The three phase DG can be connected to the grid or can be operated in islanding mode by means of a circuit breaker. The primary objective of any DG is to supply the loads with required amount of active and reactive powers and supply the extra amount of power to the grid. Here, the operating modes are of two types: grid and islanding modes. In the grid connected mode of operation, it is required to supply the grid with the amount of set point powers along with the load power. In islanding mode of operation, the DG should cater the loads with the amount of active and reactive powers, while maintaining the voltage and frequency at nominal values. The DG should also possess the seamless transition capability while transiting from one mode

to the other. Based on these objectives, a model has been developed in Matlab/Simulink and the simulation results are presented in section 5.3.

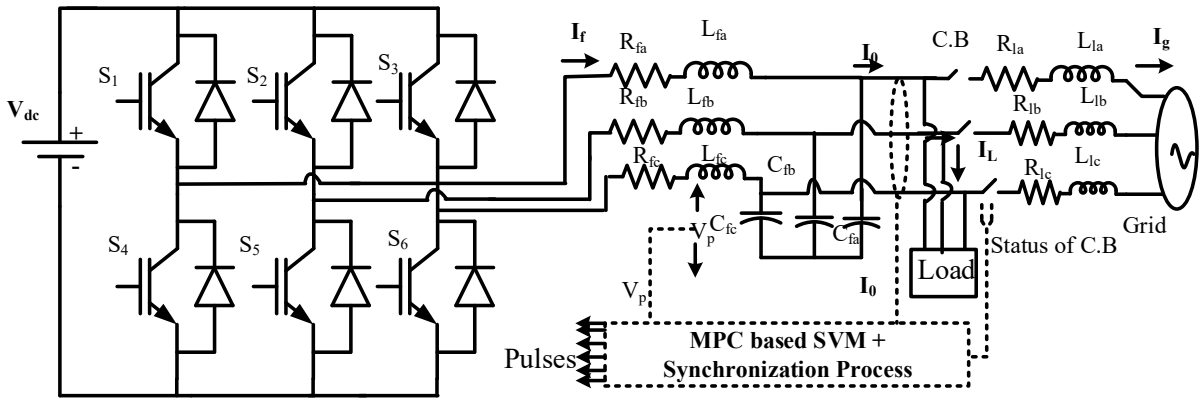

Figure 5.1 Schematic of MPC based SVM applied to three phase DG.

5.3 Simulation Results and Discussion

To verify the performance of the proposed MPC integrated with SVM, along with the seamless transition mechanism for three phase DG system, a simulation test bed is developed using Matlab/Simulink. Different case studies with all the possible operating conditions and modes are formulated and discussed in detail from Case-1 to 4, in the following subsections. The system parameters considered for simulation are presented in Table 5.1.

Table 5.1 System parameters for three phase DG

Parameters	Values
V_{dc}	750 V
V_P	(415-430) V (RMS)
V_{ref}	415 V
f_p	(49-50) Hz
R_f, L_f	0.15 Ω, 15 mH
C_f	50 μF
P	(5-15) kW
Q	(2.5-7.5) kVAr

5.3.1 Case -1: Grid connected mode

In this case, the DG is operated in grid connected mode with initial set-point of real and reactive powers ($P_{gridref}$ and $Q_{gridref}$) of 10,000W and 5,000VAr (0.9pf) respectively. The $P_{gridref}$ is changed to 15,000W (at 0.9pf) at 1 s, to examine the capability of the controller in tracking

the changes in reference powers. The Figure 5.2 shows that the developed controller is very effective in tracking the new reference powers within 0.02 s (one cycle) with zero steady state error and without any oscillations.

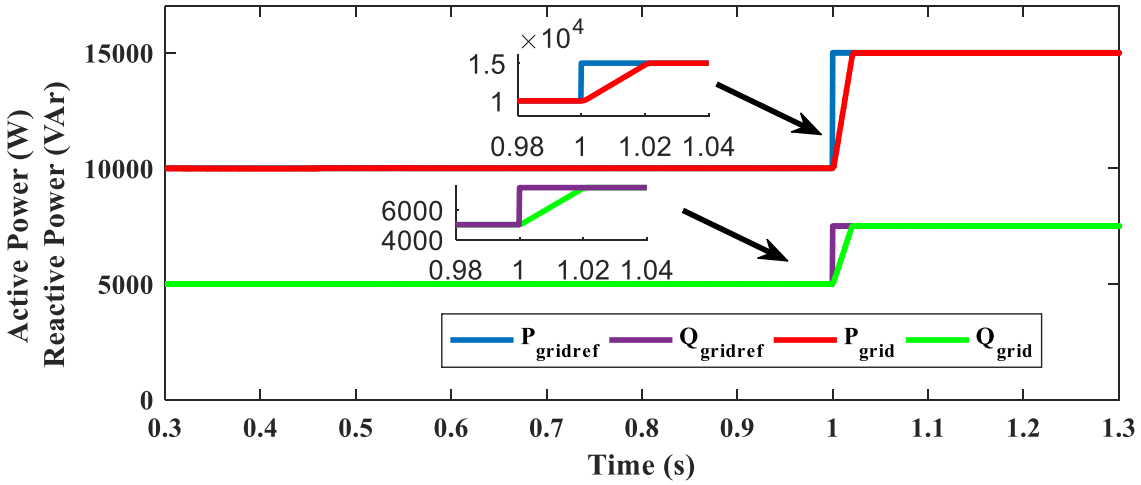

Figure 5.2 Active and reactive powers supplied to grid by DG.

5.3.2 Case-2: Islanding mode

In this case, the DG is operating in islanding mode with initial load of real and reactive powers of 5,000W and 2,500VAr (0.9pf) respectively. Since the DG is operating in off-grid mode, P_{grid} and Q_{grid} are zero. The P_{load} and Q_{load} are changed to 7,500W and 3,750VAr at 1 s, and performance of the designed controller in serving the varying load is shown in Figure 5.3.

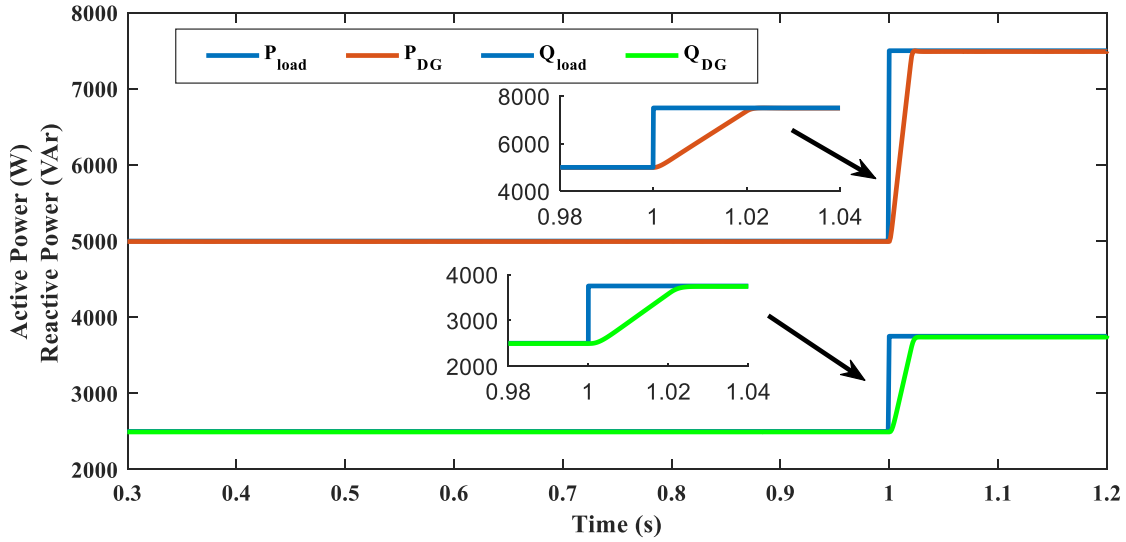

Figure 5.3 Active and reactive powers of residential loads supplied by DG.

As it is an islanding operation, to ascertain that the DG is operating at nominal voltage and frequency (415V rms, 50Hz), the output voltage, current and their total harmonic distortions (THDs) are plotted and shown in Figures 5.4 to 5.7.

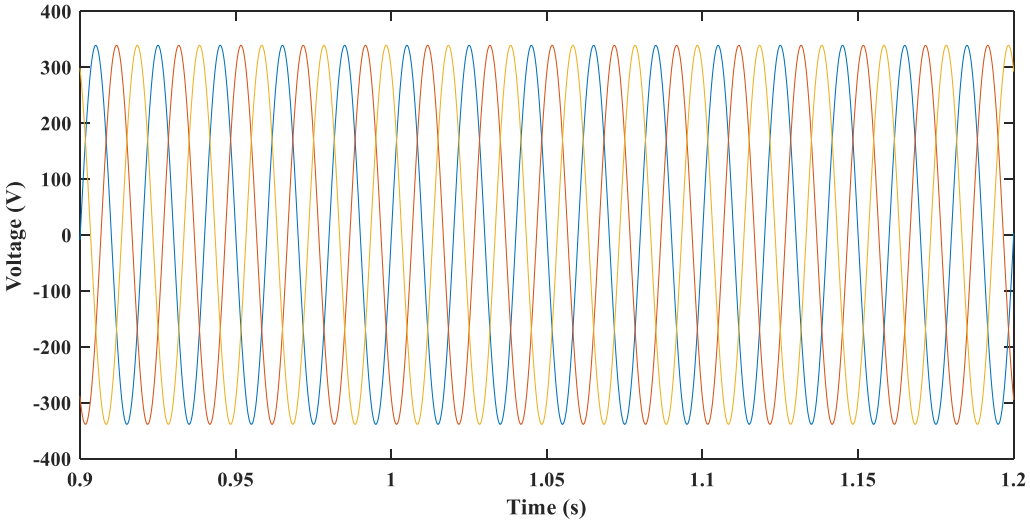

Figure 5.4 DG output voltage (V_P), feeding only residential loads.

The efficacy of the designed MPC for the single phase DG system operating in islanding mode, while feeding the changing local loads at nominal voltage and frequency with very minimum THDs can be ascertained from Figures 5.4 to 5.7. It can be observed from Figures 5.3, 5.4 and 5.6 that despite the change in connected load (P_{load} and Q_{load}) at 1 s, the inverter output voltage (V_P) is unaffected and remains there at nominal value all the time.

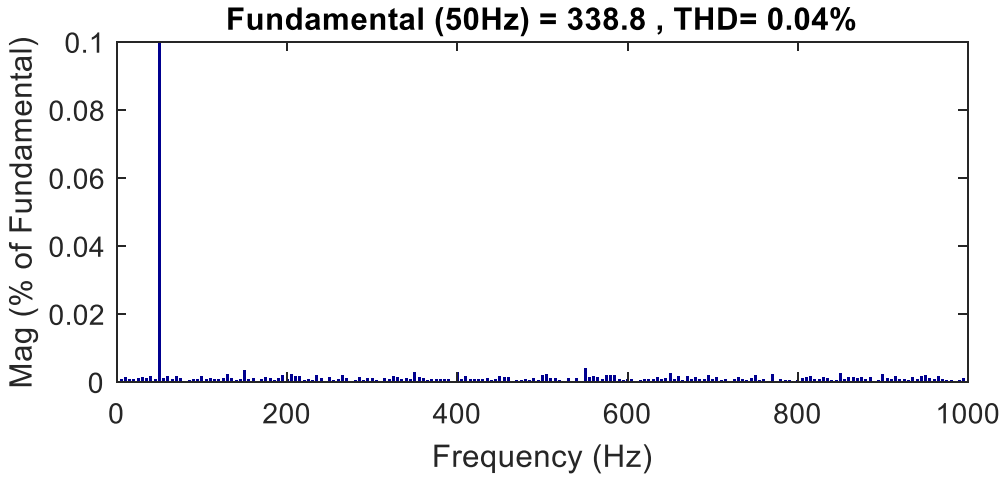

Figure 5.5 THD in voltage under off-grid mode, supplying only residential loads.

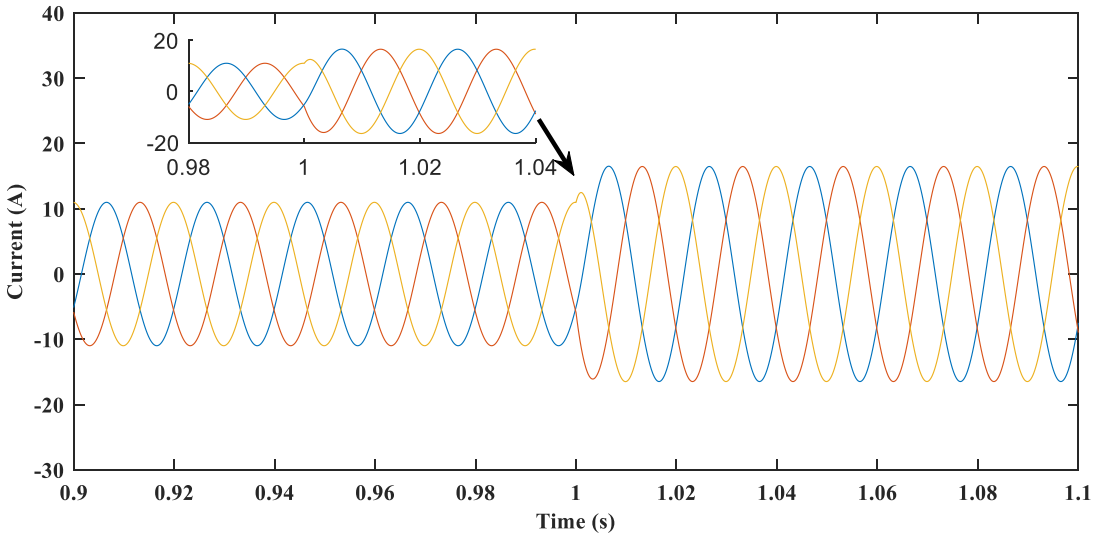

Figure 5.6 DG current in islanded mode, supplying only residential loads.

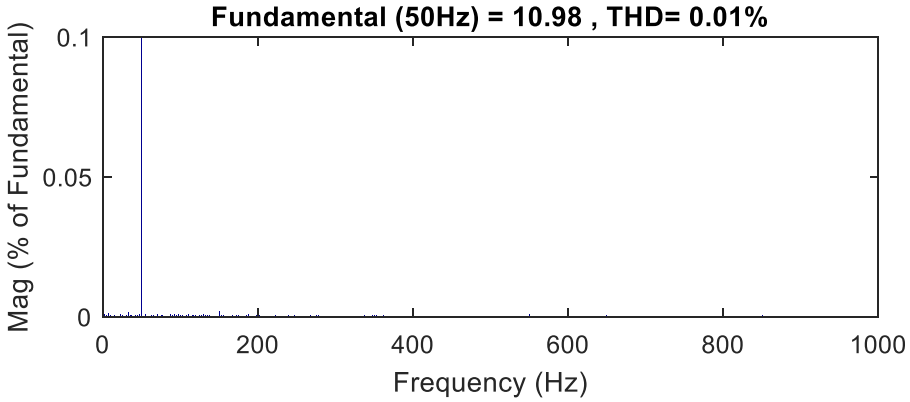

Figure 5.7 THD in current under off-grid mode, supplying only residential loads**.**

5.3.3 Case-3: Transition from grid to islanding mode

In this case, the DG is initially supplying real and reactive powers (P_{grid}, Q_{grid}) of 10,000W and 5,000VAr (0.9pf), to the grid. The residential loads (P_{load} and Q_{load}) connected in the system are considered to be 5,000W and 2,500VAr, respectively as shown in Figures 5.8 and 5.9.

At 1 s, it is considered that grid is isolated; hence the DG has to maintain its stability while feeding only the residential loads. Since the DG got isolated from grid at 1s, the grid feeding (P_{grid}, Q_{grid}) is becoming zero at 1 s, as depicted in Figures 5.8 and 5.9. Even though the grid feeding has become zero at 1 s, the DG output remains at 5,000W and 2,500VAr, which reveals the superior seamless transition performance of the proposed controller from grid connected mode to islanding mode.

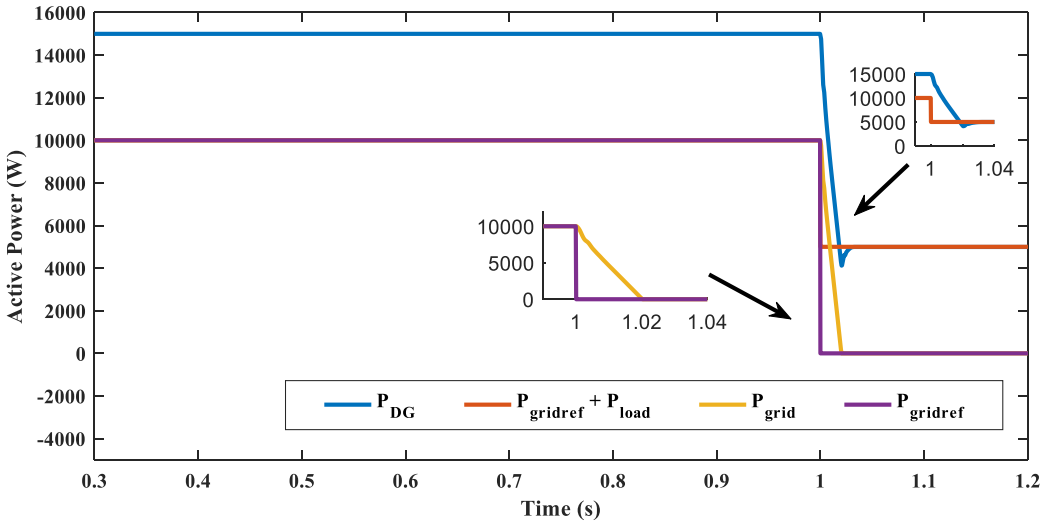

Figure 5.8 Active power during transition from grid mode to islanding mode.

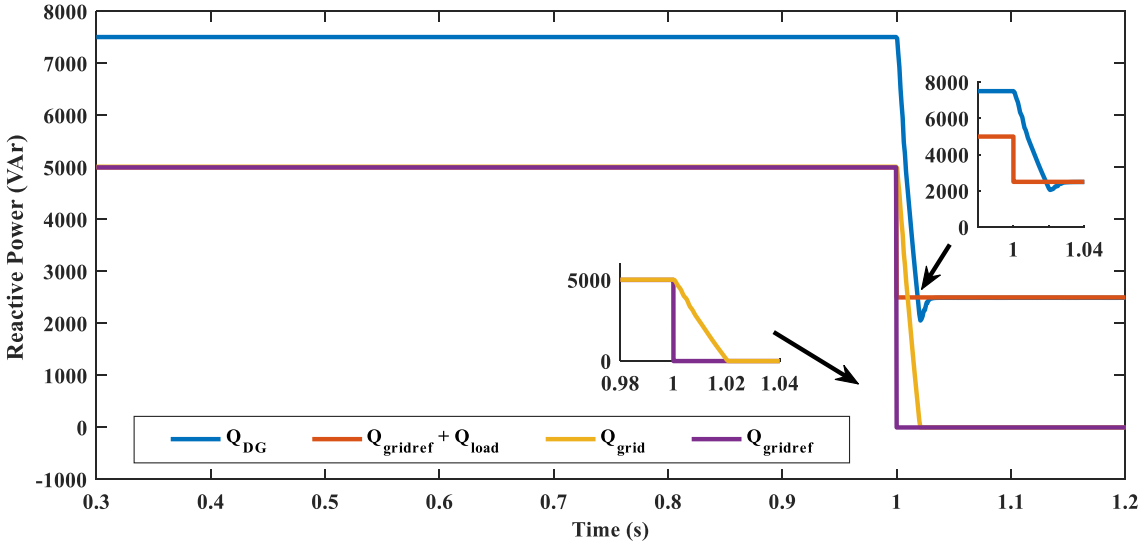

Figure 5.9 Reactive powers during transition from grid mode to islanding mode.

Figure 5.10 shows the DG output current which exhibits chattering/oscillations free response during, before and after the transition from grid connected mode to islanding mode in spite of change in system parameters resulting from isolation. Thus, it confirms the extraordinary performance of the proposed controller in achieving seamless transition. The current THD in islanding mode is 0.01% as shown in Figure 5.7 whereas the current THD in grid connected mode is 0.98% as shown in Figure 5.11.

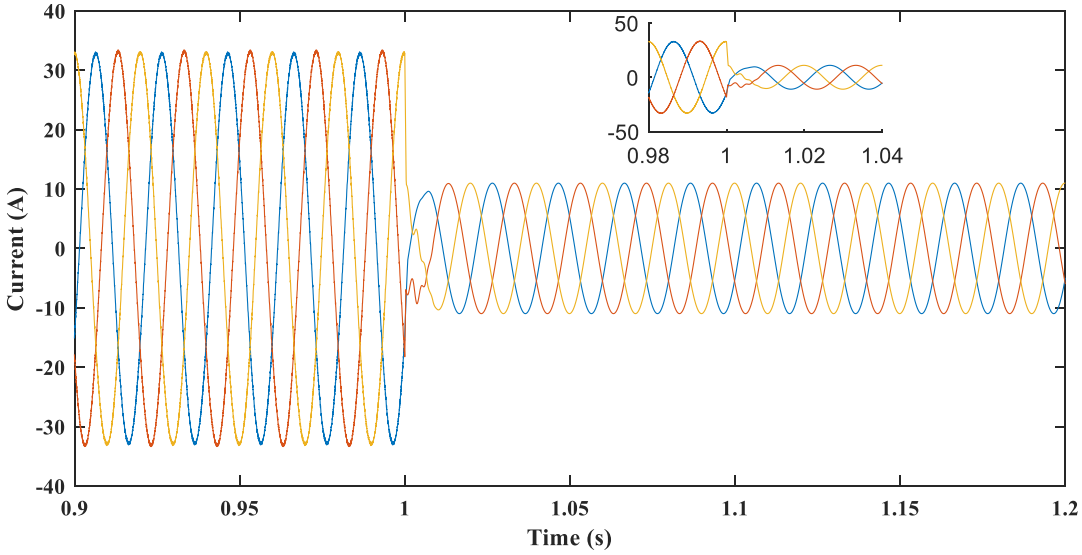

Figure 5.10 Current waveform for case-3.

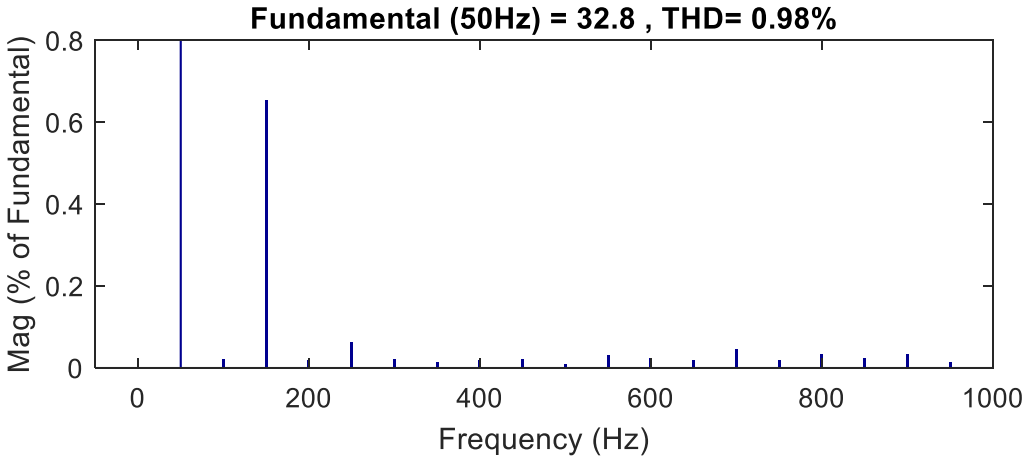

Figure 5.11 THD in current under grid connected mode.

5.3.4 Case-4: Transition from islanding to grid connected mode

The performance of the controller for resynchronization of DG with grid is studied in this case. As discussed in chapter 4, section 4.4, the DG is supplying initially its load at nominal voltage and frequency (415V (rms), 50Hz). At the same time the grid is operating at 430V (rms), 49Hz. It is decided that the DG which is operating in islanding mode is to be synchronized with the grid at 0.5 s. The grid synchronization algorithm is initiated at 0.5 s. It can be seen from Figure 5.12, that the DG voltage is having a magnitude difference of 15V (rms) and is almost 180^{o} out of phase with respect to the grid voltage at 0.5 s, that is the instant at which the grid synchronization algorithm is initiated. However, once the algorithm is initiated the DG has quickly adapted its voltage magnitude and frequency along with phase so as to match the grid references which is shown in Figure 5.12.

The counter (shown in Figure 4.5) is initiated at 0.501 s. To ensure the successful synchronization of DG with the grid, the counter is allowed to reach 1000 (= 20ms/20µs). As and when the counter reaches 1000, the MPC is toggled from off-grid mode to grid connected mode and the synchronization switch is turned ON. The power outputs of DG are shown in Figure 5.13. Since the DG is operating in islanding mode till 0.501 s, it is supplying the local load of 5,000W and 2,500VAr respectively. As the DG reference voltage has changed from nominal voltage (415V) to grid voltage (430V) at 0.5 s, the local loads start absorbing an extra power of 367.977 W ($P = V^2/R$) from 0.5 s shown in Figure 5.13. Even after synchronization at 0.501 s, the DG power remains same as the grid feeding references are kept at zero till 1.1 s. At 1.1 s, as the grid feeding references are changed to 10,000W and 5,000VAr, the DG supplies a power of 10,367.977 W (local load + grid feeding) and 5,000VAr (0.9pf) as depicted in Figure 5.13.

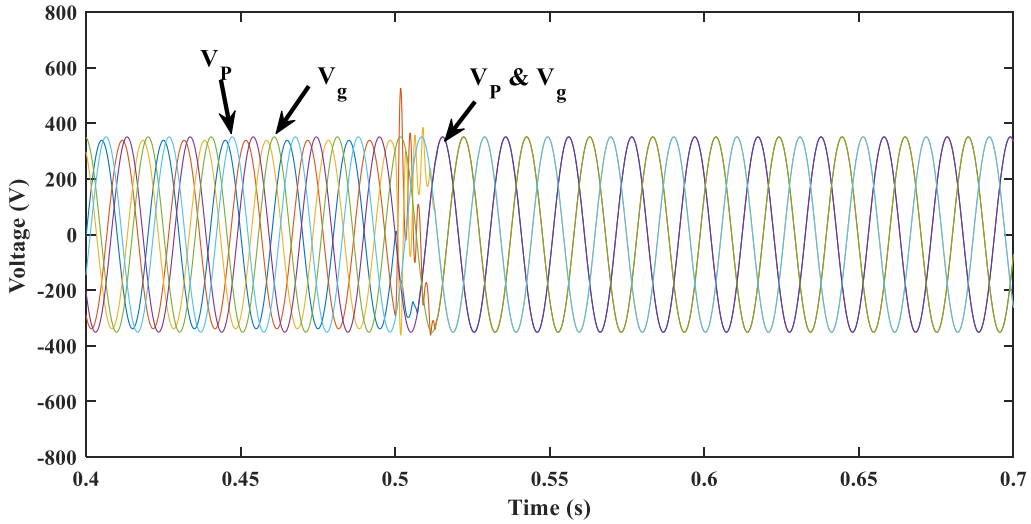

Figure 5.12 PCC and grid voltages before and after synchronization.

The DG current during different operating conditions is shown in Figure 5.14. It can be seen from Figures 5.13 and 5.14 that the moment the DG references are changed to grid references, the DG output voltage and current change their magnitude, frequency as well as phase according to the grid references from 0.5 s. Considering all the cases, the proposed MPC is exhibiting excellent performance in all the operating conditions and is also delivering extraordinary seamless response during the transitions between different modes of operation.

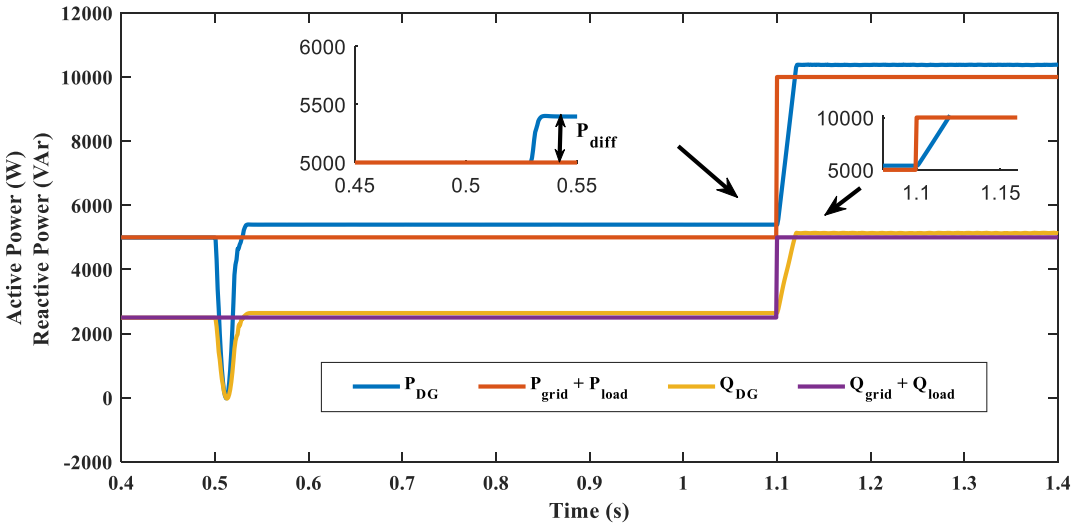

Figure 5.13 Active and reactive powers for case-4.

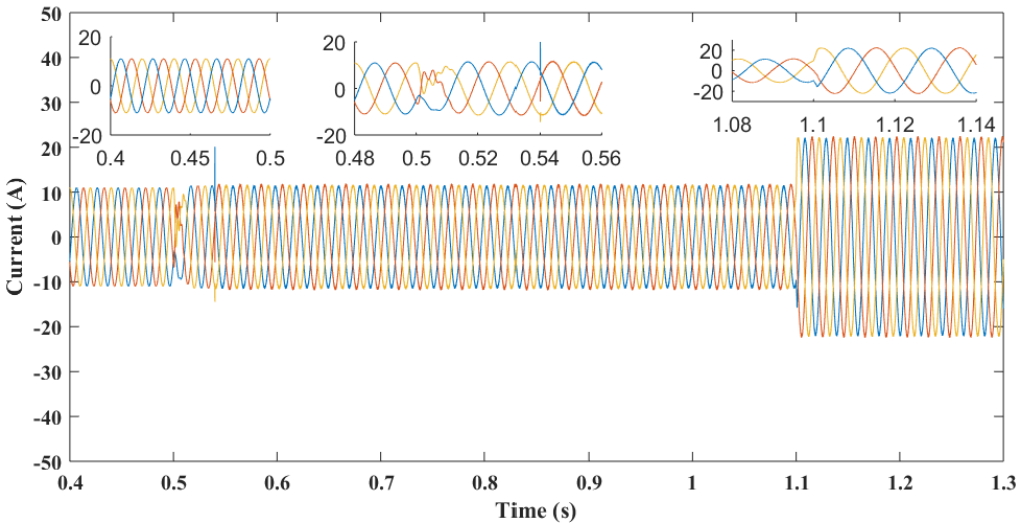

Figure 5.14 Current waveform for case-4.

From the simulation results, it can be concluded that the proposed controller is exhibiting superior seamless transition as well as suitable for systems with home appliances and the grid power injection can be adopted for the roof top solar PV based systems. Though the performance of the controller is very efficient in both the modes, the controller is to be tested for the parallel connected operation of DGs which improves the reliability and presents various problems that need to be addressed. So the parallel connected operation of DGs is a very significant problem which needs to be addressed. For the parallel connected operation of DGs, a crucial attention is necessary when they are operating in off grid operation. Therefore, the latter half of this chapter discusses the issues faced by the proposed controller when the loads are remotely placed and they need to adjust to PCC voltage.

5.4 Parallel Connected Operation of DGs

The parallel connected operation of DGs along with the problems associated with the DGs are discussed in this section. Figure 5.15 presents multiple DGs connected to PCC with line parameters. Figure 5.16 presents a three phase DG connected to utility interface which can be either grid or islanding mode of operation.

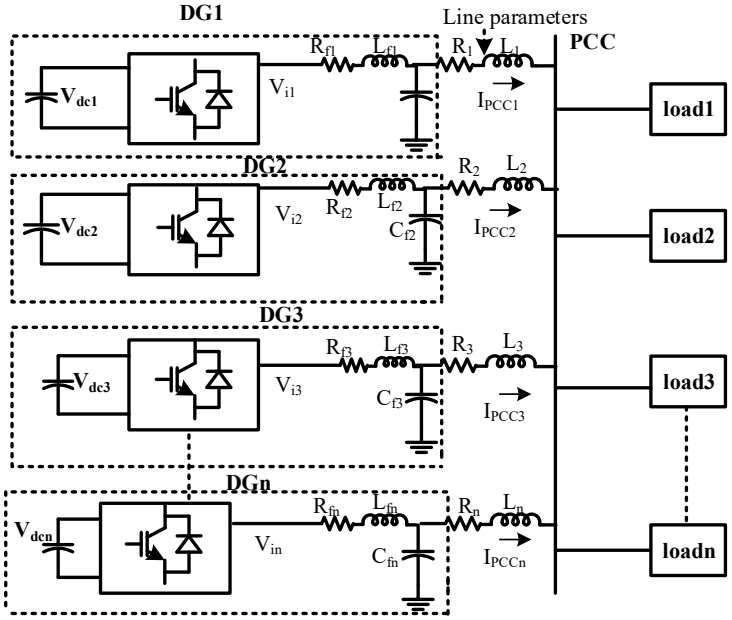

Figure 5.15 Single line diagram of multiple DGs connected to PCC.

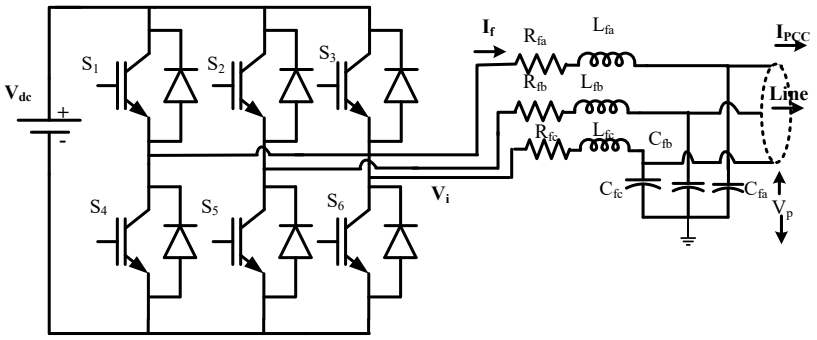

Figure 5.16 A three phase DG connected to utility interface.

5.4.1 Problem Formulation

From Figure 5.16, applying Kirchhoff's voltage law across the loop, the voltages can be represented as shown in (5.1).

$$V_i = I_f R_f + L_f \frac{dI_f}{dt} + V_p \tag{5.1}$$

Where V_i is the inverter output voltage, I_f being filter current, R_f the filter resistance, L_f, C_f being the filter inductor and capacitor, V_P is the voltage at the DG end, I_{PCC} is the current transferred to load from the DG end.

$$I_{PCC} = I_f - C_f \frac{dV_p}{dt} \tag{5.2}$$

$$V_p = V_{PCC} + I_{PCC} R_1 + L_1 \frac{dI_{PCC}}{dt} \tag{5.3}$$

Substituting (5.2) in (5.3) results in

$$V_p = V_{PCC} + \left(I_f - C_f \frac{dV_p}{dt} \right) R_1 + L_1 \frac{dI_{PCC}}{dt} \tag{5.4}$$

Simplifying (5.4), results in (5.5)

$$V_p = V_{PCC} + I_f R1 - R_1 C_f \frac{dV_p}{dt} + L_1 \frac{dI_f}{dt} - L_1 C_f \frac{d^2 V_p}{dt^2} \tag{5.5}$$

Substituting (5.1) in (5.5) and on rearranging

$$\frac{d^2 V_p}{dt^2} + \frac{R_1}{L_1} \frac{dV_p}{dt} + \frac{V_p}{C_f} \left(\frac{1}{L_1} + \frac{1}{L_f} \right) = \frac{V_i}{L_f C_f} + \frac{V_{PCC}}{L_1 C_f} + \frac{I_f}{C_f} \left(\frac{R_1}{L_1} - \frac{R_f}{L_f} \right) \tag{5.6}$$

Discretizing (5.6) results in

$$\frac{V_p(k+2) - 2V_p(k+1) + V_p(k)}{T_s^2} + \frac{R_1}{L_1} \left(\frac{V_p(k+1) - V_p(k)}{T_s} \right) + \frac{V_p(k)}{C_f} \left(\frac{1}{L_1} + \frac{1}{L_f} \right) = \begin{pmatrix} \frac{V_i(k)}{L_f C_f} + \frac{V_{PCC}(k)}{L_1 C_f} + \\ \frac{I_f(k)}{C_f} \left(\frac{R_1}{L_1} - \frac{R_f}{L_f} \right) \end{pmatrix} \tag{5.7}$$

Simplifying and rearranging (5.7) results in

$$V_p(k+2) = \begin{pmatrix} \frac{V_i(k) T_s^2}{L_f C_f} + \left(2 - \frac{R_1 T_s}{L_1} \right) V_p(k+1) + \frac{V_{PCC}(k) T_s^2}{L_1 C_f} + \left(\frac{R_1}{L_1} - \frac{R_f}{L_f} \right) \frac{I_f(k) T_s^2}{C_f} \\ + \left(\frac{R_1 T_s}{L_1} - 1 - \frac{T_s^2}{L_1 C_f} - \frac{T_s^2}{L_f C_f} \right) V_p(k) \end{pmatrix} \tag{5.8}$$

From (5.8), it is evident that the voltage that needs to be developed to meet the loads at the PCC is dependent on the line parameters and the V_{PCC}. The method of adaptive virtual impedance [96 - 97] can be adopted and adjusting the values of the line parameters, the value of the voltage can be evaluated. The procedure of adaptive virtual impedance will be tedious if the load is either increased or decreased, it needs adjustment in voltage to compensate voltage drop. Therefore, a control strategy is developed by a combination of droop and adaptive secondary voltage control. The control strategy involves two loops, which were discussed in section 5.4.2 and section 5.4.3. The comparison of the developed method with the single loop method is be discussed in section 5.4.4.

5.4.2 Power Based Control Strategy

A DG with an output voltage of $V_s\angle\delta$ is connected to the PCC ($V_{PCC}\angle 0$) as shown in Figure 5.17.

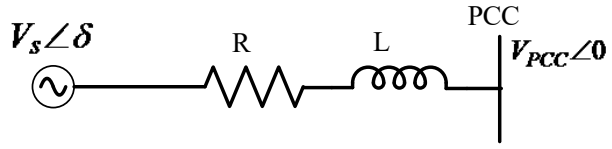

Figure 5.17 A single DG connected to PCC.

For the generalized power control strategy, a DG with output voltage with a distributed line impedance (Z) can be expressed as

$$S = P + jQ = V_{PCC} I^*_{PCC} \tag{5.9}$$

$$I_{PCC} = \left(\frac{V_s\angle\delta - V_{PCC}\angle 0}{R + jX} \right) \tag{5.10}$$

Substituting I_{PCC} in (5.9) and on simplifying, the resultant equation will be

$$P = \frac{V_{PCC}(V_s Cos\delta - V_{PCC})Cos\theta}{Z} + \frac{V_s Sin\delta V_{PCC} Sin\theta}{Z} \tag{5.11}$$

$$Q = \frac{V_{PCC}(V_s Cos\delta - V_{PCC})Sin\theta}{Z} - \frac{V_s Sin\delta V_{PCC} Cos\theta}{Z} \tag{5.12}$$

Where $Cos\theta = \frac{R}{\sqrt{R^2 + X^2}}; Sin\theta = \frac{X}{\sqrt{R^2 + X^2}}$

$Z = \sqrt{R^2 + X^2};$

Simplifying (5.11) and (5.12) the resultant will be

$$P = \frac{V_{PCC}V_s Cos(\delta - \theta)}{Z} - \frac{V_{PCC}{}^2 Cos\theta}{Z} \tag{5.13}$$

$$Q = \frac{V_{PCC}V_s Sin(\theta - \delta)}{Z} - \frac{V_{PCC}{}^2 Sin\theta}{Z} \tag{5.14}$$

Also $V_s = V_{PCC} + \Delta V$;

In case of the transmission line, (*X/R*) ratio is high, $Cos\theta \approx 1; Sin\theta \approx \theta$ whereas for the distribution system (*X/R*) ratio is always less than or equal to 1. Hence approximation cannot be done as the case for the transmission line. Extending the case for two DGs, the single line diagram for the aforesaid case is shown in Fig. 5.18. The case shown in Fig. 5.18 will have the line parameters with distances considered as the line inductance (L_1) and line resistance (R_1) of DG1 to PCC and the line resistance (R_2) and the line inductance (L_2). The voltages of DG1, DG2 are V_{S1}, V_{S2} and with angles being δ_1 and δ_2. Considering the case of two DGs and on assuming that the frequency and voltage is maintained at nominal values, the active and reactive powers transferred from DG1 to the load can be written as

$$P_1 = \frac{V_{PCC}(V_{s1}Cos\delta_1 - V_{PCC})Cos\theta}{Z_1} + \frac{V_{s1}V_{PCC}Sin\delta_1 Sin\theta}{Z_1} \tag{5.15}$$

$$Q_1 = \frac{V_{PCC}V_{s1}Sin(\theta - \delta_1)}{Z_1} - \frac{V_{PCC}{}^2 Sin\theta}{Z_1} \tag{5.16}$$

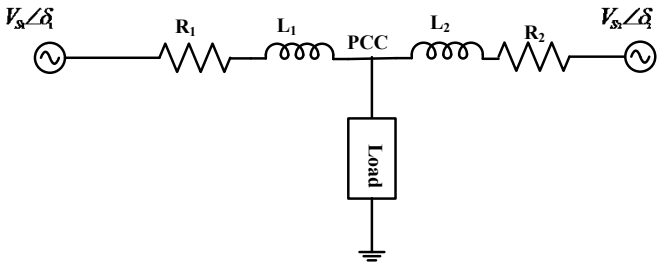

Figure 5.18 Two DGs connected to point of common coupling (PCC).

The active and reactive powers transferred from DG2 to the load can be written as

$$P_2 = \frac{V_{PCC}(V_{s2}Cos\delta_2 - V_{PCC})Cos\theta}{Z_2} + \frac{V_{s2}V_{PCC}Sin\delta_2 Sin\theta}{Z_2} \tag{5.17}$$

$$Q_2 = \frac{V_{PCC}V_{s2}Sin(\theta - \delta_2)}{Z_2} - \frac{{V_{PCC}}^2 Sin\theta}{Z_2} \tag{5.18}$$

The power sharing between the two DGs are discussed with four cases, i) if the DGs are of the same capacity and the distance between the DGs to the load is same. ii) The DGs of different capacity and the distance between the DGs to the load is same. iii) The DGs of the same capacity and the distance between the DGs to the load is different and iv) The distance between the DGs to the load as well as the DGs capacity are both different. These four cases are taken to test the versatility of the DGs and their self-adaptive capability. For case (i), the distance between the DG to the load is same. If both the distances are same, the line parameters are equal i.e., impedance(Z) and the phase angle(θ) will also be equal. Since the DGs capacity is equal, the voltage drop will be same as impedance is equal for the identical distance to PCC from DGs.

$$P_1 = P_2 = \frac{V_{PCC}(V_s Cos\delta - V_{PCC})Cos\theta}{Z} + \frac{V_s V_{PCC} Sin\delta Sin\theta}{Z} \tag{5.19}$$

$$Q_1 = Q_2 = \frac{V_{PCC}V_s Sin(\theta - \delta)}{Z} - \frac{{V_{PCC}}^2 Sin\theta}{Z} \tag{5.20}$$

For the considered load active power (P_L) and reactive power (Q_L).

$$\left.\begin{aligned} P_1 + P_2 &= P_L \\ Q_1 + Q_2 &= Q_L \end{aligned}\right\} \tag{5.21}$$

Since $P_1 = P_2$, implies that $\left.\begin{aligned} P_1 = P_2 &= \frac{P_L}{2} \\ Q_1 = Q_2 &= \frac{Q_L}{2} \end{aligned}\right\}$.

For the case (ii), the DGs are of different capacities which indicate that V_s and δ for the DGs are not equal. As the distances are equal, the line parameters are same. So, in this case, the powers from the DGs towards the load is shown in (5.22) - (5.25).

$$P_1 = \frac{V_{PCC}(V_{s1} Cos\delta_1 - V_{PCC})Cos\theta}{Z} + \frac{V_{s1} V_{PCC} Sin\delta_1 Sin\theta}{Z} \tag{5.22}$$

$$Q_1 = \frac{V_{PCC}V_{s1}Sin(\theta-\delta_1)}{Z} - \frac{{V_{PCC}}^2 Sin\theta}{Z} \tag{5.23}$$

$$P_2 = \frac{V_{PCC}(V_{s2}Cos\delta_2 - V_{PCC})Cos\theta}{Z} + \frac{V_{s2}V_{PCC}Sin\delta_2 Sin\theta}{Z} \tag{5.24}$$

$$Q_2 = \frac{V_{PCC}V_{s2}Sin(\theta-\delta_2)}{Z} - \frac{{V_{PCC}}^2 Sin\theta}{Z} \tag{5.25}$$

From (5.22) and (5.24) and (5.23) and (5.25) the difference in powers can be written as

$$P_1 - P_2 = \left(\frac{V_{PCC}(V_{s1}Cos\delta_1 - V_{s2}Cos\delta_2)Cos\theta}{Z} + \frac{V_{PCC}(V_{s1}Sin\delta_1 - V_{s2}Sin\delta_2)Sin\theta}{Z}\right) \tag{5.26}$$

$$Q_1 - Q_2 = \frac{V_{PCC}V_{s1}Sin(\theta-\delta_1)}{Z} - \frac{V_{PCC}V_{s2}Sin(\theta-\delta_2)}{Z} \tag{5.27}$$

Solving (5.21), (5.26) and (5.27)

$$\begin{aligned} P_1 &= \frac{P_L}{2} + \left(\frac{V_{PCC}(V_{s1}Cos\delta_1 - V_{s2}Cos\delta_2)Cos\theta}{2Z} + \frac{V_{PCC}(V_{s1}Sin\delta_1 - V_{s2}Sin\delta_2)Sin\theta}{2Z}\right); \\ P_2 &= \frac{P_L}{2} - \left(\frac{V_{PCC}(V_{s1}Cos\delta_1 - V_{s2}Cos\delta_2)Cos\theta}{2Z} + \frac{V_{PCC}(V_{s1}Sin\delta_1 - V_{s2}Sin\delta_2)Sin\theta}{2Z}\right) \end{aligned} \tag{5.28}$$

$$\begin{aligned} Q_1 &= \frac{Q_L}{2} + \left(\frac{V_{PCC}V_{s1}Sin(\theta-\delta_1)}{2Z} - \frac{V_{PCC}V_{s2}Sin(\theta-\delta_2)}{2Z}\right) \\ Q_2 &= \frac{Q_L}{2} - \left(\frac{V_{PCC}V_{s1}Sin(\theta-\delta_1)}{2Z} - \frac{V_{PCC}V_{s2}Sin(\theta-\delta_2)}{2Z}\right) \end{aligned} \tag{5.29}$$

From (5.28) and (5.29), it is evident that, if the load is placed equidistant from the two DGs, the sharing between the two DGs depend on the two power rating capacities of the DG. If both the capacities are same, then the case will be same as the first case which was discussed earlier. For the remaining two cases, the load shared between the two DGs are presented as shown in (5.15) – (5.18).

The variation of the frequency and voltage at the PCC resembles like that of the droop control strategy of the synchronous generator and can be shown as:

$$\omega_0 = \omega_{ref} - m(P_G - P_0) \tag{5.30}$$

$$E_0 = E_{ref} - n(Q_G - Q_0) \tag{5.31}$$

Where ω_{ref} and E_{ref} are the nominal frequency and voltage magnitude respectively, P_0 and Q_0 are the measured active and reactive powers. P_G and Q_G are the active and reactive power capacities of DG and ω_0 and E_0 are the frequency and voltage magnitude respectively. For the droop curves of P-ω and Q-E, m and n are the positive slopes.

Integrating (5.30), the equation results in

$$\delta_0 = \omega_{ref} t - \int m\left(P_G - P_0\right) dt \tag{5.32}$$

For the two DGs the different frequency and the voltage will depend on their power capacities. If power capacities are same, then (5.30) and (5.31) will be the same for both the DGs or else the equations can be written as shown below.

$$\begin{aligned} \omega_{01} &= \omega_{ref} - m_1(P_{1G} - P_1); \\ \omega_{02} &= \omega_{ref} - m_2(P_{2G} - P_2) \end{aligned} \tag{5.33}$$

$$\begin{aligned} E_{01} &= E_{ref} - n_1(Q_{1G} - Q_1); \\ E_{02} &= E_{ref} - n_2(Q_{2G} - Q_2) \end{aligned} \tag{5.34}$$

Where P_{1G}, Q_{1G} and P_{2G}, Q_{2G} are the rated generating active and reactive power capacities and m_1, n_1 and m_2, n_2 are the positive slopes of the respective DGs. The voltage drops due to the line impedances must be considered so that the voltage to be developed at the generating end should be sufficient to supply the load thereby eliminating the steady-state errors in powers.

$$\Delta V = I_{PCC}\left(R + jX\right) \tag{5.35}$$

From (5.9), I_{PCC} can be written as

$$I_{PCC} = \left(\frac{P + jQ}{V_{PCC}}\right)^* = \left(\frac{P - jQ}{V_{PCC}}\right) \tag{5.36}$$

Substituting (5.36) in (5.35) results in

$$\begin{aligned}\Delta V &= \left(\frac{P-jQ}{V_{PCC}}\right)(R+jX) \\ &= \left(\frac{PR+QX}{V_{PCC}}\right)+j\left(\frac{PX-QR}{V_{PCC}}\right)\end{aligned} \tag{5.37}$$

From (5.37), considering the real part then

$$|\Delta V| = \sqrt{\left(\frac{PR+QX}{V_{PCC}}\right)^2+\left(\frac{PX-QR}{V_{PCC}}\right)^2} \tag{5.38}$$

$$\psi_1 = \tan^{-1}\left(\frac{PX-QR}{PR+QX}\right) \tag{5.39}$$

For the increase in load, the voltage must be developed at the generating end to prevent steady state errors in the powers at loads. The voltage drop ΔV increases with the increase in load. So, the voltage that needs to be developed at the generating end must be compensating the voltage drop to maintain the PCC voltage at nominal voltage (415 V r.m.s).

5.4.3 Proposed Control Strategy

The proposed control strategy predominantly comprises two loops. The primary control employs droop control and the secondary control for the restoration of frequency and voltage at PCC. The droop control determines the power to be shared among different DGs to maintain the PCC voltage and frequency at nominal values whereas the adaptive secondary voltage provides the information of the voltage drop to be compensated to restore the PCC voltage and frequency to nominal values if the primary control fails. The proposed control strategy is presented in Figure 5.19. The primary and secondary control for a single DG is shown in Figure 5.19 (a) and Figure 5.19 (b) presents the proposed modified droop control. The primary control for a single DG is developed based on the droop control which is free of the conventional d-q transformations.

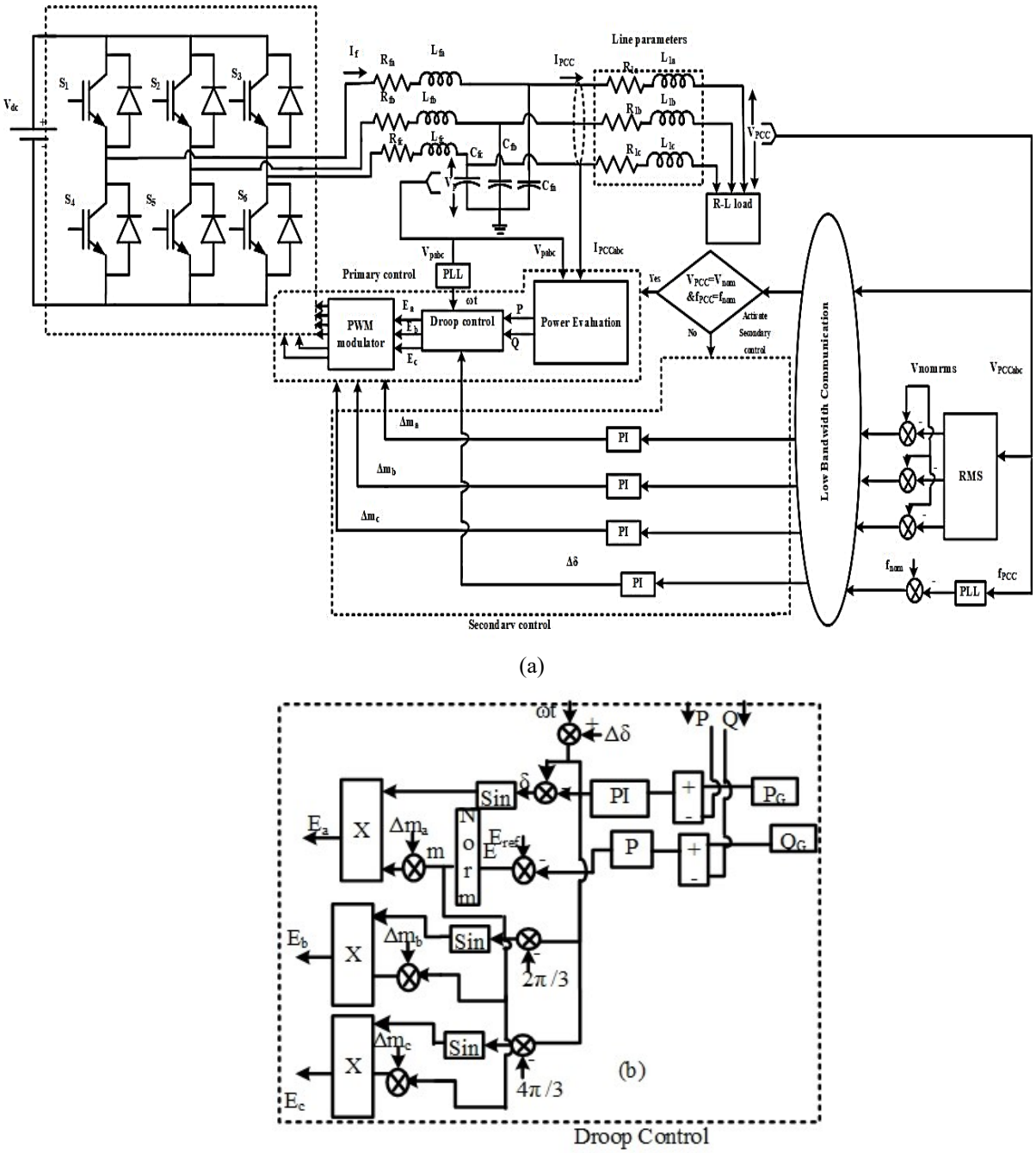

Figure 5.19 Proposed Control strategy. (a). Primary and secondary control for a single DG. (b). Inner view of droop control.

The power control based approach is followed rather than the conventional outer current loop and inner voltage loop based approach. The control strategy is developed based on (5.31) and (5.32) for the control of active and reactive powers respectively. Equation (5.31) describes the voltage control to supply the loads with the required amount of active and reactive powers, whereas (5.32) presents the control of frequency to meet the load demand. Based on (5.32), a PI controller is considered instead of an integrator whereas for the control of voltage from

(5.31), a proportional controller is considered. Figure 5.19(b) presents the block diagram of droop control consisting of the inputs i.e., powers evaluated and the phase angle sensed from the DG. The primary control also consists of two inputs from the secondary control Δm and $\Delta\delta$ to be incorporated for the generation of switching pulses using pulse width modulator (PWM). Till the activation of the secondary control, the values of the inputs from secondary control are zero.

From Figure 5.19 (b), the values of $\Delta\delta$, Δm, δ and E can be written as

$$\Delta\delta = \left(f_{nom} - f_{PCC}\right)\left(K_{psf} + \frac{k_{Isf}}{s}\right) \tag{5.40}$$

Where f_{nom} is the nominal frequency (50 Hz), f_{pcc} is the frequency *at PCC*. K_{psf}, k_{Isf} are the gains of PI controller in secondary control for frequency.

$$\Delta m = \left(K_{psv} + \frac{k_{Isv}}{s}\right)\left(V_{nomrms} - V_{pccrms}\right) \tag{5.41}$$

Where K_{psv}, k_{Isv} are the PI control gain parameters in secondary control for voltage, V_{nomrms}, V_{PCCrms} are the rms values of nominal voltage and PCC voltage respectively.

$$\delta = \left(\omega t + \Delta\delta\right) - \left(P_G - P\right)\left(K_P + \frac{K_I}{s}\right) \tag{5.42}$$

$$E = E_{ref} - K_{pv}\left(Q_G - Q\right) \tag{5.43}$$

where $\Delta\delta$=0, till the secondary control is activated, E_{ref}= 415 V (rms), K_P *and* K_I are gains of PI control parameters whereas K_{pv} is the gain of proportional controller for voltage of primary control. The obtained value in (5.43) is normalized and the output after normalization is treated as modulation index m, i.e., $m=E/E_{ref}$. The values of E_a, E_b, E_c can be represented in (5.44) as

$$\begin{aligned} E_a &= \left(m + \Delta m_a\right)\sin\delta \\ E_b &= \left(m + \Delta m_b\right)\sin\delta \\ E_c &= \left(m + \Delta m_c\right)\sin\delta \end{aligned} \tag{5.44}$$

Where the values of Δm_a, Δm_b, Δm_c are equal to zero till the activation of secondary control. After the generation of the modulation signals (E_a, E_b, E_c), the modulation signals are compared with the carrier to generate switching pulses to DG. The system parameters considered for simulation as well as HIL are presented in Table 5.1.

Table 5.2 System parameters

Parameters	**DG1**	**DG2**
V_{dc}	750 V	750 V
V_{PCC}	415 V (RMS)	415 V (RMS)
f_{nom}	50 Hz	50 Hz
K_P	$2x10^{-4}$ Hz/W	$4x10^{-4}$ Hz/W
K_I	$2x10^{-3}$ Hz/W	$4x10^{-3}$ Hz/W
K_{pv}	$5x10^{-4}$ V/VAr	$5x10^{-4}$ V/VAr
K_{Psv}	0.001	0.001
K_{Isv}	0.5	0.6
K_{psf}	0.001	0.001
K_{Isf}	0.2	0.3
P_G	20 kW/30 Kw	20 kW
L_f	15 mH	15 mH
C_f	50 µF	50 µF
Line parameters *R, L*	0.5 Ω, 1 mH	0.25 Ω, 0.5 mH
P_{load}, Q_{load}	(10-15) kW, (5-7.5) kVAr	

5.4.4 Simulation Results and Discussions

To verify the performance of the developed control strategy, the simulation results for the various cases are done in MATLAB/ Simulink are presented.

5.4.4.1 Case-1: DG with equal capacities and line parameters

For Case-1, the DG capacities are equal and the distance between the load to the DGs (i.e., the line parameters) is equal. Initially, the load is 10kW and 5kVAr respectively. At 0.6 s, the load is increased by 5kW and 2.5kVAr to test the performance of the controller. The load powers at PCC and the powers shared by two DGs are shown in Figure 5.20. As the line parameters are equal and the power capacities are same, the active and reactive powers shared by two DGs are equal as shown in Figures 5.20 and 5.21. The voltage and current at PCC are shown in Figures 5.22 and 5.23 respectively.

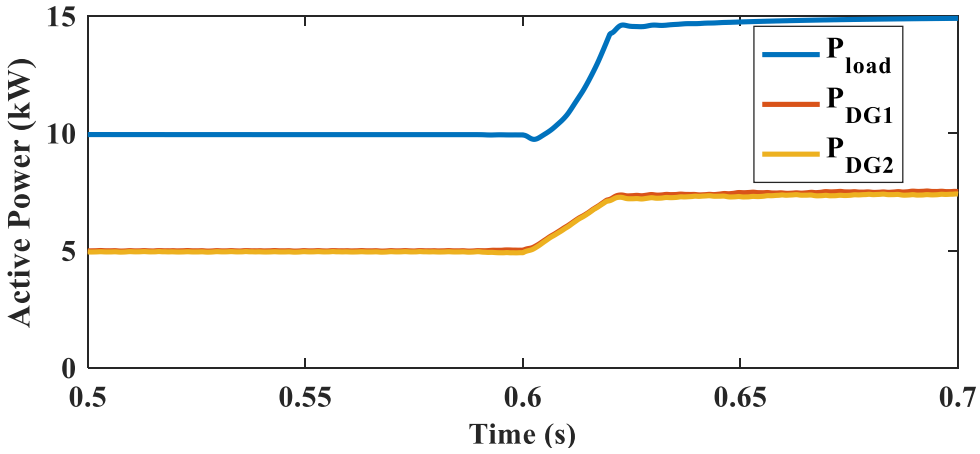

Figure 5.20 Active Powers shared by DGs.

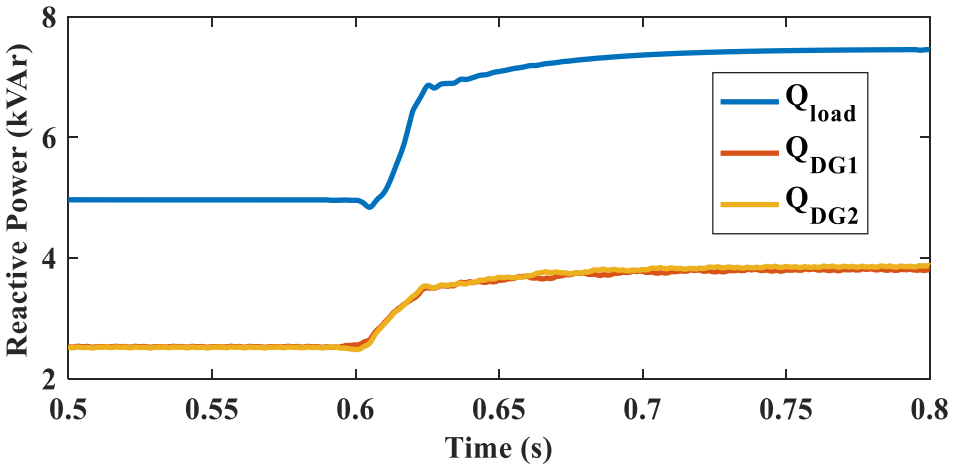

Figure 5.21 Reactive Powers shared by DGs.

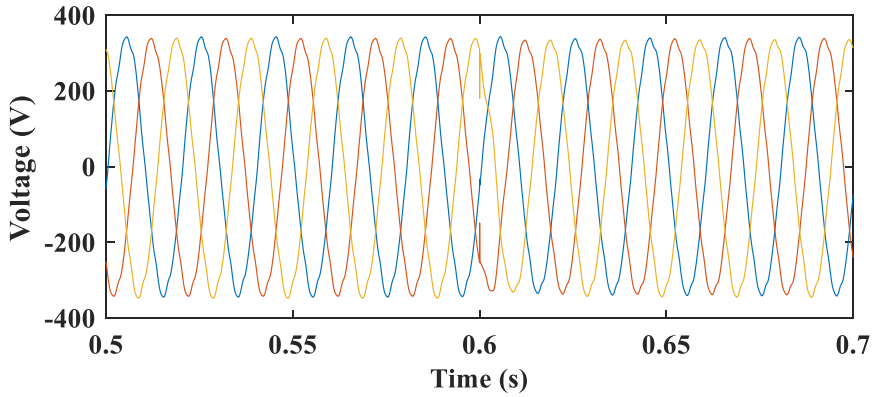

Figure 5.22 Load Voltages at PCC.

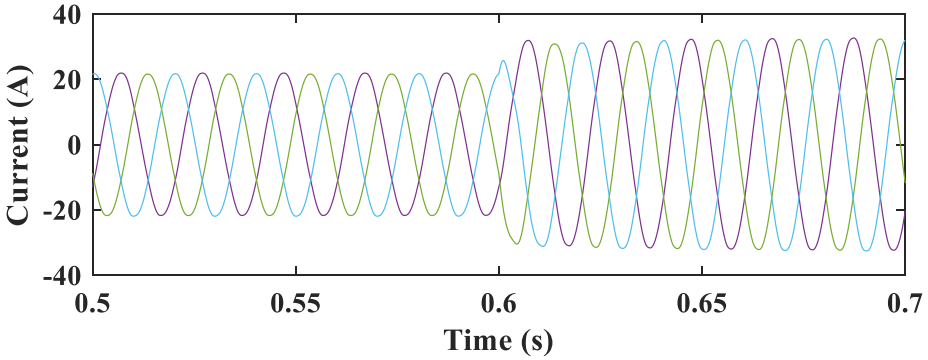

Figure 5.23 Load currents at PCC.

5.4.4.2 Case 2: DG with different capacities and line parameters

For Case-2, the DG capacities and the line parameters are not equal. The load is considered same as in case-1. At 0.6 s, the load is increased to 5kW and 2.5kVAr to test the performance of the controller. The load active and reactive powers at PCC and powers shared by two DGs are as shown in Figures 5.24 and 5.25. The active powers shared between the two DGs are in the ratio of 2:1 because the controller parameters are in the ratio 1:2. The reactive powers shared between the two DGs depend on the line voltage drop which is presented in (5.37). Figures 5.26 and 5.27 present the voltages and currents at PCC. In Figure 5.26, it can be observed that even for the change in load, the voltage always remains the same as the nominal voltage.

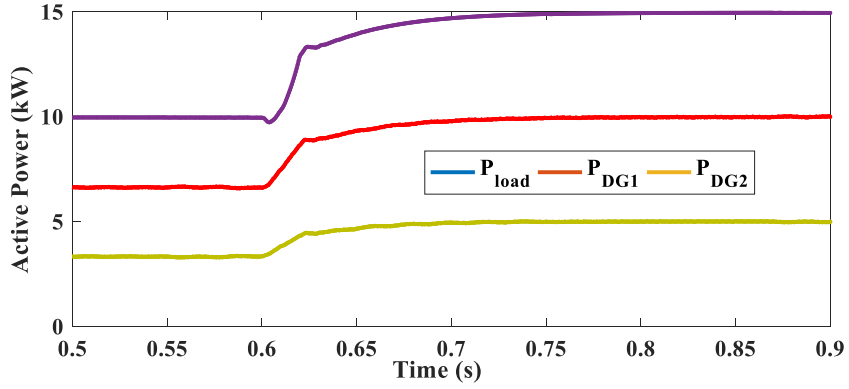

Figure 5.24 Active Powers shared by DGs.

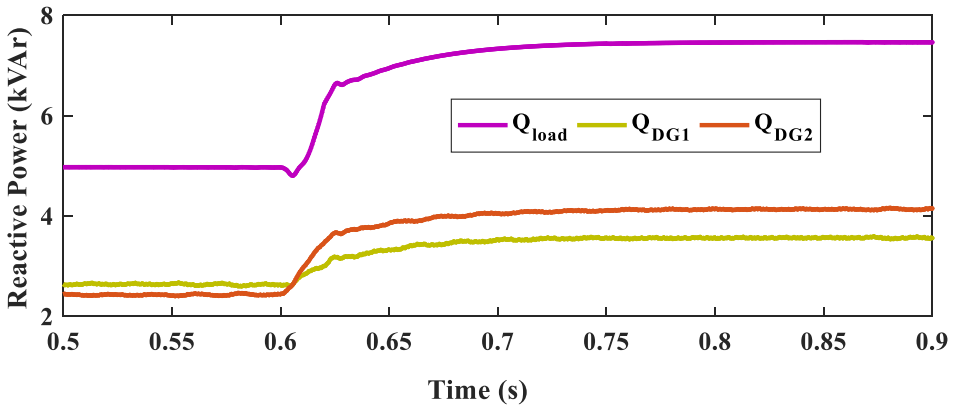

Figure 5.25 Reactive Powers shared by DGs.

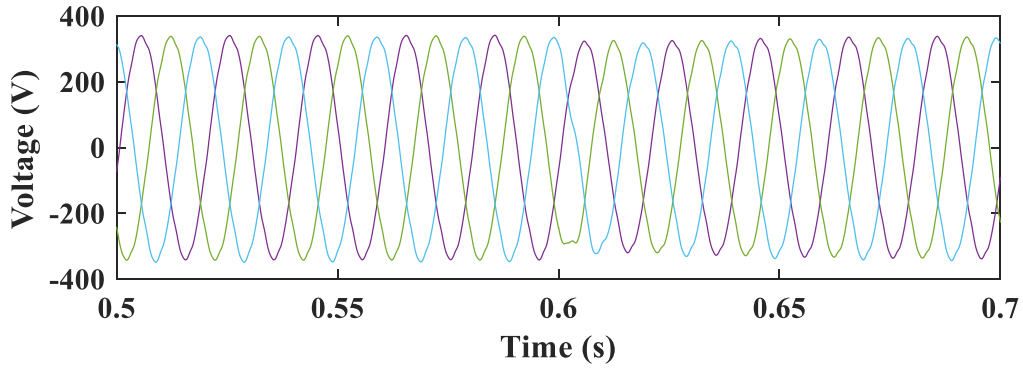

Figure 5.26 Load Voltages at PCC.

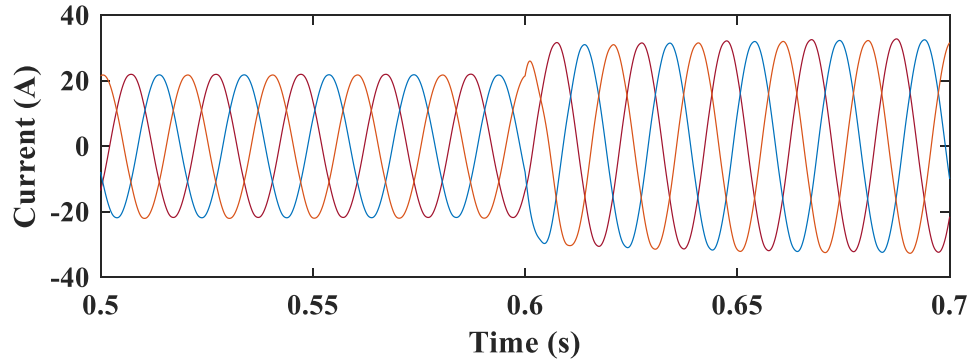

Figure 5.27 Load Currents at PCC.

5.4.4.3 Case-3: DG2 is disconnected

Case-3 presents the dynamic performance of the controller with the loads considered same as in cases 1 and 2 except at 1 s; as DG2 is out due to fault and DG1 is supplying the full load. The responses for the active power and reactive powers are shown in Figures 5.28 and 5.29. The voltage and currents at PCC are shown in Figures 5.30 and 5.31 respectively.

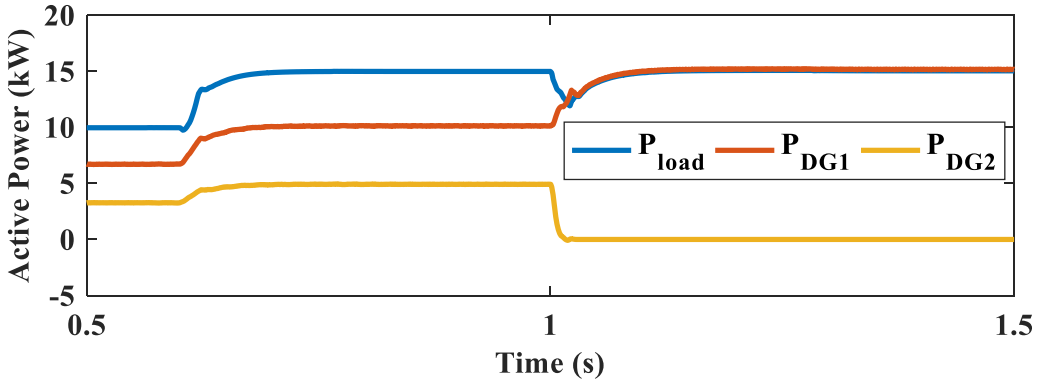

Figure 5.28 Active Powers shared by DGs.

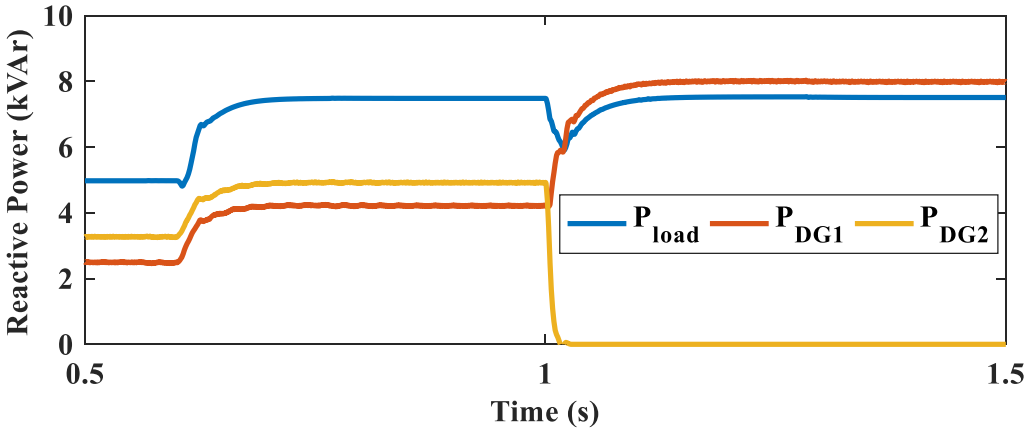

Figure 5.29 Reactive Powers shared by DGs.

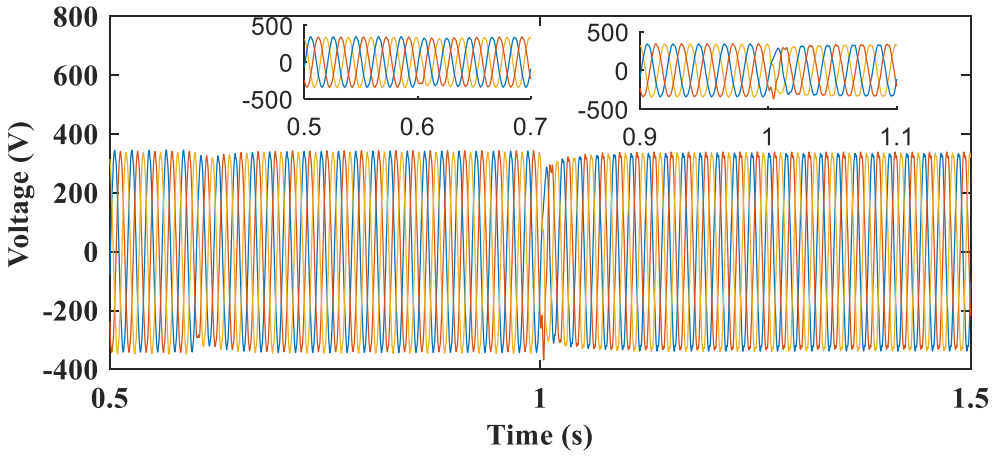

Figure 5.30 Load Voltages at PCC with DG2 disconnected.

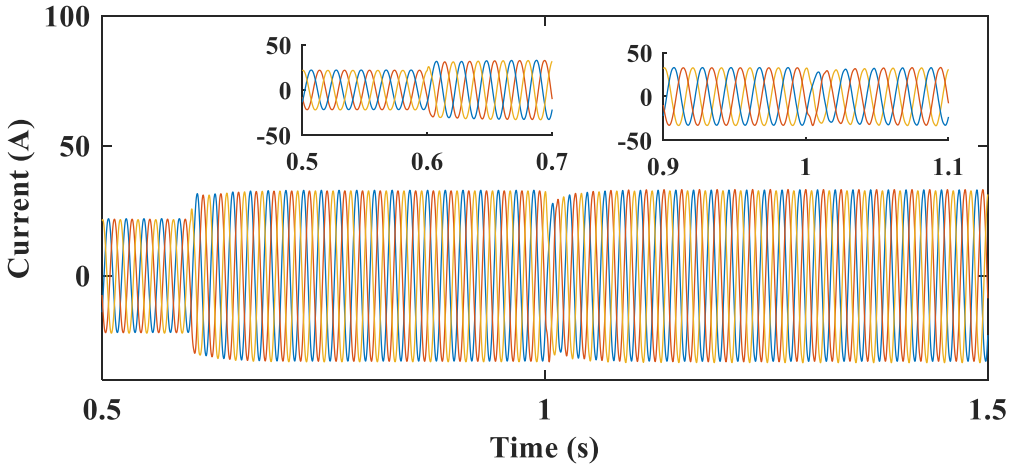

Figure 5.31 Load Currents at PCC with DG2 disconnected.

5.4.4.4 Case-4: DG2 is back into operation

Case-4 presents the dynamic performance of the controller with the load operated by DG1, and it is seen that in Case-3, DG2 is out of service. At t=1.5 s, DG2 is back into operation and the load is being shared by two DGs. The performance of the controller with the load shared by the DGs is shown in Figures 5.32 and 5.33. The voltage and currents at PCC are shown in Figures 5.34 and 5.35, whereas Figures 5.32-5.35 shows the seamless transition of the DGs.

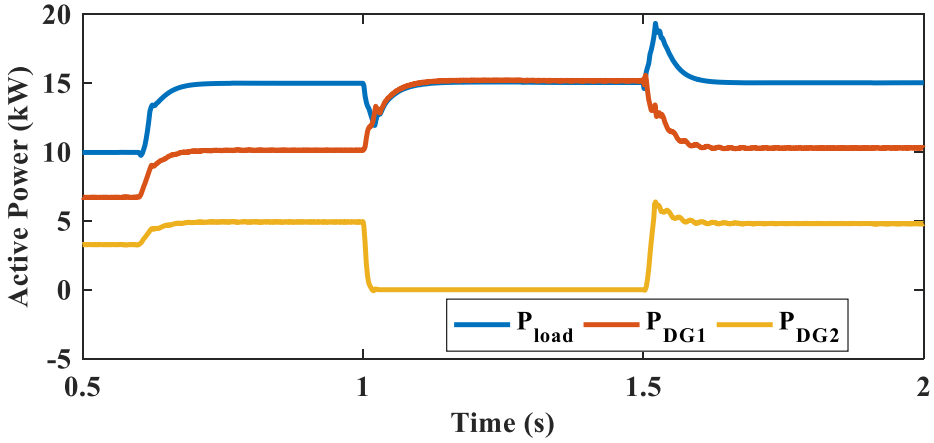

Figure 5.32 Active Powers shared by DGs.

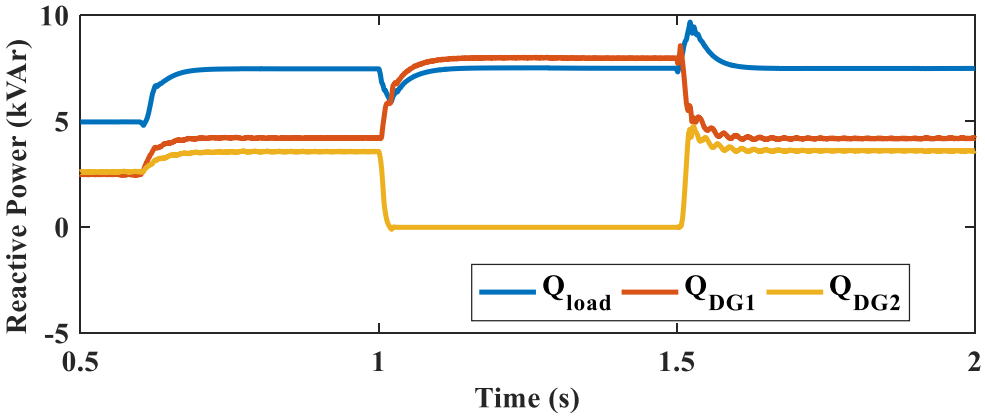

Figure 5.33 Reactive Powers shared by DGs.

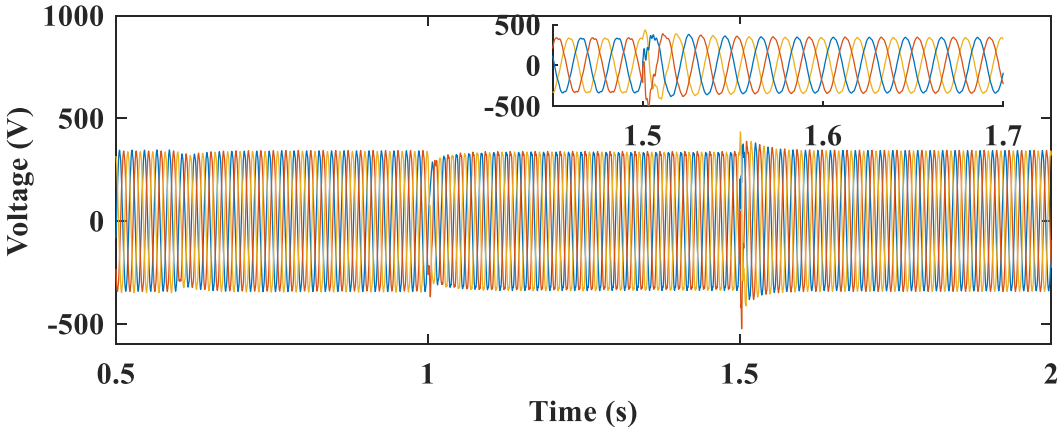

Figure 5.34 Load Voltages at PCC with DG2 back into operation.

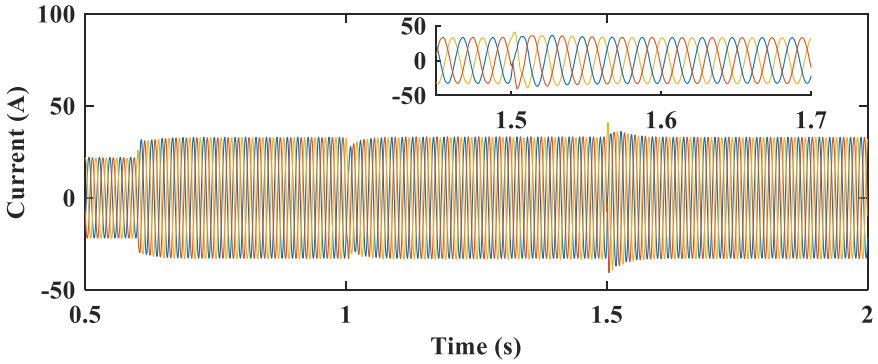

Figure 5.35 Load Currents at PCC with DG2 back into operation.

5.4.5 Hardware-In-Loop (HIL) Results

For different cases considered for the simulation, HIL results are performed in OPAL-RT. The HIL set-up is shown in Figure 5.36. The two DGs are considered in a single OPAL-RT

simulator whereas the other simulator consists of the DSO where the loads are connected. The set-up consists of a personal computer and a laptop with which the communication is done to the OPAL-RT simulators by using ethernet cables. The low bandwidth communication signals are assumed to be the signals from the second simulator with delays passed through analog outputs of second simulator. The analog outputs of second simulator are given as inputs of the first simulator. The initiation of the secondary control will be done automatically when the primary control fails i.e., the analog outputs of the simulator are non-zero. In this way, the controller takes decisions based on the analog output signals received from distribution system operator (DSO).

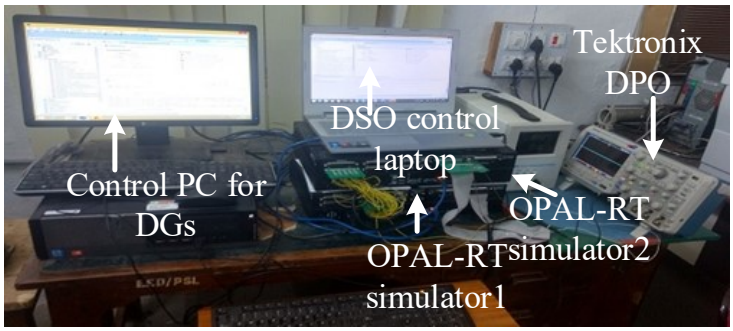

Figure 5.36 HIL set-up.

Figure 5.37 presents the load active powers shared by the DGs and the load active power present at DSO with the controller parameters ratio as (1:2) whereas Figure 5.38 presents the load power at equal controller parameters for two DGs. Hence it can be observed that in Figure. 5.37, the ratio of sharing between the two DGs is in the ratio of 2:1; whereas in Figure 5.38, the load shared by the DGs is equal.

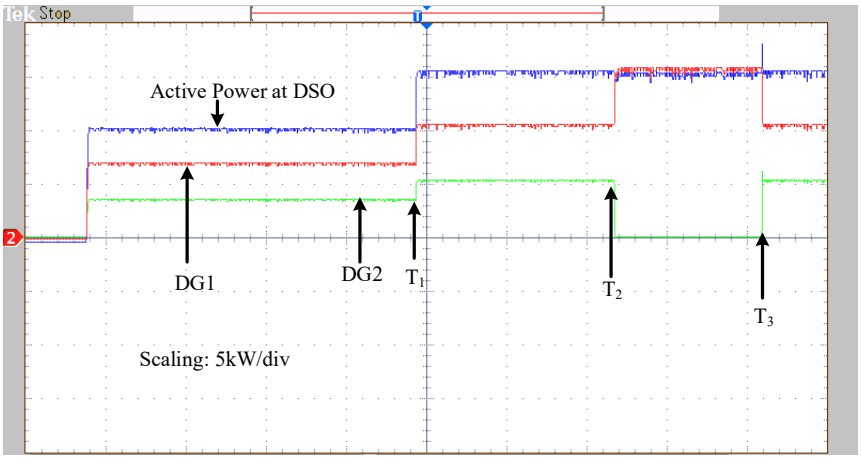

Figure 5.37 Load active powers and powers shared by DGs with unequal values of controller.

At T_1, a load change is done to evaluate the performance of the controller and correspondingly the load sharing between the DGs is increased; however, the ratio of the power sharing between the DGs is unaffected as there is no change in the controller parameter values. At T_2, DG2 is disconnected with some fault and it is observed that DG1 takes the entire load power. At T_3, DG2 is brought back into operation and the active power sharing of both the DGs remains the same. It can be seen from Figure 5.38, that the sharing of the powers between the two DGs is same because of the same controller parameters.

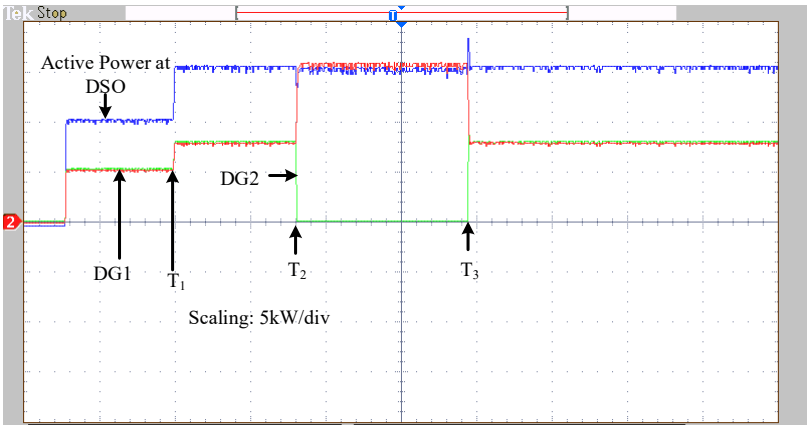

Figure 5.38 Load active powers and powers shared by DGs with equal values of controller.

The load reactive powers shared by two DGs are shown in Figures 5.39 and 5.40. The reactive power at unequal distances is shown in Figure 5.39, whereas Figure 5.40 presents the reactive powers with equal distances.

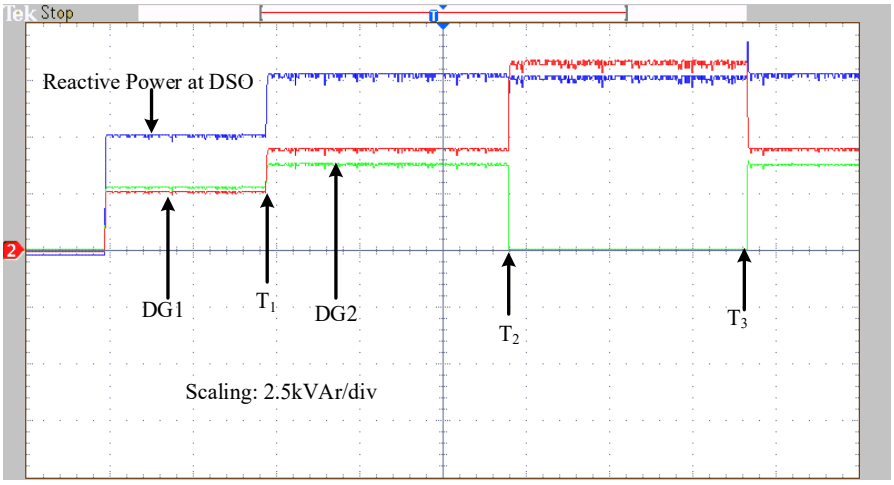

Figure 5.39 Load reactive powers and powers shared by DGs with unequal distances.

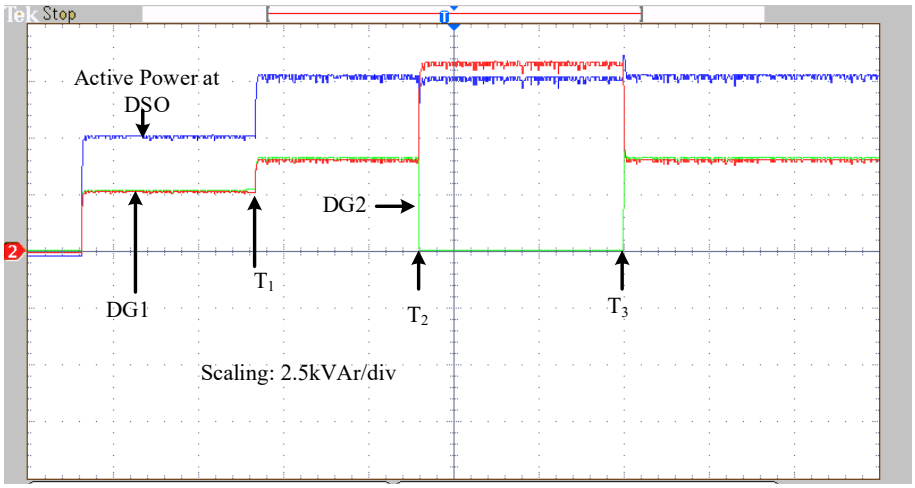

Figure 5.40 Load reactive powers and powers shared by DGs with equal distances.

At T_1, the load reactive power is changed to observe the performance of the controller. In the proposed control strategy, the reactive power sharing takes place on the basis of the line voltage drop. The line parameters of DG1 to load are twice that of DG2. Therefore, in order to compensate the drop in line voltage, it is observed that the reactive power sharing of DG1 is a little more (500W) than DG2s share of reactive power during load change, i.e., an additional amount (500W) of reactive power is taken as a share of DG. At T_2, the DG2 is out due to fault and DG1 has the entire share of reactive power. At T_3, DG2 is brought back into operation and the reactive power sharing of both the DGs remains the same. It can be seen in Figure 5.40, that the sharing of the powers between the two DGs is same because of equal distances.

Figures 5.41 and 5.42 present the load voltages and load currents at PCC. The scaling is presented in Figure 5.41 i.e., 1 V is equivalent to 48 V and in Figure 5.42, 1 A is equivalent to 11 A. In Figure 5.41, the corrective action is done by using secondary voltage control strategy at T_2, where the DG2 is out of action and the DG1 is made to share the complete load. The DSO will be placed in the second simulator of OPAL-RT where the communication delays are introduced. In this case, communication delay of 20 ms is introduced. Even with the introduction of communication delays, it can be observed that the voltages at PCC is brought again to the nominal voltages at PCC. In Figure 5.42, the instant of T_1, is shown as there is change in load active and reactive power at T_1. In all the above cases, it can be observed that there is a seamless transition in the load sharing of powers which is essential for the smart grid network. The comparison of the proposed controller with the conventional droop is presented in Table 5.2.

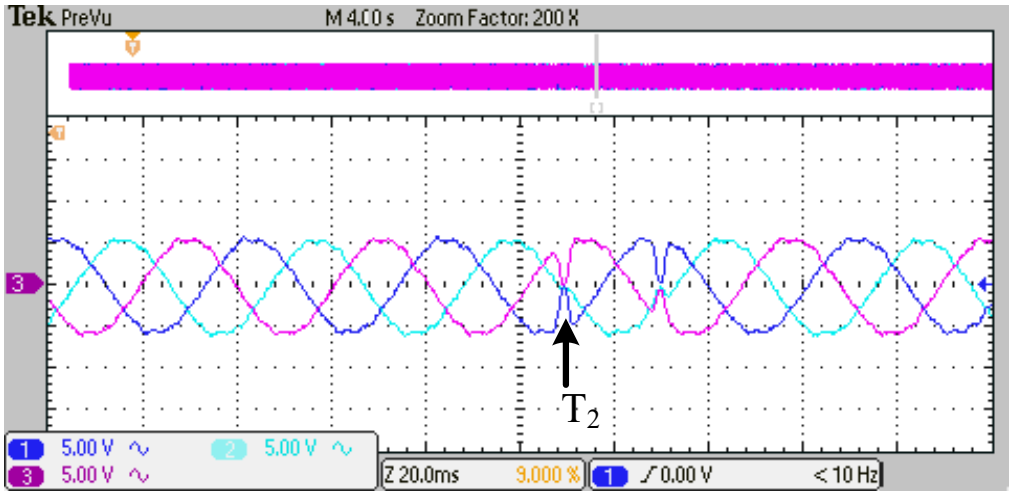

Figure 5.41 Load Voltages at PCC during secondary control operation.

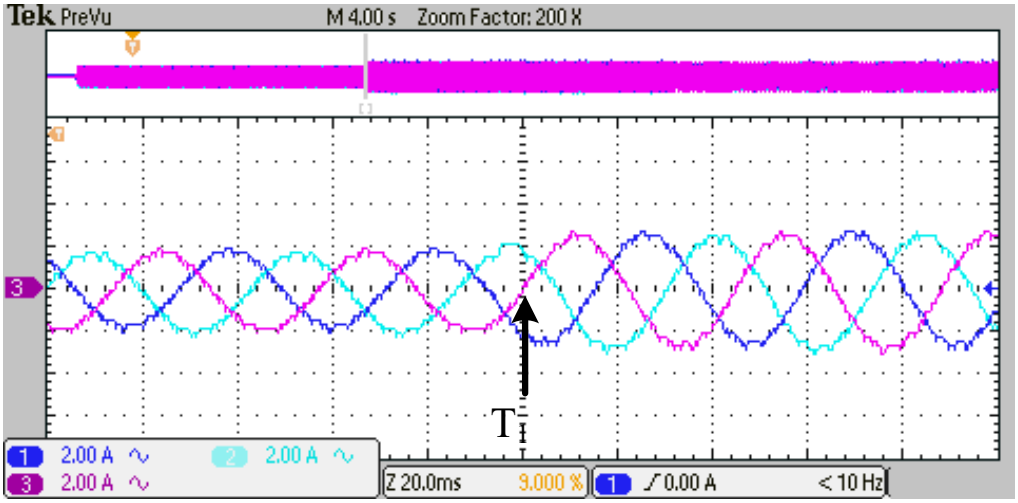

Figure 5.42 Load currents at PCC during load change.

Table 5.3 Comparison of conventional droop with proposed control strategy

Control technique	Conventional droop	Proposed control strategy
Approach	• *P*-ω and *Q*-*V* droop	• Each inverter sends output *P* and *Q* to a central controller • Central controller evaluates the reference *P* and *Q* for each inverter • Inverter supplies the load by adjusting phase and amplitude to achieve required *P* and *Q*.
Communications	• No	• Yes
Active power sharing performance	• Achieves active power sharing with slow transient response	• Achieves active power sharing with fast response (0.1s)
Reactive power sharing	• Not able to achieve reactive power sharing under line impedance mismatch conditions	• Able to achieve reactive power sharing regardless of line impedance conditions.

Voltage frequency variation	• There will be a trade-off between active power sharing and frequency regulation	• Frequency is fixed as the adjustment is only applied to the angle of reference voltage.
Voltage amplitude regulation	• There is a trade-off between reactive power sharing and amplitude regulation.	• Amplitude varied based on the reactive power sharing requirement.
Other advantages	• Easy to implement	• Ability to share active and reactive power based on specified ratio. • No system failure even if there is communication loss. • Communication between inverters and central controller can be used for optimization of available power (economic dispatch)

5.5 Summary

In this chapter, MPC integrated with SVM for the control of three phase DG to operate in grid connected as well as in off-grid modes is discussed. A simple PLL free grid synchronization mechanism along with seamless transition control between grid connected mode and off-grid mode are developed. The proposed MPC integrated with SVM is examined for delivering the set-point powers in grid connection mode, supplying the local load at the nominal voltage and frequency in off-grid mode, for smooth transitions between these modes. The performance of the proposed control scheme for three phase DG is confirmed through simulations. The performance of the controller proved to be very much efficient in both the grid as well as off grid connected modes. The proposed methodology is free of weighting factors, unlike seamless transition strategies using MPC references.

The parallel connected DGs have been discussed along with the problems associated with decentralized coordination control methods. In subsequent sections of the chapter, a control strategy is proposed which is free of conventional d-q transformations and eliminates the use of filters. The filters which make the system sluggish, thereby increasing the cost and reducing the system transient response, are eliminated in the proposed control strategies. The performance of the proposed control strategies is validated through different cases of simulation and the hardware-in-loop implementation of the considered cases of the simulation is performed. The simulation and HIL results indicate seamless transition of the DGs which are essentials for the smart grid network. Though the controller exhibits superior performance compared to the conventional droop, the dynamic performance of the proposed control strategy must be tested with multiple DGs. The multiple DGs must consist of a diesel generator along

with the DGs to study the dynamic performance of the controller which is discussed in chapter 6.

Chapter 6

Coordinated Control Operation of the Distributed Generators along with Diesel Generator

Chapter 6
Coordinated Control Operation of the Distributed Generators along with Diesel Generator

6.1 Introduction

The DGs which are photo-voltaic based will not be able to operate during night as well as snow fall countries. So, the operation of diesel generator in conjunction with the conventional DGs should be studied. In view of this, a diesel generator is connected along with two other DGs. The primary as well as secondary control strategies are proposed in this chapter. The primary control decides the power shared between two distributed generators as the other distributed generator i.e., the diesel generator is operated in constant power and voltage mode. The secondary control strategy allows the distributed generators to restore the frequency and voltage to nominal values. The developed control strategies always maintain the frequency and voltage at nominal values and they possess adaptability for smart grid interconnection. The performance of the proposed control strategies is validated through different case studies of simulation; Hardware-in-loop is also implemented using OPAL-RT.

6.2 Proposed Control Strategy

The above issues are addressed using the proposed control strategy, which is effective in meeting the requirements. The proposed control strategy has two loops i.e., one for power droop control and the other based on adaptive secondary voltage control. The power droop control gives an idea of the amount of power to be transferred to the load at PCC whereas the adaptive dc link voltage control helps in determining the dc link voltage to maintain the PCC voltage at nominal value (415 V r.m.s). The control strategy of droop as well as the secondary voltage control is presented in Figure 6.1. For the adaptive secondary voltage control, the difference in r.m.s values of the voltage are sensed at the distribution system operator (DSO) end and are sent to the individual DG units. By sending the difference (error) in the r.m.s values, the PI controller develops different modulation indexes for different phases. Similarly, for frequency adjustment, the frequency is sensed at the DSO and subtracted from the nominal values. The resultant value (error) is passed through a PI controller and the difference in the phase adjustment ($\Delta\delta$) is given to the primary control. At the DG end, the switching pulses are

given to the DG in such a way that it compensates the voltage drop and at the PCC, the load is always maintained at nominal values of voltage and frequency at PCC. Similarly, for the diesel generator, the voltage and frequency that are sensed at the load point are given to the speed regulator and voltage regulator to maintain the load voltage and frequency at nominal values. Figure 6.2 presents the single line diagram of control strategy with single DG along with diesel generator (DG3). The proposed control strategy uses the low bandwidth communications (LBC) for the transfer of data which has communication dependency as low and the viability, sharing accuracy and voltage quality are very high which are essential aspects for the development of the coordination control strategy. Also, the proposed control strategy is free of the conventional (d-q) transformations.

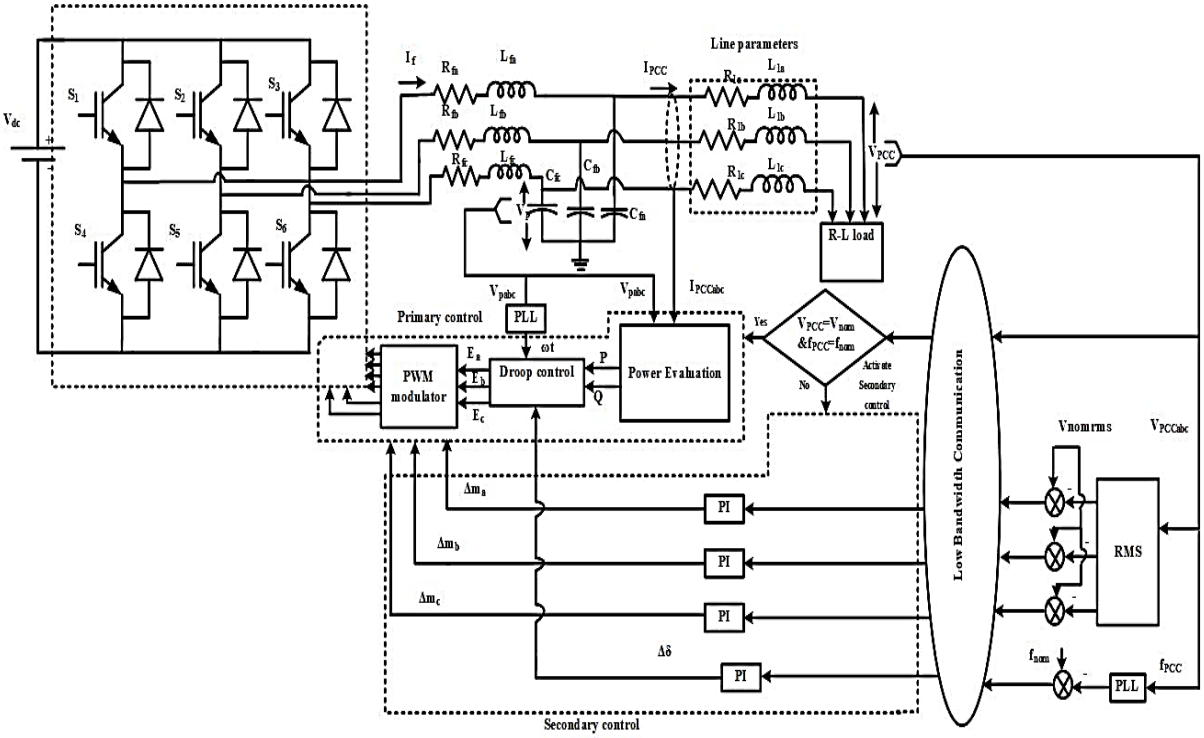

(a)

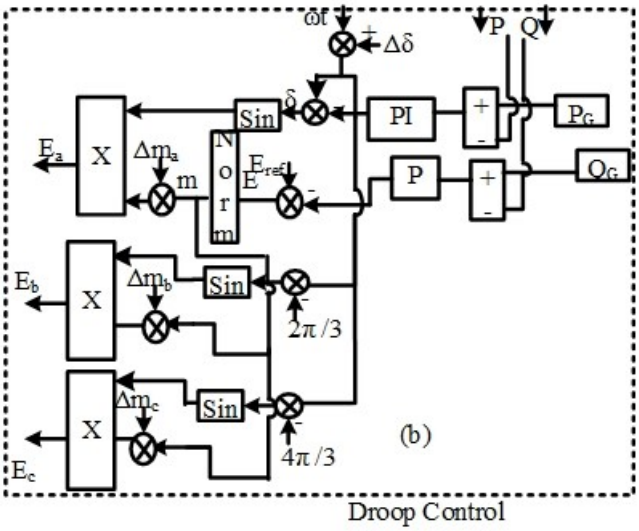

Figure 6.1 Proposed control strategy for single DG. (a) Primary and Secondary control. (b) Droop control.

From the DSO, the centralized system sends the difference in voltage and frequency values to the diesel generator as well as to two other DGs. Based on the difference in the values of the voltage and frequency, the control operator will set the controller values and adjust the controller values to dispatch the power as directed by the centralized controller.

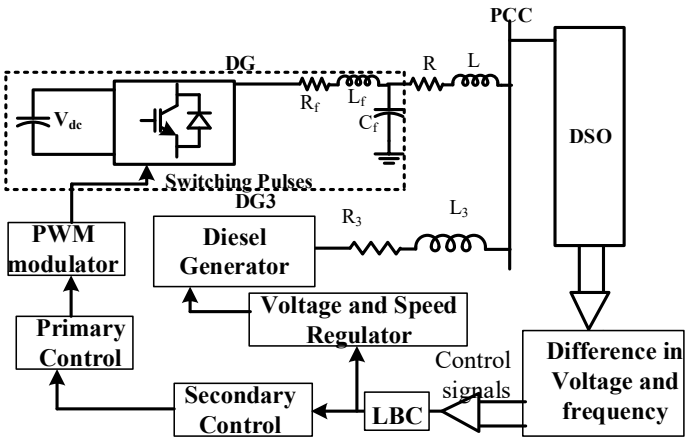

Figure 6.2 Single line diagram of control strategy with single DG and diesel generator.

Table 6.1 System parameters

Parameters	DG1	DG2	DG3 (Diesel generator)
V_{dc}	750 V	750 V	-
V_{PCC}	415 V (RMS)	415 V (RMS)	415 V (RMS)
f_{nom}	50 Hz	50 Hz	50 Hz
K_P	$2x10^{-4}$ Hz/W	$4x10^{-4}$ Hz/W	-
K_I	$2x10^{-3}$ Hz/W	$4x10^{-3}$ Hz/W	-
K_{pv}	$5x10^{-4}$ V/VAr	$5x10^{-4}$ V/VAr	-
K_{Psv}	0.001	0.001	10
K_{Isv}	0.5	0.6	8
K_{psf}	0.001	0.001	-

K_{Isf}	0.2	0.3	5
P_G	20 kW/30 kW	20 kW	5 kW
L_f	15 mH	15 mH	-
C_f	50 μF	50 μF	-
Line parameters *R, L*	0.5 Ω, 1 mH	0.25 Ω, 0.5 mH	0.25 Ω, 0.5 mH
P_{load} Q_{load}	(10-15 kW), (5- 7.5) kVAr		

6.3 Simulation Results and Discussions

The performance of the proposed control strategy is verified using MATLAB / Simulink simulations for various case studies. This section consists of the different cases that are suitable for the coordinated control operation of DGs.

6.3.1 Case-1: Three DGs operating in parallel

In Case-1, the DG capacities and the distance between the load to the DGs (i.e., the line parameters) are not the same. As mentioned earlier, the diesel generator is operated in constant power and constant voltage mode and the generator supplies active power of 4.1kW rated capacity. The parameters are considered as mentioned in Table 6.1. Initially, the load is 10kW and 5kVAr respectively. At 1.05 s, the load is increased to 5kW and 2.5kVAr to test the performance of the controller. The power delivered at PCC and the power shared by two DGs are depicted in Figure 6.3. As the line parameters and the power capacities are not same, the active powers shared by the two DGs are not equal and are shared based on the parameters of the controller of two DGs as presented in Figure 6.3. The comparison of the active power of the proposed method (P_{prop}) with the traditional method (P_{trad}) (conventional d-q transformations) is shown in Figure 6.3. It can be observed from Figure 6.3, that the traditional method comprising d-q transformation takes 0.8 s to settle down whereas the proposed method settles at almost 0.2 s. Figure 6.4 presents the comparison of the reactive powers for proposed (Q_{prop}) along with the traditional method (Q_{trad}). The reactive power delivered to PCC for the traditional method takes more time when compared with the proposed method. In both traditional as well as the proposed method, it can be seen that the reactive power shared by DG1 is more compared to DG2 because the line voltage drop is higher; therefore, the reactive power required to compensate the line voltage drop is more. The voltage and current at PCC are indicated in Figures 6.5 and 6.6 respectively. The Figures 6.3 to 6.6, present smooth transition during the load variation.

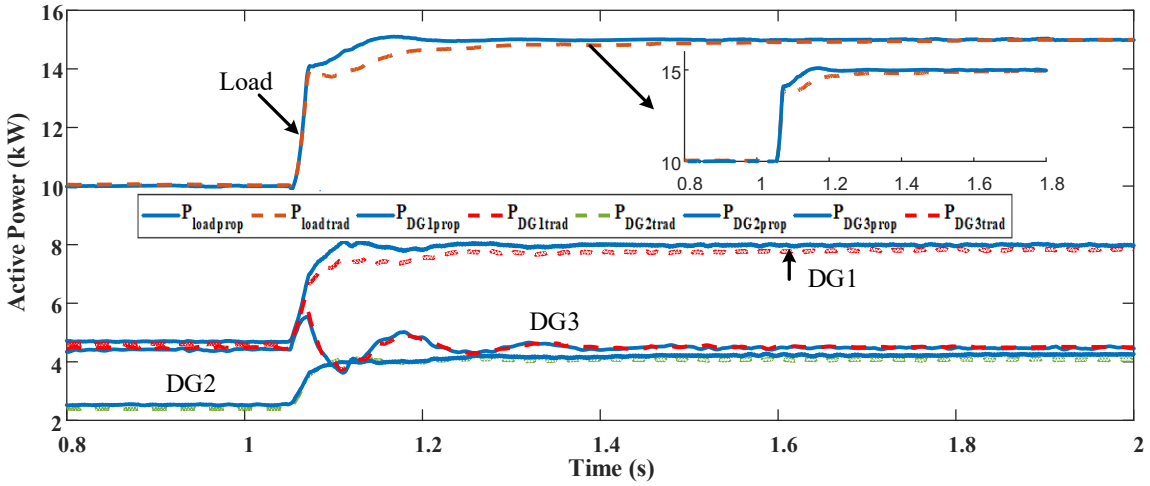

Figure 6.3 Active Powers shared by DGs.

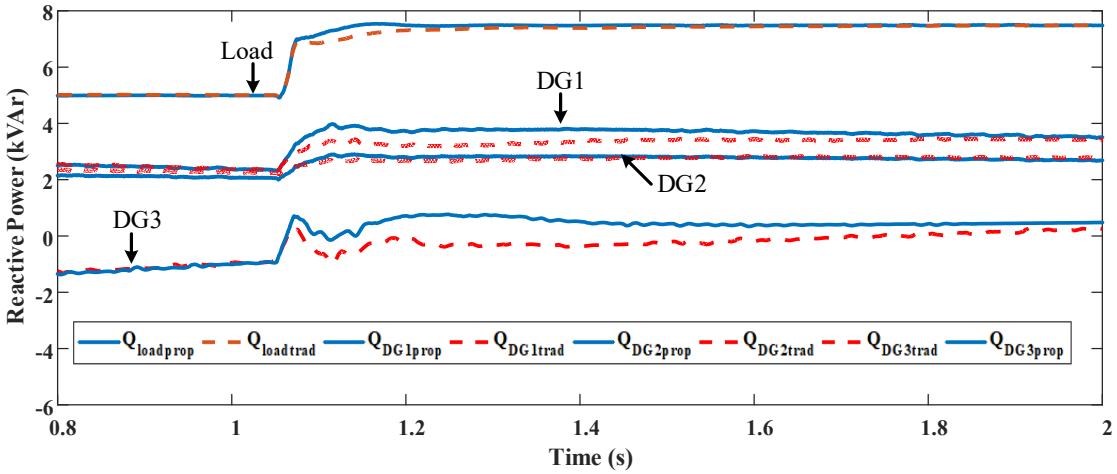

Figure 6.4 Reactive Powers shared by DGs.

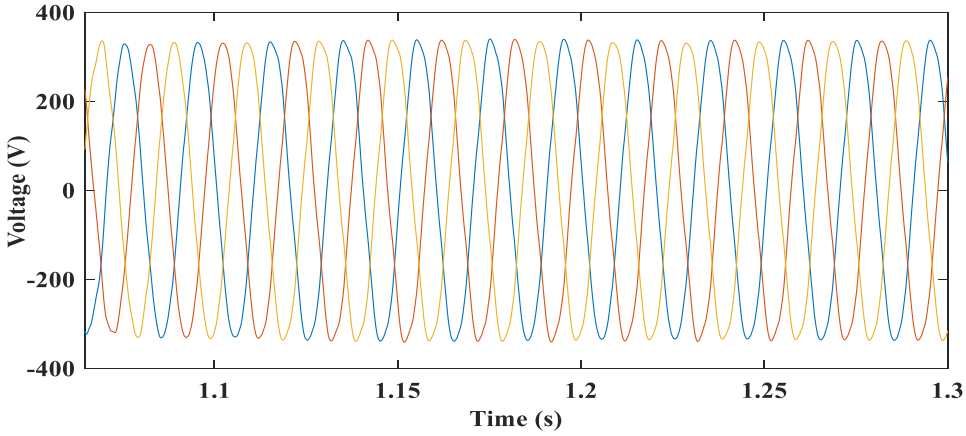

Figure 6.5 Load Voltages at PCC.

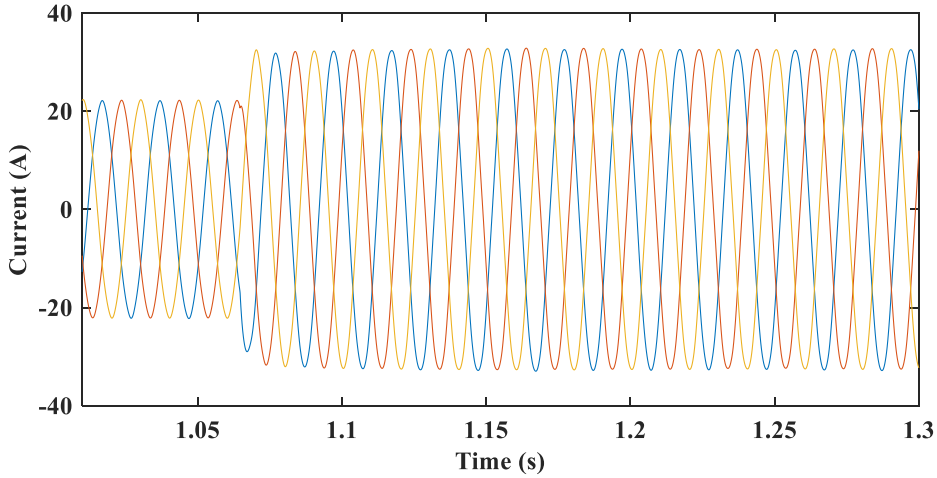

Figure 6.6 Load currents at PCC.

6.3.2 Case-2: DG2 is disconnected

For Case-2, it is assumed that DG2 is not able to supply the load due to fault and is disconnected. Therefore, the load is being supplied by DG1 and the diesel generator DG3. Figure 6.7 depicts a comparison of the proposed control with the traditional control for active powers. It is assumed that DG2 is out with the fault at 2.52 s and it can be observed that the active power supplied by DG2 is zero and the active powers are supplied by DG1 and DG3 only.

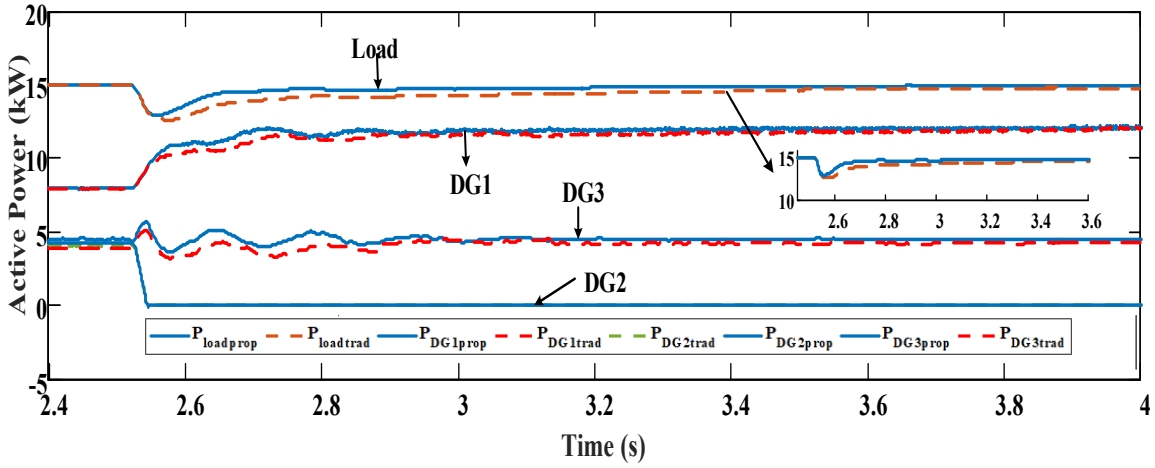

Figure 6.7 Active Powers shared by DGs.

As DG2 is out with fault, the reactive power of the load is supplied by DG1 and it is presented in Figure 6.8. It can be observed that the proposed control performs better in terms of controller speed when compared with the traditional control in supplying the required amount of active and reactive powers. The time taken by the proposed control in delivering the

active and reactive powers is 0.2 s, whereas the traditional control takes 1.1 s. Figures 6.9 and 6.10 present the voltage and currents of loads at PCC.

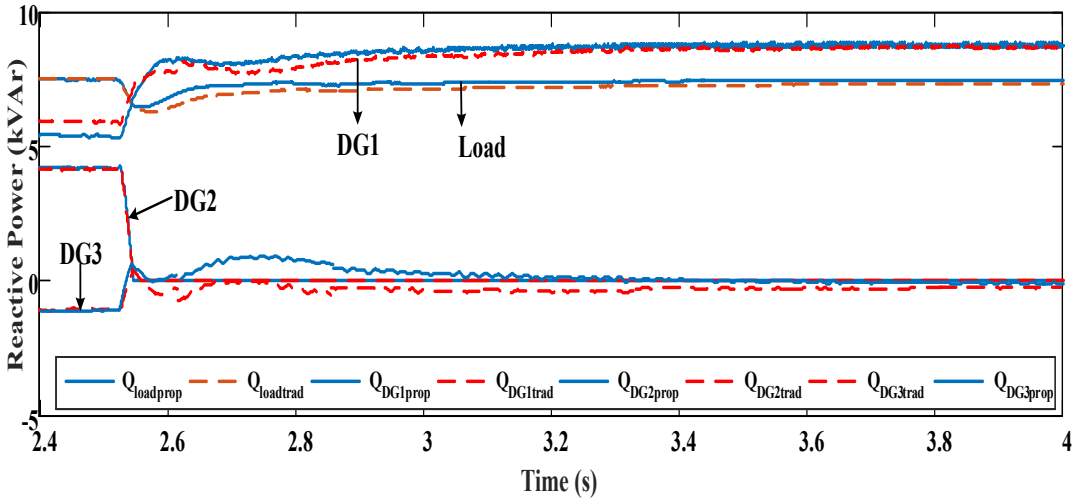

Figure 6.8 Reactive Powers shared by DGs.

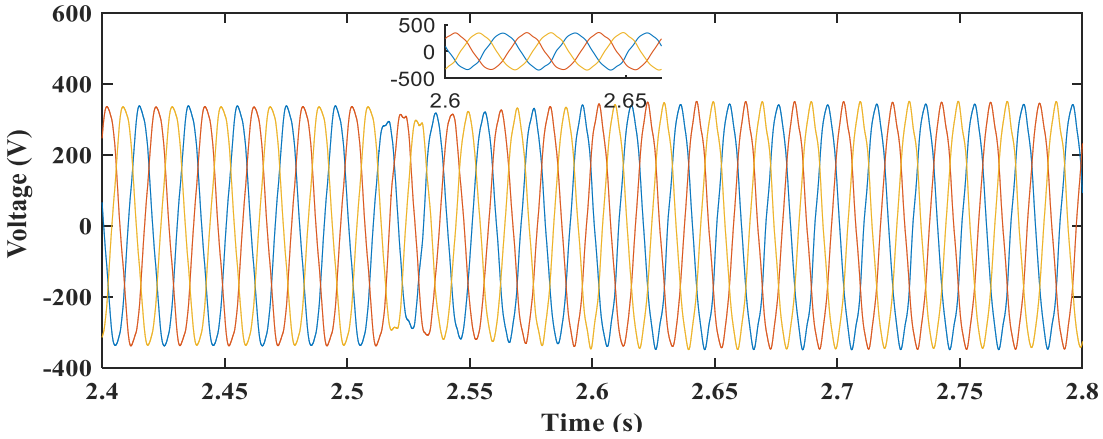

Figure 6.9 Load Voltages at PCC with DG2 disconnected.

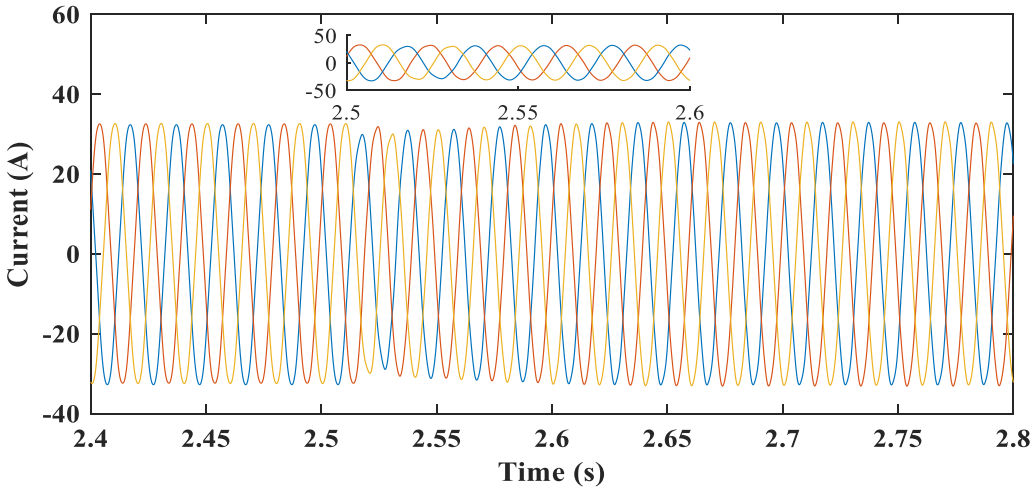

Figure 6.10 Load Currents at PCC with DG2 disconnected.

6.3.3 Case 3: DG2 is back into operation

Case-3 presents the dynamic performance of the controller with the same loads considered for case-1 and case-2. At 4.15 s, DG2 is brought back into operation and all the DG's are supplying the load. The responses for the active power and reactive powers and comparison of the proposed and traditional control of active and reactive powers are shown in Figures 6.11 and 6.12.

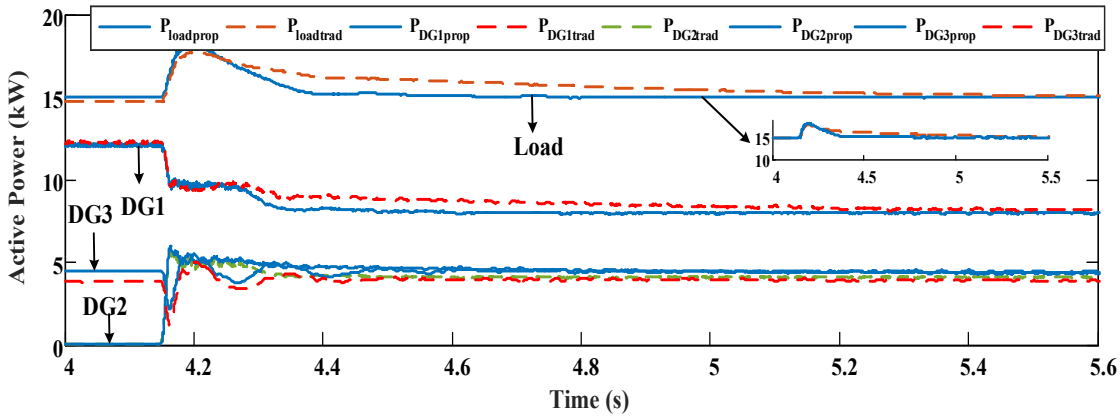

Figure 6.11 Active Powers shared by DGs.

The controller is very effective in bringing back the powers to normal values when both DGs are in operation. The time taken by the proposed control is 0.35 s whereas the traditional control takes 1.05 s in delivering the load with required power.

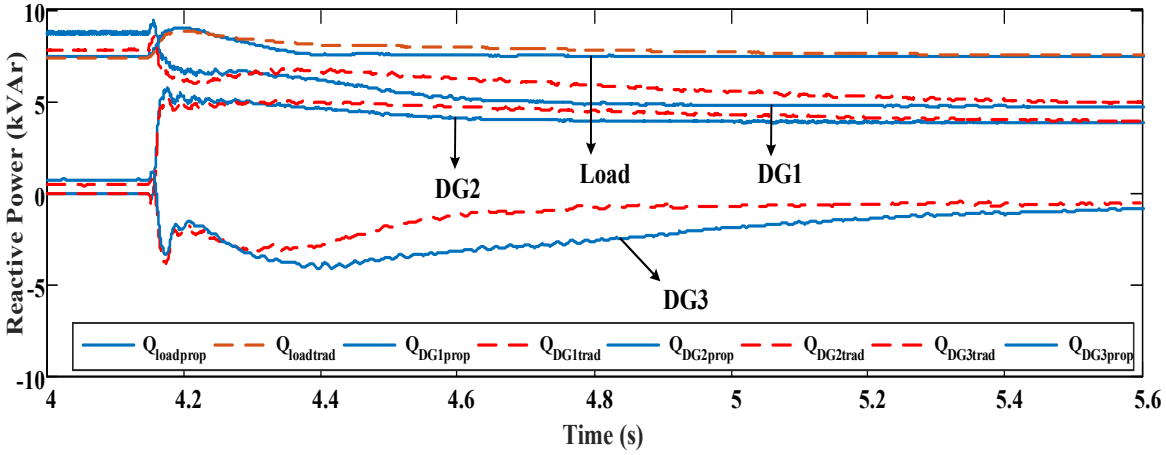

Figure 6.12 Reactive Powers shared by DGs.

Figures 6.13 and 6.14 present the voltage and currents at PCC whereas the Figures 6.11-6.14 present the seamless transition. Therefore, the controller is effective in delivering the

required amount of active and reactive power. From the simulation results it is evident that the proposed control strategies show superior performance compared with the traditional controller.

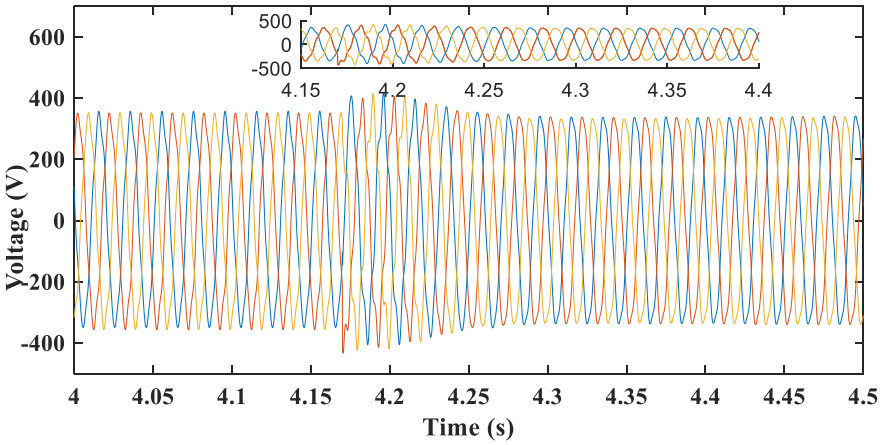

Figure 6.13 Load Voltages at PCC.

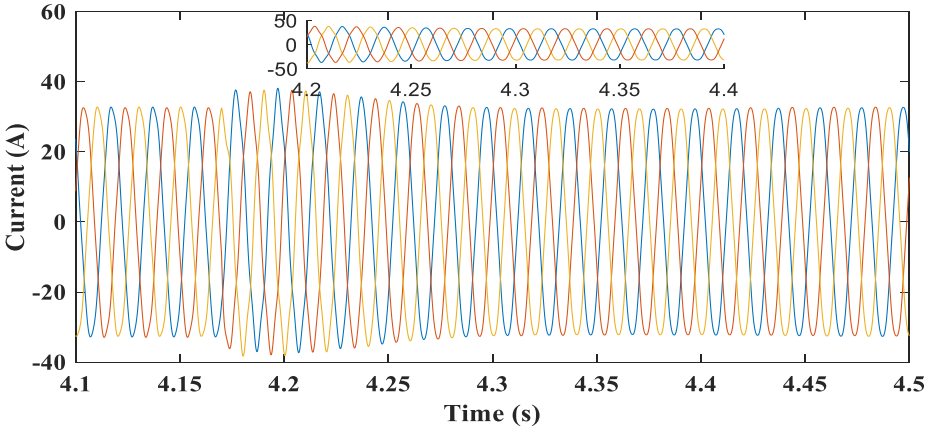

Figure 6.14 Load Currents at PCC.

6.4 Validation of Robustness of Proposed Control

To validate the robustness of the proposed control, a parameter variation of 10% increase in all the parameters i.e., both filter parameters (R_f, L_f, C_f) and line parameters (R,L) . All the three cases discussed are considered for the proposed control for the evaluation of robustness.

6.4.1 Case 1: Change in Load and Three DGs are operating in parallel

Case 1 considers the load change and the three DGs are operating in parallel. At 1.05 s, the load is increased to 5kW and 2.5kVAr to test the performance of the controller. The active and reactive powers delivered to the load and by the three DGs are presented with a red dotted

line in Figures 6.15 and 6.16 respectively. The results presented indicate the robustness of the proposed control.

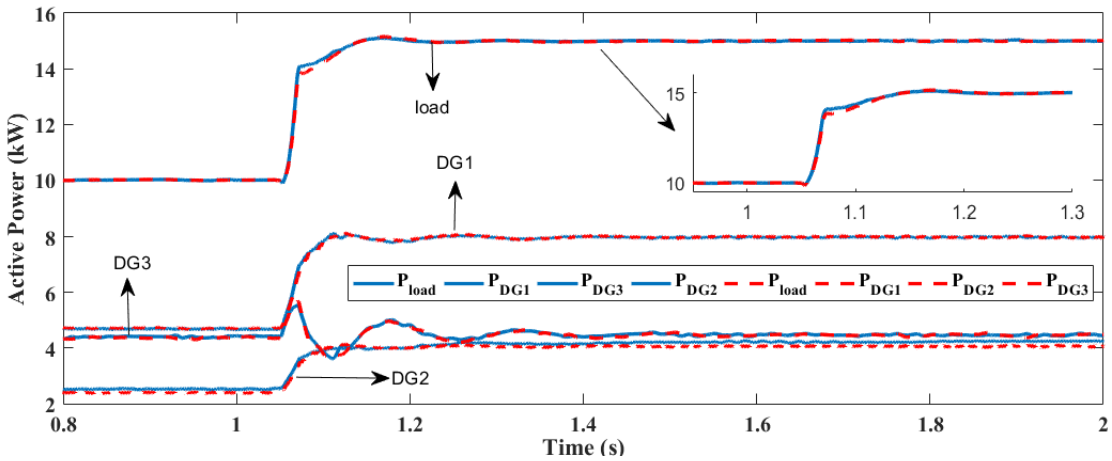

Figure 6.15 Active power with and without parameter variation for case1.

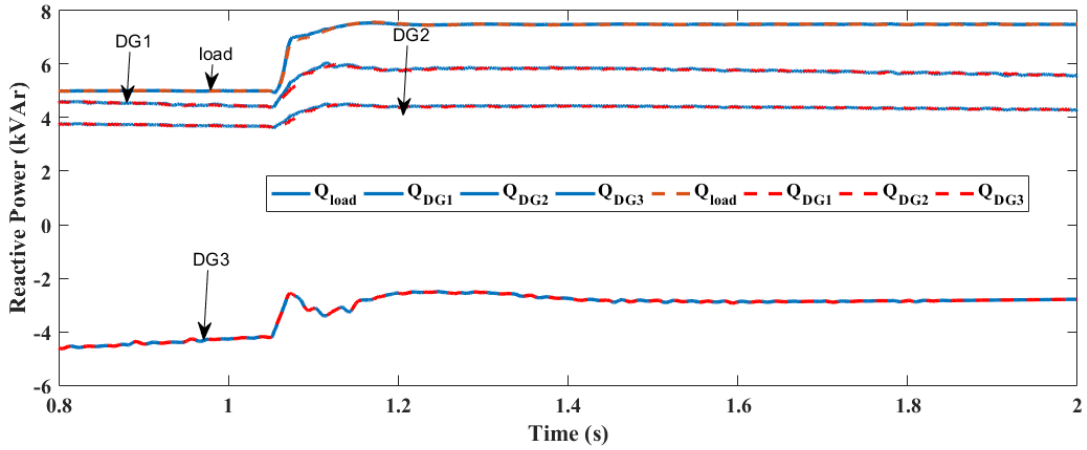

Figure 6.16 Reactive power with and without parameter variation for case1.

6.4.2 Case2: DG2 is disconnected

Case 2 considers DG2 being disconnected and the two DGs are operating in parallel. At 2.55 s, the DG2 is disconnected to test the dynamic performance of the controller. The active and reactive powers delivered to the load and by the three DGs are presented with a red dotted line in Figures 6.17 and 6.18 respectively. The results presented indicate the robustness of the proposed control.

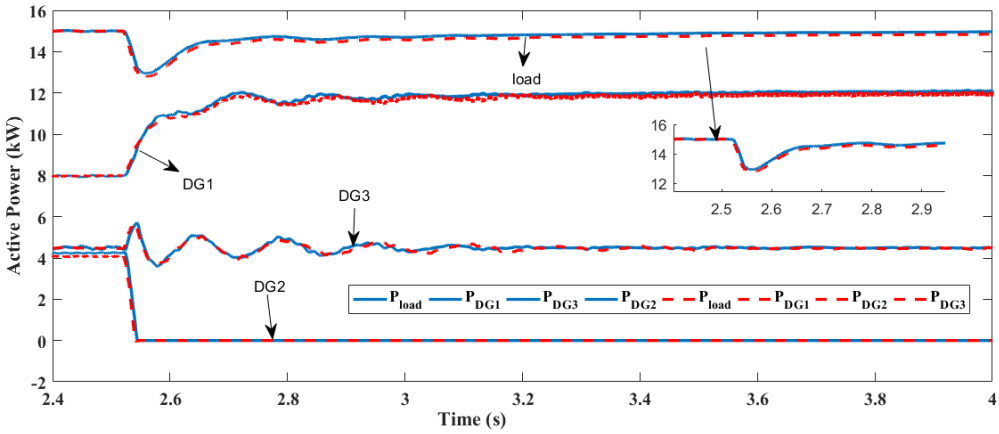

Figure 6.17 Active power with and without parameter variation for case2.

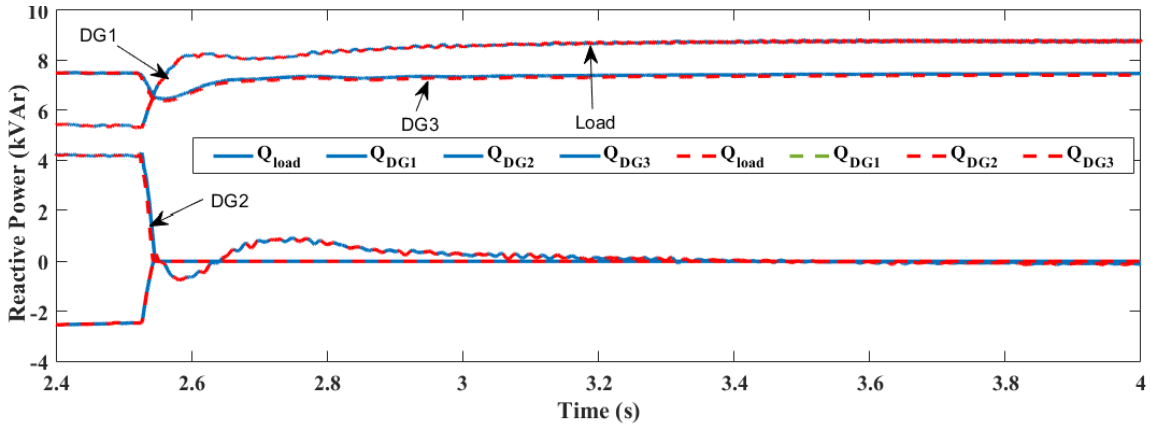

Figure 6.18 Reactive power with and without parameter variation for case2.

6.4.3 Case 3: DG2 is brought back into operation

Case 3 considers DG2 brought back into operation and the two DGs are operating in parallel. At 4.15 s, the DG2 is disconnected to test the dynamic performance of the controller. The active and reactive powers delivered to the load and by the three DGs are presented with a red dotted line in Figures 6.19 and 6.20 respectively. The results presented indicate the robustness of the proposed control.

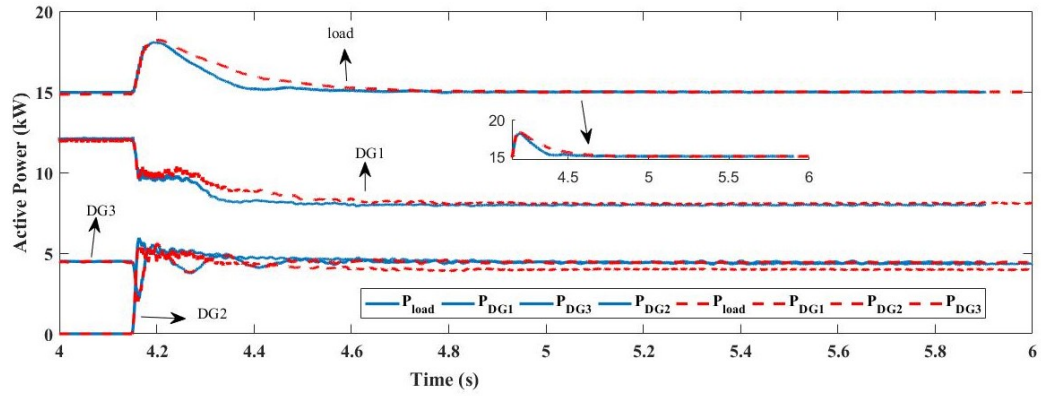

Figure 6.19 Active power with and without parameter variation for case3.

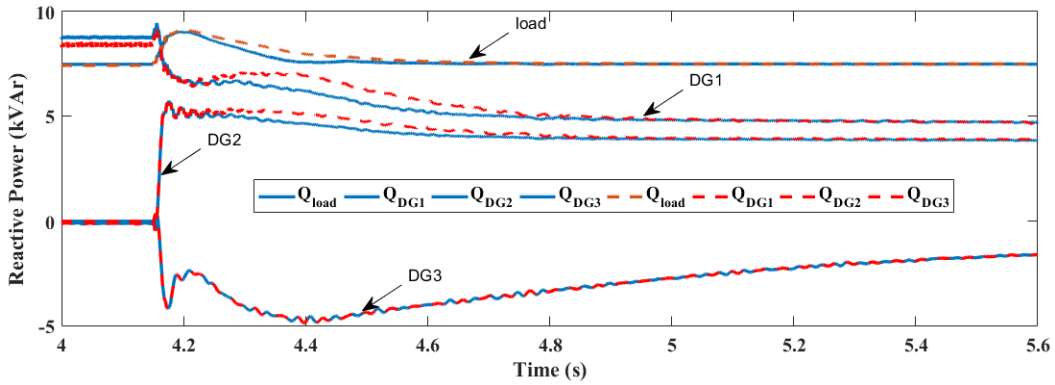

Figure 6.20 Reactive power with and without parameter variation for case3.

From the three cases, it is evident that the proposed control is robust which is essential for any control strategy.

6.5 Hardware-In-Loop (HIL) Results

The HIL results are performed in OPAL-RT for different cases considered for the simulation. The HIL set-up is shown in Figure 6.15. The three DGs are considered in a single OPAL-RT simulator whereas the other simulator consists of DSO where the loads are connected. The set-up consists of a personal computer (PC) and a laptop with which communication is carried out to the OPAL-RT simulators by using ethernet cables. The low bandwidth communication signals are assumed as the signals from the second simulator with delays passed through analog outputs of second simulator.

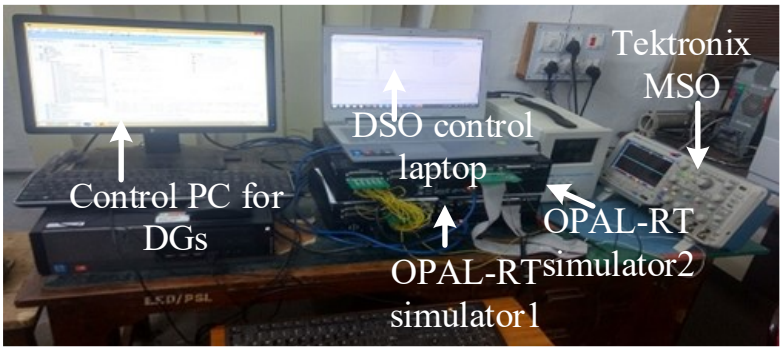

Figure 6.21 HIL set-up.

The analog outputs of second simulator are given as analog inputs to the first simulator. The initiation of the secondary control will be done automatically when the primary control fails i.e., the analog outputs of the second simulator are non-zero. In this way, the controller takes the decisions based on the analog output signals received from DSO. Figure 6.16 presents the load active power shared by the DGs and the load active power present at DSO with controller ratio (1:2). The DG3 is operated in constant power and constant voltage mode. Therefore, the DG3 i.e., the diesel generator is operated with a fixed amount of power.

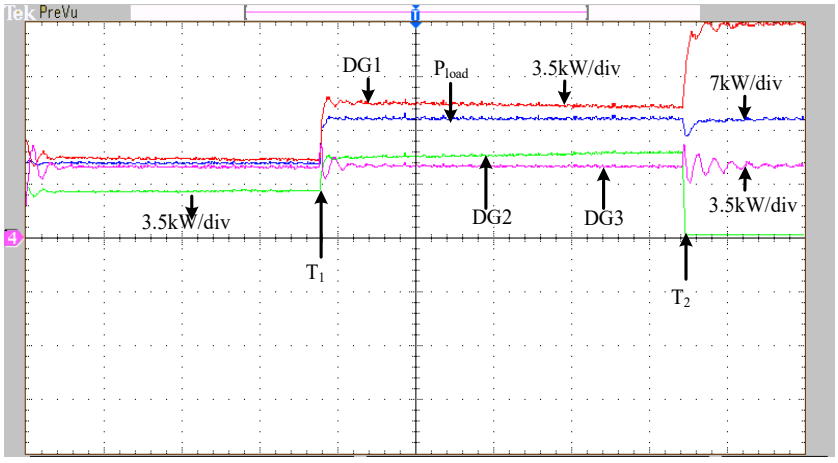

Figure 6.22 Load active powers and powers shared by DGs.

The other two DGs share load in the inverse ratio of their droop constants. Hence it can be observed in Figure 6.16 that the ratio of sharing between the two DGs is 2:1. At T_1, a load change of 5 kW is done to evaluate the performance of the controller and correspondingly the load sharing between the DGs increases; however, the ratio of the power sharing between the DGs is unaffected as there is no change in controller values. At T_2, the DG2 is disconnected with some fault and it is observed that the DG1 is sharing the entire load power along with DG3.

The load reactive powers shared by the three DGs are presented in Figure 6.17. At T_1, the load reactive power is changed from 5 kVAr to 7.5 kVAr to test the performance of the controller. The proposed control strategy shows that the reactive power sharing takes place on the basis of line voltage drop. The line parameters of DG1 to load are twice that of the DG2. So, in order to compensate the drop in line voltage, it is observed that the reactive power sharing of DG1 is 750 VAr more than DG2's share of reactive power during load change. An additional amount of reactive power is taken as a share of DG1. At T_2, the DG2 is out due to fault and the DG1 has the entire share of reactive power along with DG3.

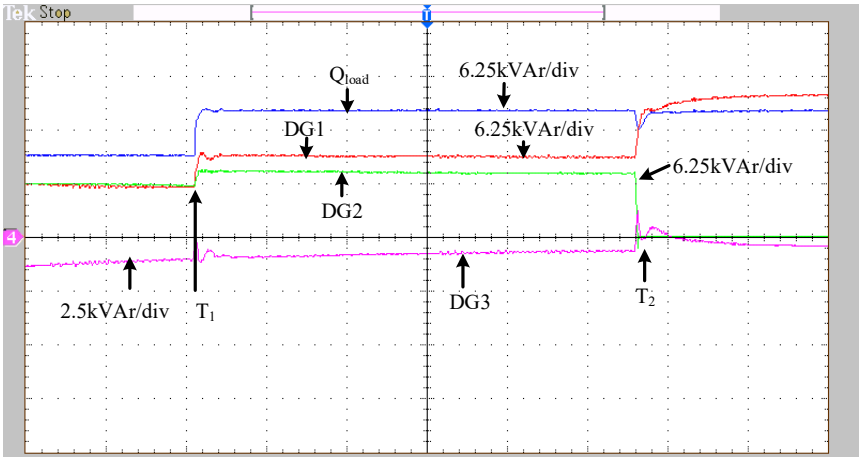

Figure 6.23 Load reactive powers and powers shared by DGs.

Figures 6.18 and 6.19 present the load voltages and load currents at PCC at the point of change in the load. The scaling of the voltage is presented in Figure 6.18.

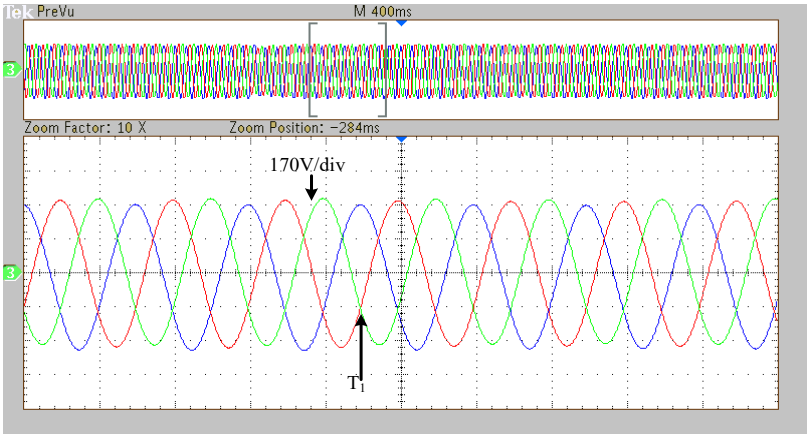

Figure 6.24 Load Voltages at PCC during load change.

In Figure 6.19, at the instant of T_1, there is change in active load and reactive power of 5 kW and 2.5 kVAr respectively, shows the change in the currents at the time instant T_1. In

Figure 6.20, the voltage at PCC is presented. Corrective action is taken by using the secondary voltage control strategy at T_2, where DG2 is out of action and DG1 is made to share the complete load. As the DSO will be placed in the second simulator of OPAL-RT where the communication delays are introduced. Here a communication delay of 20 ms is considered and it is assumed that the transferring of data for the individual DG is through optical fiber cable. Even with communication delays, it shows clearly that the voltages at PCC are brought again to nominal values. In all the above cases, it can be observed that there is a seamless transition in the load sharing of powers of the DGs which are essential for the smart grid network.

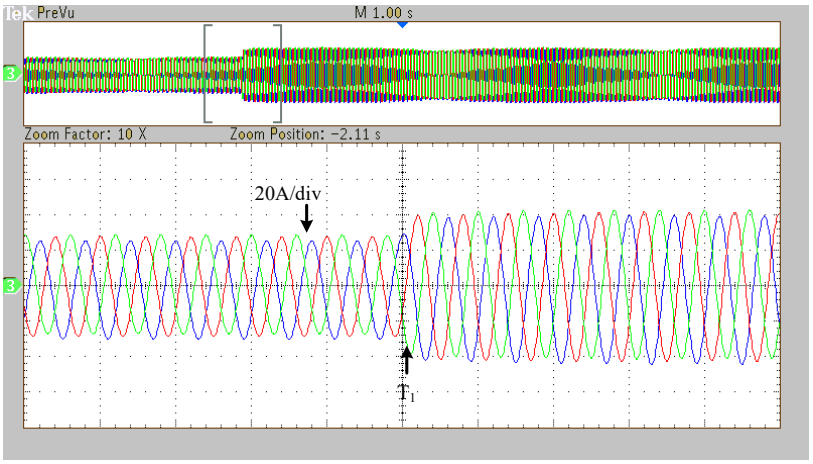

Figure 6.25 Load currents at PCC during load change.

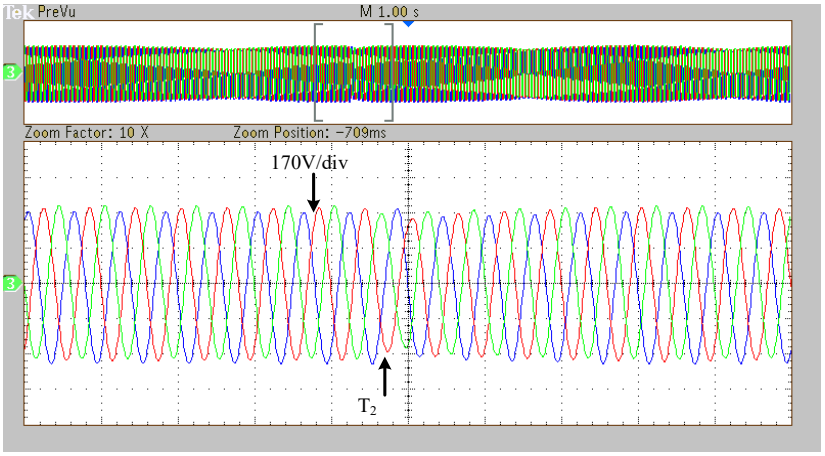

Figure 6.26 Load Voltages at PCC with DG2 disconnected.

A tabular column is formulated and the time taken by the proposed control and the traditional control (d-q transformations) are presented in Table 6.2.

Table 6.2 Time comparison between traditional and Proposed Control

Cases Considered	Traditional Control (d-q transformations)	Proposed Control
Case-1	0.8s	0.2s
Case-2	1.1s	0.2s
Case-3	1.05s	0.35s

6.6 Summary

This chapter presented the dynamic performance of the proposed controller when the DGs are connected with a diesel generator. The proposed control strategies are effective in maintaining the voltage and frequency to nominal values and the elimination of filters drastically improves the performance and the powers and voltages are quickly settling down to their values as per controller parameters. The primary control decides the power shared between the two distributed generators along with the diesel generator with voltage and frequency maintained at nominal values at the point of common coupling (PCC). The secondary control strategy allows the distributed generators to restore the voltage and frequency to nominal values if the primary control fails. The proposed control strategy is free of conventional d-q transformation which eliminates the discrete filters and thereby increases the speed of the controller. The communication delays are introduced and it is found that the effect of communication delay also does not affect the controller performance. Therefore, the proposed controller is quick in bringing the voltage and frequency to settle to their nominal values and robust. Hence, the controller can be used for real-time applications.

Chapter 7

Conclusions

Chapter 7
Conclusions

7.1 General Overview

Distributed generation offers several advantages such as: enhanced reliability, reduction in peak power requirements, improvement in power quality, provision of ancillary services including reactive power supply and helps in reducing the carbon emissions. Though distributed generation offers the advantages, it needs suitable control strategies to make it user friendly and efficient. The literature reported different control methodologies for DGs for grid as well as islanding operation. Based on the methodologies adopted for grid and off grid operation, the research objectives were identified and addressed in the thesis. In view of above context, this thesis presents research work on control methodologies of distributed generation.

7.2 Summary of Important Findings

i. **Development of Current Reference Generation Schemes for Single Phase Grid Connected Inverter:**

Two current reference generation schemes viz. i) Simplified active and reactive power control (SRPC) and ii) Modified scalar control along with the conventional scalar reference generation scheme are developed. The performance of MPC based SVM and ASDM for control of active and reactive powers of single phase grid connected DG is verified with different current reference generation schemes. The scalar reference generation scheme results in steady state error. Though the modified scalar reference generation scheme renders zero steady state error, it induces delay in power tracking and tuning of PI controller is tedious. The MPC based SVM in combination with SRPC has the advantage of quick, accurate and stable control when compared with ASDM. Although the modified scalar reference generation scheme and SRPC have error correction mechanisms, but their performance with ASDM is very poor. Therefore, it is concluded that that MPC based SVM with SRPC is the best combination among considered reference generation and modulation schemes.

ii. **Model Predictive Controller for Single Phase Distributed Generator with Seamless Transition between Grid and Off-Grid Modes:**

MPC integrated with SVM for the control of single phase DG to operate in grid connected as well as in off-grid modes is presented. A simple PLL free grid synchronization mechanism along with seamless transition control between grid connected mode and off-grid mode is developed. The developed MPC integrated with SVM is examined for delivering the set-point powers in grid connection mode, supplying the local load at the nominal voltage and frequency in off-grid mode and for smooth transitions between these modes. The designated performance of the developed control scheme for single phase DG is confirmed through simulations, which are further validated on an experimental test bed. The performance of the controller proved to be very efficient in both the grid as well as off grid connected modes and the proposed methodology is free of weighting factors unlike seamless transition strategies using MPC references.

iii. Model Predictive Controller for Three Phase Distributed Generator with Seamless Transition between Grid and Off-Grid Modes:

MPC integrated with SVM for the control of three phase DG to operate in grid connected as well as in off-grid modes is discussed. A simple PLL free grid synchronization mechanism along with seamless transition control between grid connected mode and off-grid mode is developed. The developed MPC integrated with SVM is examined for delivering the set-point powers in grid connection mode, supplying the local load at nominal voltage and frequency in off-grid mode and for smooth transitions between these modes. The performance of the developed control scheme for three phase DG is confirmed through simulations. The performance of the controller is proved to possess superior performance in both the grid as well as off grid connected modes and the proposed methodology is free from weighting factors.

iv. Distributed Control Strategy for the Coordinated Control Operation of Distributed Generators:

A control strategy is proposed which is free of conventional d-q transformations and eliminates the use of filters. The filters should be eliminated which makes the system sluggish, thereby increasing the cost and reducing the system transient response. The performance of the proposed control strategies is validated through different cases of simulation and the hardware-in-loop (HIL) implementation of the considered cases of the simulation is performed. The simulation and HIL results indicate the seamless

transition of the DGs, which are essential for the smart grid operation. The proposed controller exhibits superior performance when compared to the conventional droop method.

v. **Control Strategies for the Coordinated Control Operation of the Distributed Generators along with Diesel Generator:**

The dynamic performance of the proposed controller with the DGs are connected along with a diesel generator. The proposed control strategies are effective in maintaining the voltage and frequency at nominal values and the elimination of filters, drastically improves the performance as well as fast settling time. The primary control decides the power shared between the two distributed generators along with the diesel generator, with voltage and frequency maintained at nominal values at the point of common coupling (PCC). The secondary control strategy allows the distributed generators to restore the voltage and frequency to nominal values if the primary control fails. The proposed control strategy is free of conventional d-q transformations which eliminates the discrete filters and thereby increases the speed of the controller. It is observed that the effect of communication delays does not significantly affect the controller performance as well as fast settling time in bringing the voltage and frequency values to nominal values.

7.3 Scope for Future work

Any research never ends without leaving an open window for further research. The following aspects may be looked at by future researchers:

- The application of the developed objectives to multilevel inverter topologies would be a very interesting topic.
- Investigations on application of multi-agent system for the distributed generation to study the distributed coordination of DGs.
- Application of real time communication into the developed control methodologies would provide an innovative idea to investigate.

References

[1] http://www.ren21.net/wp-content/uploads/2018/06/17-8652_GSR2018_FullReport_web_-1.pdf

[2] F. Blaabjerg, M. Liserre, and K. Ma, "Power electronics converters for wind turbine systems," *IEEE Trans. Ind. Appl.*, vol. 48, no. 2, pp. 708-719, March/April.2012.

[3] J. M. Guerrero, F. Blaabjerg, T. Zhelev, K. Hemmes, E. Monmasson, S. Jemei. M. P. Comech, R. Granadino, and J. I. Frau, "Distributed generation: Toward a new energy paradigm," *IEEE Magazine Ind. Electron.*, vol. 4, no. 1, pp. 52-64, March 2010.

[4] A. Luo, Y. Chen, Z. Shuai, and C. Tu, "An improved reactive current detection and power control method for single-phase photovoltaic gridconnected DG system," *IEEE Trans. Energy Convers.,* vol. 28, no. 4, pp. 823–831, Dec. 2013.

[5] A. Cagnano, E. De Tuglie, M. Liserre, and R. A. Mastromauro, "Online optimal reactive power control strategy of PV inverters," *IEEE Trans. Ind. Electron.,* vol. 58, no. 10, pp. 4549–4558, Oct. 2011.

[6] Marco Liserre*,* Frede Blaabjerg and Steffan Hansen*,* "Design and Control of an *LCL*-Filter-Based Three-Phase Active Rectifier," *IEEE Trans. Ind. Electron*, vol. 41, no. 5, pp. 1281-1290, Sept. 2005.

[7] R. Teodorescu, F. Blaabjerg, M. Liserre, and P. Chiang Loh, "Proportional-resonant controllers and filters for grid-connected voltage source converters," *Proc. IEE, Electr*. *Power Appl.*, vol. 53, no. 5, pp. 750–762, Sep. 2006.

[8] Alejandro G. Yepes*,* Francisco D. Freijedo*,* Jesu´s Doval-Gandoy*,* O´ scar Lo´pez, Jano Malvar and Pablo Fernandez-Comesa˜na*,* "Effects of Discretization Methods on the Performance of Resonant Controllers," *IEEE Trans. Power Electron,* vol. 25, no. 7, pp. 1692-1712, July 2010.

[9] S. Deo, C. Jain, and B. Singh, "A PLL-less scheme for single-phase grid interfaced load compensating solar PV generation system," *IEEE Trans. Ind. Informat.,* vol. 11, no. 3, pp. 692–699, Jun. 2015.

[10] C. Attaianese, M. D. Monaco, and G. Tomasso, "High performance digital hysteresis control for single source cascaded inverters," *IEEE Trans. Ind. Informat.,* vol. 9, no. 2, pp. 620–629, May 2013.

[11] R F. Wu, X. Li and J. Duan, "Improved Elimination Scheme of Current Zero-Crossing Distortion in Unipolar Hysteresis Current Controlled Grid-Connected Inverter," *IEEE Trans. Ind. Informat.,* vol. 11, no. 5, pp. 1111-1118, Oct. 2015.

[12] Z. Yao and L. Xiao, "Control of Single-Phase Grid-Connected Inverters with Nonlinear Loads," in *IEEE Transactions on Ind. Electron.*, vol. 60, no. 4, pp. 1384-1389, April 2013.

[13] C. Meza, D. Biel, D. Jeltsema, and J. M. A. Scherpen, "Lyapunov-based control scheme for single-phase grid-connected PV central inverters," *IEEE Trans. Control Syst. Technol.,* vol. 20, no. 2, pp. 520–529, Mar. 2012.

[14] Chen J, Yao W,Zhang C, Ren Y, Jiang L. "Design of robust MPPT controller for grid-connected PMSG based wind turbine via perturbation observation based nonlinear adaptive control," Ren. Energy. vol.134, pp.478–95, 2019.

[15] M. A. Hannan, Z. A. Ghani, A. Mohamed and M. N. Uddin, "Real-Time Testing of a Fuzzy-Logic-Controller-Based Grid-Connected Photovoltaic Inverter System," in *IEEE Trans. Ind. Appl.*, vol. 51, no. 6, pp. 4775-4784, Nov.-Dec. 2015.

[16] H. R. Baghaee, M. Mirsalim and G. B. Gharehpetian, "Performance Improvement of Multi-DER Microgrid for Small- and Large-Signal Disturbances and Nonlinear Loads: Novel Complementary Control Loop and Fuzzy Controller in a Hierarchical Droop-Based Control Scheme," in *IEEE Sys. Jour.*, vol. 12, no. 1, pp. 444-451, March 2018.

[17] V. S. C. Raviraj and P. C. Sen, "Comparative study of proportional-integral, sliding mode, and fuzzy logic controllers for power converters," *IEEE Trans. Ind. Appl*., vol. 33, no. 2, pp 518-524, 1997.

[18] Sekhar, P.C., Mishra, S., "Sliding mode based feedback linearizing controller for grid connected multiple fuel cells scenario," Int. J. Electr. Power Energy Syst., 2014, vol.60, pp. 190–202.

[19] N. Altin, S. Ozdemir, H. Komurcugil and I. Sefa, "Sliding-Mode Control in Natural Frame with Reduced Number of Sensors for Three-Phase Grid-Tied LCL-Interfaced Inverters," in *IEEE Trans.Ind. Electron.*, vol. 66, no. 4, pp. 2903-2913, April 2019.

[20] P. Cortes, M. P. Kazmierkowski, R. M. Kennel, D. E. Quevedo and J. Rodriguez, "Predictive control in power electronics and drives," *IEEE Trans. Ind. Electron*, vol. 55, no. 12, pp. 4312-4324, December 2008.

[21] D. Zhi, L. Xu, and B. W. Williams, "Model-based predictive direct power control of doubly fed induction generators," *IEEE Trans. Power Electron.,* vol. 25, no. 2, pp. 341-351, Feb. 2010.

[22] A. Bouafia, J. P. Gaubert and F. Krim, "Predictive direct power control of threephase pulsewidth modulation (PWM) rectifier using space-vector modulation (SVM)," *IEEE Trans. Power Electron.,* vol. 25, no. 1, pp. 228-236, January 2010.

[23] J. M. Espí, J. Castelló, R. García-Gil, G. Garcerá, and E. Figueres, "An adaptive robust predictive current control for three-phase grid-connected inverters," *IEEE Trans. Ind. Electron*, vol. 58, no. 8, pp. 3537-3546, August 2011.

[24] Q. Zeng and L. Chang, "An advanced SVPWM-based predictive current controller for three-phase inverters in distributed generation systems," *IEEE Trans. Ind. Electron*, vol. 55, no. 3, pp. 1235-1246, Mar. 2008.

[25] O. Kukrer, "Discrete-time control of voltage-fed three-phase PWM inverters," *IEEE Trans. Ind. Electron*, vol. 11, no. 2, pp. 260-269, Mar. 1996.

[26] R. E. Betz, B. J. Cook, and S. J. Henriksen, "A digital current controller for three phase voltage source inverters," in Conf. Rec. IEEE IAS Annu. Meeting, New Orleans, LA, Oct. 2003, pp. 722-729.

[27] Y. Nishida, O. Miyashita, T. Haneyoshi, H. Tomita, and A. Maeda, "A predictive instantaneous-current PWM controlled rectifier with AC-side harmonic current reduction," *IEEE Trans. Ind. Electron*, vol. 44, no. 3, pp. 337-343, Jun. 1997.

[28] S.-M. Yang and C.-H. Lee, "A deadbeat current controller for field oriented induction motor drives," *IEEE Trans. Power Electron.,* vol. 17, no. 5, pp. 772-778, Sep. 2002.

[29] P. Cortés, G. Ortiz, J. I. Yuz, J. Rodríguez, S. Vazquez, and L. G. Franquelo, "Model predictive control of an inverter with output LC filter for UPS applications," *IEEE Trans. Ind. Electron.,* vol. 56, no. 6, pp. 1875-1883, February 2009.

[30] S. Kouro, P. Cortes, R. Vargas, U. Ammann and J. Rodriguez, "Model predictive control─A simple and powerful method to control power converters," *IEEE Trans. Ind. Electron.,* vol. 56, no. 6, pp. 1826-1838, June 2009.

[31] Bin Wu, High- Power Converters and AC Drives, Wiley-IEEE Press, Mar. 2006.

[32] Liu, T., Xia, Ch., Shi, T., "Robust model predictive current control of grid-connected converter without alternating current voltage sensors," *IET Power Electron*., vol. 7, No. 12, pp. 2934–2944, 2014.

[33] V. Yaramasu, M. Rivera, B. Wu and J. Rodriguez, "Model Predictive Current Control of Two-Level Four-Leg Inverters—Part I: Concept, Algorithm, and Simulation Analysis," *IEEE Trans. Power. Electron*, vol. 28, no. 7, pp. 3459-3468, Jul. 2013.

[34] S. Kwak, S. Kim and J. Park, "Predictive Current Control Methods with Reduced Current Errors and Ripples for Single-Phase Voltage Source Inverters," in *IEEE Trans. Ind. Informat.*, vol. 11, no. 5, pp. 1006-1016, Oct. 2015.

[35] L. Li, H. Nian, L. Ding and B. Zhou, "Direct power control of DFIG system without phase-locked loop under unbalanced and harmonically distorted voltage," *IEEE Trans. Energy Conver*., vol. 33, no. 1, pp. 395-405, 2017.

[36] R. Errouissi, S. M. Muyeen, A. Al-Durra and S. Leng, "Experimental Validation of a Robust Continuous Nonlinear Model Predictive Control Based Grid-Interlinked Photovoltaic Inverter," in *IEEE Trans. Ind. Electron*, vol. 63, no. 7, pp. 4495-4505, July 2016.

[37] S. A. Larrinaga, M. A. Rodriguez, E. Oyarbide and J. R. T. Apraiz, "Predictive control strategy for DC/AC converters based on direct power control," *IEEE Trans. Ind. Electron.,* vol. 54, no. 3, pp. 1261-1271, June 2007.

[38] P. Antoniewicz, and M. P. Kazmierkowski, "Virtual-Flux-Based predictive direct power control of AC/DC converters with online inductance estimation," *IEEE Trans. Ind. Electron.,* vol. 55, no. 12, pp. 4281-4390, December 2008.

[39] J. Hu and Z. Zhu, "Investigation on switching patterns of direct power control strategies for grid-connected DC – AC converters based on power variation rates," *IEEE Trans. Power Electron.,* vol. 26, no. 12, pp. 3582-3598, December 2011.

[40] R. Morales-Caporal, and M. Pacas, "Encoderless predictive direct torque control for synchronous reluctance machines at very low and zero speed," *IEEE Trans. Ind. Electron.,* vol. 55, no. 12, pp. 4408-4416, December 2008.

[41] G. Abad, M. A. Rodriguez, and J. Poza, "Two-level VSC based predictive direct power control of the doubly fed induction machine with reduced power ripple at low constant switching frequency," *IEEE Trans. Energy. Convers.,* vol. 23, no. 2, pp. 570-580, Jun. 2008.

[42] G. Abad, M. A. Rodriguez, and J. Poza, "Two-level VSC based predictive direct torque control of the doubly fed induction machine with reduced torque and flux ripples at low constant switching frequency," *IEEE Trans. Power Electron.,* vol. 23, no. 3, pp. 1050-1061, May. 2008.

[43] G. Abad, M. A. Rodriguez, and J. Poza, "Three-level NPC converter-based predictive direct power control of the doubly fed induction machine at low constant switching frequency," *IEEE Trans. Ind. Electron.,* vol. 55, no. 12, pp. 4417-4429, 2008.

[44] S. Vazquez, A. Marquez, R. Aguilera, D. Quevedo, J. I. Leon and L. G. Franquelo, "Predictive Optimal Switching Sequence Direct Power Control for Grid-Connected Power Converters," *IEEE Trans. Ind. Electron*, vol. 62, no. 4, pp. 2010-2020, Apr. 2015.

[45] T. Kawabata and S. Higashino, "Parallel Operation of Voltage Source Inverters," *IEEE Trans. Ind.* Appl., vol. 24, pp. 281-287, no. 2, 1988.

[46] M. C. Chandorkar, D. M. Divan, and R. Adapa, "Control of parallel connected inverters in standalone AC supply systems," *IEEE Trans. Ind.* Appl., vol. 29, no. 1, pp. 136-143, 1993.

[47] J. M. Guerrero, L. G. de Vicuna, J. Matas, M. Castilla and J. Miret, "A wireless controller to enhance dynamic performance of parallel inverters in distributed generation systems," *IEEE Trans. Power Electron.*, vol. 19, no. 5, pp. 1205-1213, 2004.

[48] J. M. Guerrero, J. Matas, V. Luis Garcia de, M. Castilla, and J. Miret, "Decentralized Control for Parallel Operation of Distributed Generation Inverters Using Resistive Output Impedance," *IEEE Trans. Ind. Electron.*, vol. 54, no. 2, pp. 994-1004, 2007.

[49] R. Majumder, A. Ghosh, G. Ledwich, and F. Zare, "Angle droop versus frequency droop in a voltage source converter based autonomous microgrid," *IEEE Power and Energy Society General Meeting* 2009, pp.1-8.

[50] R. Majumder, B. Chaudhuri, A. Ghosh, G. Ledwich, and F. Zare, "Improvement of Stability and Load Sharing in an Autonomous Microgrid Using Supplementary Droop Control Loop," *IEEE Trans. Power Sys*., vol. 25, no. 2, pp. 796-808, 2010.

[51] W. Yao, M. Chen, J. Matas, M. Guerrero, and Z. Qian, "Design and Analysis of the Droop Control Method for Parallel Inverters Considering the Impact of the Complex Impedance on the Power Sharing," *IEEE Trans. Ind. Electron*, vol. 58, no. 2, pp. 576-588, Feb. 2011.

[52] K. Jaehong, J. M. Guerrero, P. Rodriguez, R. Teodorescu, and N. Kwanghee, "Mode Adaptive Droop Control with Virtual Output Impedances for an Inverter-Based Flexible AC Microgrid," *IEEE Trans. Power Electron*, vol. 26, no. 3, pp. 689-701, 2011.

[53] Z. Qing-Chang, "Robust Droop Controller for Accurate Proportional Load Sharing Among Inverters Operated in Parallel," *IEEE Trans. Ind. Electron*, vol. 60, no. 4, pp. 1281-1290, 2013.

[54] C. T. Lee, C. C. Chu, and P. T. Cheng, "A New Droop Control Method for the Autonomous Operation of Distributed Energy Resource Interface Converters," *IEEE Trans. Power Electron*, vol. 28, no. 4, pp. 1980-1993, 2013.

[55] Y. Mohamed and E. F. El-Saadany, "Adaptive Decentralized Droop Controller to Preserve Power Sharing Stability of Paralleled Inverters in Distributed Generation Microgrids," *IEEE Trans. Power Electron*, vol. 23, no. 6, pp. 2806-2816, 2008.

[56] L. Yun Wei and K. Ching-Nan, "An Accurate Power Control Strategy for Power-Electronics-Interfaced Distributed Generation Units Operating in a Low-Voltage Multi-bus Microgrid," *IEEE Trans. Power Electron*, vol. 24, no. 12, pp. 2977-2988, 2009.

[57] A. Seon-Ju, P. Jin-Woo, C. Il-Yop, M. Seung-Il, K. Sang-Hee, and N. SoonRyul, "Power-Sharing Method of Multiple Distributed Generators Considering Control Modes and Configurations of a Microgrid," *IEEE Trans. Power Deliv.*, vol. 25, no. 3, pp. 2007-2016, 2010.

[58] E. Rokrok and M. E. H. Golshan, "Adaptive voltage droop scheme for voltage source converters in an islanded multibus microgrid,", *IET Generation, Transmission and Distribution,* vol. 4, no. 5, pp. 562-578, 2010.

[59] E. Barklund, N. Pogaku, M. Prodanovic, C. Hernandez-Aramburo, and T. C. Green, "Energy Management in Autonomous Microgrid Using Stability Constrained Droop Control of Inverters," *IEEE Trans. Power Electron*, vol. 23, no. 5, pp. 2346-2352, 2008.

[60] G. Diaz, C. Gonzalez-Moran, J. Gomez-Aleixandre, and A. Diez, "Scheduling of Droop Coefficients for Frequency and Voltage Regulation in Isolated Microgrids," *IEEE Trans. Power Sys.*, vol. 25, no. 1, pp.489-496, 2010.

[61] M. N. Marwali, J. Jin-Woo, and A. Keyhani, "Control of distributed generation systems - Part II: Load sharing control," *IEEE Trans. Power Electron.*, vol. 19, no. 6, pp. 1551-1561, 2004.

[62] C. Il-Yop, L. Wenxin, D. A. Cartes, E. G. Collins, and M. Seung-Il, "Control Methods of Inverter-Interfaced Distributed Generators in a Microgrid System," *IEEE Trans. Ind.* Appl., vol. 46, no. 3, pp. 1078-1088, 2010.

[63] M. Savaghebi, A. Jalilian, J. C. Vasquez, and J. M. Guerrero, "Autonomous Voltage Unbalance Compensation in an Islanded Droop-Controlled Microgrid," *IEEE Trans. Ind. Electron.*, vol. 60, no. 4, pp. 1390-1402, 2013.

[64] R. Majumder, G. Ledwich, A. Ghosh, S. Chakrabarti, and F. Zare, "Droop Control of Converter-Interfaced Microsources in Rural Distributed Generation," *IEEE Trans. Power Deliv*., vol. 25, no. 4, pp. 2768-2778, 2010.

[65] Z. Yao and M. Hao, "Theoretical and Experimental Investigation of Networked Control for Parallel Operation of Inverters," *IEEE Trans. Ind. Electron.*, vol. 59, no. 4, pp. 1961-1970, 2012.

[66] J. M. Guerrero, J. C. Vasquez, J. Matas, L. G. de Vicuna, and M. Castilla, "Hierarchical Control of Droop-Controlled AC and DC Microgrids – A General Approach Toward Standardization," *IEEE Trans. Ind. Electron.*, vol. 58, no. 1, pp. 158-172, 2011.

[67] H. Ming, H. Haibing, X. Yan, and J. M. Guerrero, "Multilayer Control for Inverters in Parallel Operation Without Intercommunications," *IEEE Trans. Power Electron.*, vol. 27, no. 8, pp. 3651-3663, 2012.

[68] M. Savaghebi, A. Jalilian, J. C. Vasquez, and J. M. Guerrero, "Secondary Control for Voltage Quality Enhancement in Microgrids," *IEEE Trans. Smart Grid*, vol. 3, no. 4, pp. 1893-1902, 2012.

[69] J. C. Vasquez, J. M. Guerrero, M. Savaghebi, J. Eloy-Garcia, and R.Teodorescu, "Modeling, Analysis, and Design of Stationary-Reference-Frame Droop-Controlled Parallel Three-Phase Voltage Source Inverters," *IEEE Trans. Ind.* Electron., vol. 60, no. 4, pp. 1271-1280, 2013.

[70] J. M. Guerrero, L. Hang, and J. Uceda, "Control of Distributed Uninterruptible Power Supply Systems," *IEEE Trans. Ind. Electron.*, vol. 55, no. 8, pp. 2845-2859, 2008.

[71] C. Jiann-Fuh and C. Ching-Lung, "Combination voltage-controlled and current-controlled PWM inverters for UPS parallel operation," *IEEE Trans. Power Electron.*, vol. 10, no. 5, pp. 547-558, 1995.

[72] H. Van Der Broeck and U. Boeke, "A simple method for parallel operation of inverters," Telecommunications Energy Conference, 1998. INTELEC. Twentieth International, 1998, pp. 143-150.

[73] T. Caldognetto and P. Tenti, "Microgrids Operation Based on Master–Slave Cooperative Control," in *IEEE Jour. Emer. Select. Top. Power Electron*, vol. 2, no. 4, pp. 1081-1088, Dec. 2014.

[74] C. Wang, P. Yang, C. Ye, Y. Wang and Z. Xu, "Improved V/F Control Strategy for Microgrids Based on Master–Slave Control Mode," *IET Renewable Power Generation*, vol. 10, no. 9, pp. 1356-1365, 10 2016.

[75] P. Jain, V. Agarwal and B. P. Muni, "Hybrid Phase Locked Loop for Controlling Master-Slave Configured Centralized Inverters in Large Solar Photovoltaic Power Plants," *IEEE Trans. Ind. Appl.*, vol. 54, no. 4, pp. 3566-3574, July-Aug. 2018.

[76] Tsai-Fu Wu, Yu-Kai Chen and Yong-Heh Huang, "3C strategy for inverters in parallel operation achieving an equal current distribution," *IEEE Trans. Ind. Electron.*, vol. 47, no. 2, pp. 273-281, April 2000.

[77] T. M. L. Assis and G. N. Taranto, "Automatic Reconnection from Intentional Islanding Based on Remote Sensing of Voltage and Frequency Signals," *IEEE Trans. Smart Grid*, vol. 3, no. 4, pp. 1877-1884, Dec. 2012.

[78] A. Bellini, S. Bifaretti and F. Giannini, "A Robust Synchronization Method for Centralized Microgrids," *IEEE Trans. Ind. Appl.*, vol. 51, no. 2, pp. 1602-1609, March-April 2015.

[79] Y. Panov and M. M. Jovanovic, "Loop Gain Measurement of Paralleled DC–DC Converters with Average-Current-Sharing Control," *IEEE Trans. Power Electron*, vol. 23, no. 6, pp. 2942-2948, Nov. 2008.

[80] S. Tolani and P. Sensarma, "An Instantaneous Average Current Sharing Scheme for Parallel UPS Modules," *IEEE Trans. Ind. Electron.*, vol. 64, no. 12, pp. 9210-9220, Dec. 2017.

[81] M. S. Golsorkhi, M. Savaghebi, D. D. Lu, J. M. Guerrero and J. C. Vasquez, "A GPS-Based Control Framework for Accurate Current Sharing and Power Quality Improvement in Microgrids," *IEEE Trans. Power Electron.*, vol. 32, no. 7, pp. 5675-5687, July 2017.

[82] Y. Deng, Y. Tao, G. Chen, G. Li and X. He, "Enhanced Power Flow Control for Grid-Connected Droop-Controlled Inverters with Improved Stability," *IEEE Trans.Ind. Electron.*, vol. 64, no. 7, pp. 5919-5929, July 2017.

[83] S. Peyghami, H. Mokhtari, P. C. Loh, P. Davari and F. Blaabjerg, "Distributed Primary and Secondary Power Sharing in a Droop-Controlled LVDC Microgrid with Merged AC and DC Characteristics," *IEEE Trans. Smart Grid*, vol. 9, no. 3, pp. 2284-2294, May 2018.

[84] M. S. Golsorkhi, D. J. Hill and H. R. Karshenas, "Distributed Voltage Control and Power Management of Networked Microgrids," *IEEE Jour. Emer. Select. Top. Power Electron*, vol. 6, no. 4, pp. 1892-1902, Dec. 2018.

[85] J. Rocabert, A. Luna, F. Blaabjerg, and P. Rodriguez, "Control of power converters in AC microgrids," *IEEE Trans. Power Electron*., vol. 27, no. 11, pp. 4734–4739, Nov. 2012.

[86] S. M. Ashabani and Y. A. R. I. Mohamed, "A Flexible Control Strategy for Grid-Connected and Islanded Microgrids With Enhanced Stability Using Nonlinear Microgrid Stabilizer," *IEEE Trans Smart Grid*, vol. 3, no. 3, pp. 1291-1301, Sept. 2012.

[87] Á. Molina-García, R. A. Mastromauro, T. García-Sánchez, S. Pugliese, M. Liserre and S. Stasi, "Reactive Power Flow Control for PV Inverters Voltage Support in LV Distribution Networks," *IEEE Trans. Smart Grid*, vol. 8, no. 1, pp. 447-456, Jan. 2017.

[88] S. Vazquez, J. A. Sanchez, M. R. Reyes, J. I. Leon and J. M. Carrasco, "Adaptive Vectorial Filter for Grid Synchronization of Power Converters Under Unbalanced and/or Distorted Grid Conditions," *IEEE Trans. Ind. Electron*, vol. 61, no. 3, pp. 1355-1367, Mar.2014.

[89] Y. Han, M. Luo, X. Zhao, J. M. Guerrero and L. Xu, "Comparative Performance Evaluation of Orthogonal-Signal-Generators-Based Single-Phase PLL Algorithms— A Survey," *IEEE Trans. Power Electron*, vol. 31, no. 5, pp. 3932-3944, May 2016.

[90] S. Golestan, J. M. Guerrero and J. C. Vasquez, "Single-Phase PLLs: A Review of Recent Advances," in *IEEE Trans. Power Electron*, vol. 32, no. 12, pp. 9013-9030, Dec. 2017.

[91] R. Teodorescu and F. Blaabjerg, "Flexible control of small wind turbines with grid failure detection operating in stand-alone and grid-connected mode," *IEEE Trans. Power Electron*, vol. 19, no. 5, pp. 1323-1332, Sept. 2004.

[92] G. G. Talapur, H. M. Suryawanshi, L. Xu and A. B. Shitole, "A Reliable Microgrid with Seamless Transition Between Grid Connected and Islanded Mode for Residential Community with Enhanced Power Quality," *IEEE Trans. Ind. Appl*, vol. 54, no. 5, pp. 5246-5255, Sept.-Oct. 2018.

[93] G. Lou, W. Gu, J. Wang, J. Wang and B. Gu, "A Unified Control Scheme Based on a Disturbance Observer for Seamless Transition Operation of Inverter-Interfaced Distributed Generation," *IEEE Trans. Smart Grid*, vol. 9, no. 5, pp. 5444-5454, Sept. 2018.

[94] X. Li, H. Zhang, M. B. Shadmand and R. S. Balog, "Model Predictive Control of a Voltage-Source Inverter with Seamless Transition Between Islanded and Grid-Connected Operations," *IEEE Trans. Ind. Electron*, vol. 64, no. 10, pp. 7906-7918, Oct. 2017.

[95] M. Ciobotaru, R. Teodorescu, and F. Blaabjerg, "A new single-phase PLL structure based on second order generalized integrator," in *Proc. 37th IEEE Power Electron. Spec. Conf.*, Jun. 2006, pp. 1–6.

[96] J. Zhang, J. Shu, J. Ning, L. Huang and H. Wang, "Enhanced Proportional Power Sharing Strategy Based on Adaptive Virtual Impedance in Low-Voltage Networked Microgrid," *IET Gener. Transm. Distrib.,* vol. 12, no. 11, pp. 2566-2576, Jun. 2018.

[97] Y. Hu, J. Xiang, Y. Peng, P. Yang and W. Wei, "Decentralised Control for Reactive Power Sharing using Adaptive Virtual Impedance," *IET Gener. Transm. Distrib.*, vol. 12, no. 5, pp. 1198-1205, Mar. 2018.

Publications

Referred Journal Publications:

[1] Perumalla Chandra Sekhar and T. Ratna Rahul, “Model Predictive Controller for Single Phase Distributed Generator with Seamless Transition between Grid and Off-Grid Modes”, *IET Generation, Transmission & Distribution*, vol. 13, no.10, pp. 1829 –1837, May. 2019. DOI: 10.1049/iet-gtd.2018.6345.

[2] T. Ratna Rahul and Perumalla Chandra Sekhar, “Investigation of Current Reference Schemes for Control of Single Phase Inverter using Model Predictive Control and Asynchronous Sigma Delta Modulation”, *Institution of Engineers India*, 2019. https://doi.org/10.1007/s40031-019-00405-z.

Conferences:

[1] T. Ratna Rahul and D. M. Vinod Kumar, “Distributed Control Strategy for the Coordinated Control Operation of the Distributed Generators”. *2018 8th IEEE India International Conference on Power Electronics (IICPE),* JAIPUR, India, 2018, pp. 1-6.

[2] P. C. Sekhar, S. Pandit and Ratna Rahul T., "Analysis of asynchronous sigma-delta modulation scheme for real and reactive power control in grid connected single phase inverters," *2016 IEEE Power and Energy Society General Meeting (PESGM),* Boston, MA,2016, pp. 1-5.doi: 10.1109/PESGM.2016.7741630.

[3] P. C. Sekhar and T. R. Rahul, "Analysis of model predictive control for the active and reactive power in three phase grid connected inverters," *2016 International Conference on Next Generation Intelligent Systems (ICNGIS),* Kottayam, India, 2016, pp. 1-5. doi: 10.1109/ICNGIS.2016.7854028.

Journal Communicated:

[1] T. Ratna Rahul and D. M. Vinod Kumar: “Control Strategies for the Coordinated Control Operation of the Distributed Generators along with Diesel Generator”, to Elsevier Energy Journal.

Curriculum-Vitae

Name	:	Ratna Rahul Tupakula
Date of Birth	:	01st August 1988
Gender	:	Male
Contact number	:	+91 9490634363
Email id	:	ratna.rahul1988@gmail.com

Academic Qualifications:

Program	University	Percentage of marks	Year of completion
M. Tech. (Control Systems)	JNTU Anantapur	82.21	2011
B. Tech. (EEE)	JNTU Anantapur	70.58	2009